

Figure 9.43 Variation of $M_{\gamma q}$ with H/h and ϕ' (After Neeley *et al.*, 1973. With permission from ASCE.)

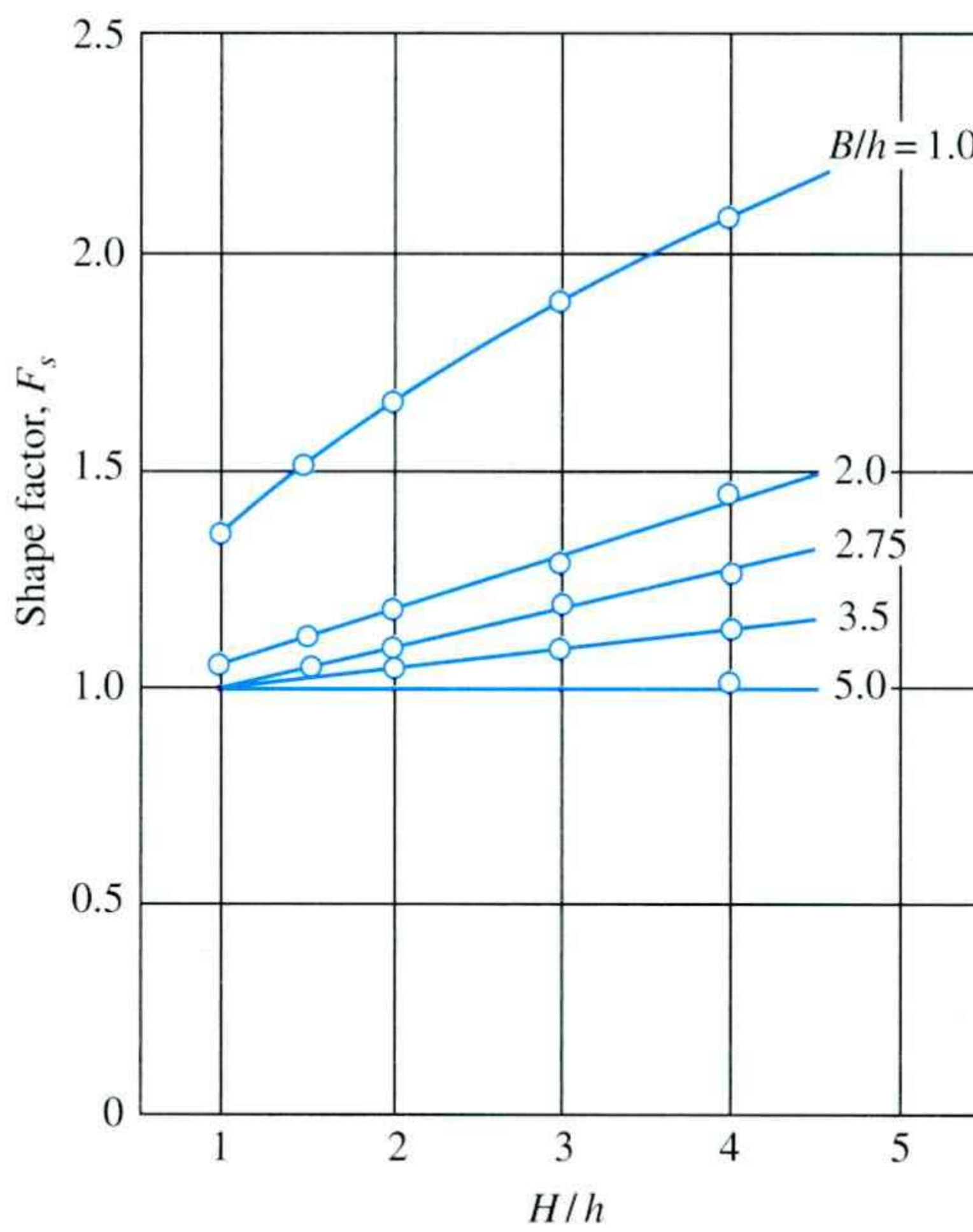


Figure 9.44 Variation of shape factor with H/h and B/h (After Neeley *et al.*, 1973. With permission from ASCE.)

Empirical Correlation Based on Model Tests

Ghaly (1997) used the results of 104 laboratory tests, 15 centrifugal model tests, and ⁹ field tests to propose an empirical correlation for the ultimate resistance of single anchors. The correlation can be written as

$$P_{\text{ult}} = \frac{5.4}{\tan \phi'} \left(\frac{H^2}{A} \right)^{0.28} \gamma A H \quad (9.94)$$

where A = area of the anchor = Bh .

Ghaly also used the model test results of Das and Seeley (1975) to develop a load-displacement relationship for single anchors. The relationship can be given as

$$\frac{P}{P_{\text{ult}}} = 2.2 \left(\frac{u}{H} \right)^{0.3} \quad (9.95)$$

where u = horizontal displacement of the anchor at a load level P .

Equations (9.94) and (9.95) apply to single anchors (i.e., anchors for which $S'/B = \infty$). For all practical purposes, when $S'/B \approx 2$ the anchors behave as single anchors.

Factor of Safety for Anchor Plates

The allowable resistance per anchor plate may be given as

$$P_{\text{all}} = \frac{P_{\text{ult}}}{\text{FS}}$$

where FS = factor of safety.

Generally, a factor of safety of 2 is suggested when the method of Ovesen and Stromann is used. A factor of safety of 3 is suggested for P_{ult} calculated by Eq. (9.94).

Spacing of Anchor Plates

The center-to-center spacing of anchors, S' , may be obtained from

$$S' = \frac{P_{\text{all}}}{F}$$

where F = force per unit length of the sheet pile.

Example 9.11

Refer to Figure 9.41a. Given: $B = h = 0.4 \text{ m}$, $S' = 1.2 \text{ m}$, $H = 1 \text{ m}$, $\gamma = 16.51 \text{ kN/m}^3$, and $\phi' = 35^\circ$. Determine the ultimate resistance for each anchor plate. The anchor plates are made of concrete and have thicknesses of 0.15 m.

Solution

From Figure 9.39a for $\phi' = 35^\circ$, the magnitude of K_a is about 0.26.

$$\begin{aligned} W &= Ht\gamma_{\text{concrete}} = (1 \text{ m})(0.15 \text{ m})(23.5 \text{ kN/m}^3) \\ &= 3.525 \text{ kN/m} \end{aligned}$$

From Eq. (9.89),

$$\begin{aligned} K_p \sin \delta' &= \frac{W + \frac{1}{2}\gamma H^2 K_a \sin \phi'}{\frac{1}{2}\gamma H^2} \\ &= \frac{3.525 + (0.5)(16.51)(1)^2(0.26)(\sin 35)}{(0.5)(16.51)(1)^2} = 0.576 \end{aligned} \quad (9.94)$$

From Figure 9.39b with $\phi' = 35^\circ$ and $K_p \sin \delta' = 0.576$, the value of $K_p \cos \delta'$ is about 4.5. Now, using Eq. (9.88),

$$\begin{aligned} P'_{\text{ult}} &= \frac{1}{2}\gamma H^2(K_p \cos \delta' - K_a \cos \phi') \\ &= (\frac{1}{2})(16.51)(1)^2[4.5 - (0.26)(\cos 35)] = 35.39 \text{ kN/m} \end{aligned}$$

In order to calculate P'_{us} let us assume the sand to be loose. So, C_{ov} in Eq. (9.90) is equal to 14. Hence,

$$P'_{\text{us}} = \left[\frac{C_{\text{ov}} + 1}{C_{\text{ov}} + \left(\frac{H}{h} \right)} \right] P'_{\text{ult}} = \left[\frac{14 + 1}{14 + \left(\frac{1}{0.4} \right)} \right] = 32.17 \text{ kN/m}$$

$$\frac{S' - B}{H + h} = \frac{1.2 - 0.4}{1 + 0.4} = \frac{0.8}{1.4} = 0.571$$

For $(S' - B)/(H + h) = 0.571$ and loose sand, Figure 9.41b yields

$$\frac{B_e - B}{H - h} = 0.229$$

So

$$\begin{aligned} B_e &= (0.229)(H + h) + B = (0.229)(1 + 0.4) + 0.4 \\ &= 0.72 \end{aligned}$$

Hence, from Eq. (9.91)

$$P_{\text{ult}} = P'_{\text{us}} B_e = (32.17)(0.72) = \mathbf{23.16 \text{ kN}}$$

Example 9.12

Refer to a *single anchor* given in Example 9.11 using the stress characteristic solution. Estimate the ultimate anchor resistance. Use $m = 0$ in Figure 9.43.

Solution

Given: $B = h = 0.4 \text{ m}$ and $H = 1 \text{ m}$.

Thus,

$$\frac{H}{h} = \frac{1 \text{ m}}{0.4 \text{ m}} = 2.5$$

$$\frac{B}{h} = \frac{0.4 \text{ m}}{0.4 \text{ m}} = 1$$

From Eq. (9.93),

$$P_{\text{ult}} = M_{\gamma q} \gamma h^2 B F_s$$

From Figure 9.43, with $\phi' = 35^\circ$ and $H/h = 2.5$, $M_{\gamma q} \approx 18.2$. Also, from Figure 9.44, with $H/h = 2.5$ and $B/h = 1$, $F_s \approx 1.8$. Hence,

$$P_{\text{ult}} = (18.2)(16.51)(0.4)^2(0.4)(1.8) \approx \mathbf{34.62 \text{ kN}}$$

Example 9.13

Solve Example Problem 9.12 using Eq. (9.94).

Solution

From Eq. (9.94),

$$P_{\text{ult}} = \frac{5.4}{\tan \phi'} \left(\frac{H^2}{A} \right)^{0.28} \gamma A H$$

$$H = 1 \text{ m}$$

$$A = B h = (0.4 \times 0.4) = 0.16 \text{ m}^2$$

$$P_{\text{ult}} = \frac{5.4}{\tan 35} \left[\frac{(1)^2}{0.16} \right]^{0.28} (16.51)(0.16)(1) \approx \mathbf{34.03 \text{ kN}}$$

9.18

Holding Capacity of Anchor Plates in Clay ($\phi = 0$ Condition)

Relatively few studies have been conducted on the ultimate resistance of anchor plates in clayey soils ($\phi = 0$). Mackenzie (1955) and Tschebotarioff (1973) identified the nature of variation of the ultimate resistance of strip anchors and beams as a function of H , h , and c (undrained cohesion based on $\phi = 0$) in a nondimensional form based on laboratory model test results. This is shown in the form of a nondimensional plot in Figure 9.45 (P_{ult}/hBc versus H/h) and can be used to estimate the ultimate resistance of anchor plates in saturated clay ($\phi = 0$).

9.19

Ultimate Resistance of Tiebacks

According to Figure 9.46, the ultimate resistance offered by a tieback in sand is

$$P_{\text{ult}} = \pi d l \bar{\sigma}'_o K \tan \phi' \quad (9.96)$$

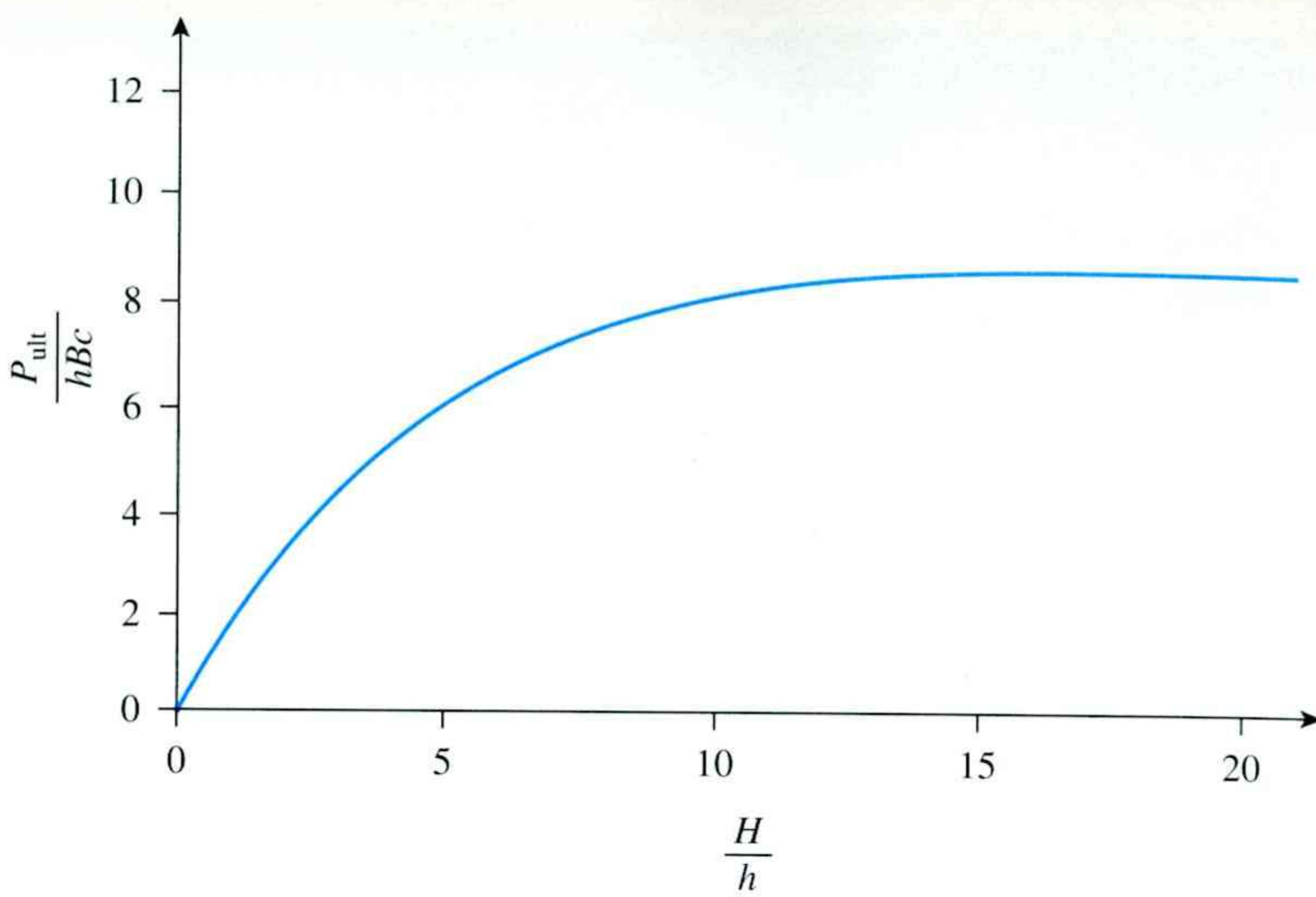


Figure 9.45 Experimental variation of $\frac{P_{\text{ult}}}{hB_c}$ with H/h for plate anchors in clay
(Based on Mackenzie (1955) and Tschebotarioff (1973))

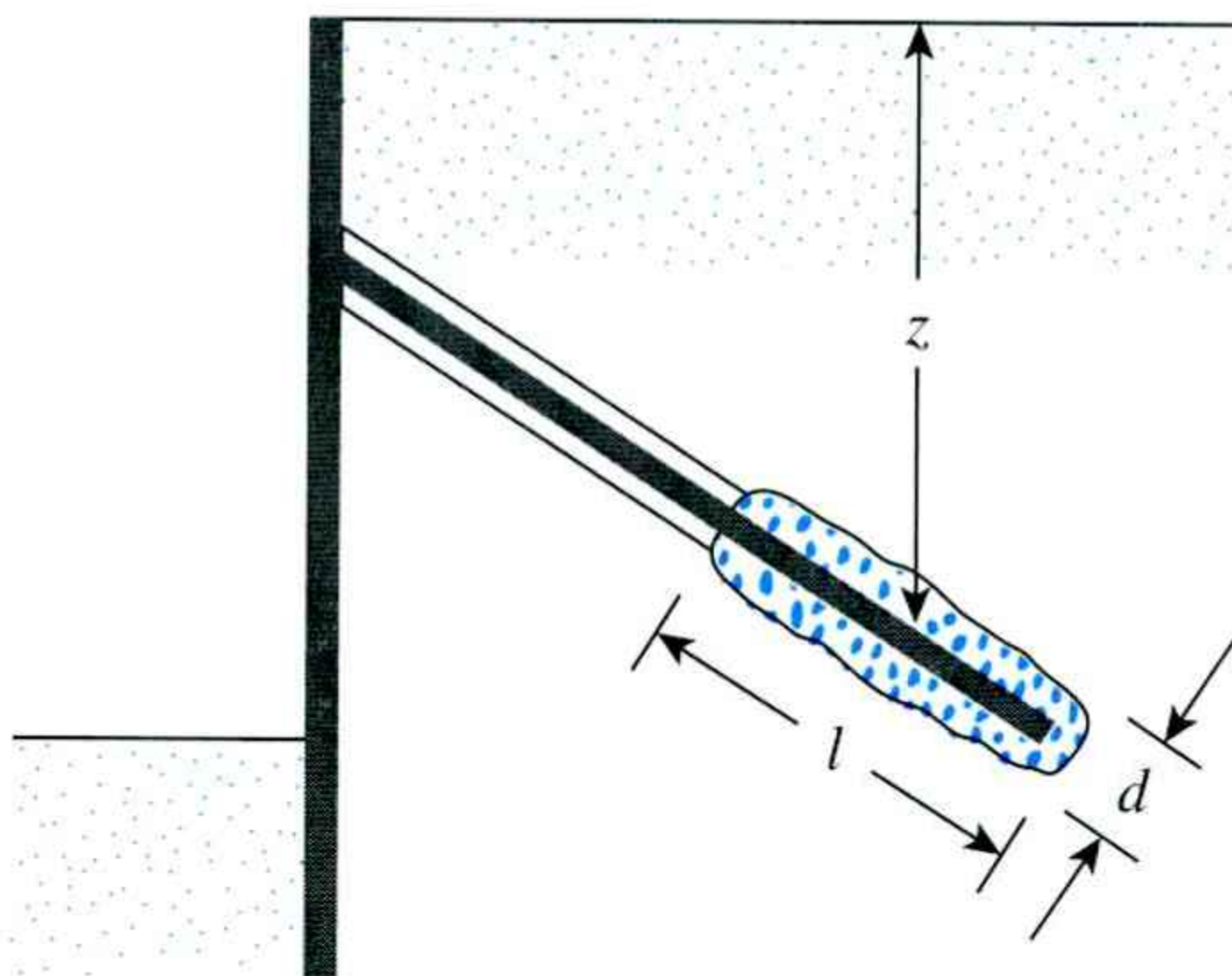


Figure 9.46 Parameters for defining the ultimate resistance of tiebacks

where

ϕ' = effective angle of friction of soil

$\bar{\sigma}'_o$ = average effective vertical stress ($=\gamma z$ in dry sand)

K = earth pressure coefficient

The magnitude of K can be taken to be equal to the earth pressure coefficient at rest (K_o) if the concrete grout is placed under pressure (Littlejohn, 1970). The lower limit of K can be taken to be equal to the Rankine active earth pressure coefficient.

In clays, the ultimate resistance of tiebacks may be approximated as

$$P_{\text{ult}} = \pi d l c_a \quad (9.97)$$

where c_a = adhesion.

The value of c_a may be approximated as $\frac{2}{3}c_u$ (where c_u = undrained cohesion). A factor of safety of 1.5 to 2 may be used over the ultimate resistance to obtain the allowable resistance offered by each tieback.

Problems

- 9.1** Figure P9.1 shows a cantilever sheet pile wall penetrating a granular soil. Here, $L_1 = 4 \text{ m}$, $L_2 = 8 \text{ m}$, $\gamma = 16.1 \text{ kN/m}^3$, $\gamma_{\text{sat}} = 18.2 \text{ kN/m}^3$, and $\phi' = 32^\circ$.
- What is the theoretical depth of embedment, D ?
 - For a 30% increase in D , what should be the total length of the sheet piles?
 - Determine the theoretical maximum moment of the sheet pile.
- 9.2** Redo Problem 9.1 with the following: $L_1 = 3 \text{ m}$, $L_2 = 6 \text{ m}$, $\gamma = 17.3 \text{ kN/m}^3$, $\gamma_{\text{sat}} = 19.4 \text{ kN/m}^3$, and $\phi' = 30^\circ$.
- 9.3** Refer to Figure 9.10. Given: $L = 3 \text{ m}$, $\gamma = 16.7 \text{ kN/m}^3$, and $\phi' = 30^\circ$. Calculate the theoretical depth of penetration, D , and the maximum moment.
- 9.4** Refer to Figure P9.4, for which $L_1 = 2.4 \text{ m}$, $L_2 = 4.6 \text{ m}$, $\gamma = 15.7 \text{ kN/m}^3$, $\gamma_{\text{sat}} = 17.3 \text{ kN/m}^3$, and $\phi' = 30^\circ$, and $c = 29 \text{ kN/m}^2$.
- What is the theoretical depth of embedment, D ?
 - Increase D by 40%. What length of sheet piles is needed?
 - Determine the theoretical maximum moment in the sheet pile.
- 9.5** Refer to Figure 9.14. Given: $L = 4 \text{ m}$; for sand, $\gamma = 16 \text{ kN/m}^3$; $\phi' = 35^\circ$; and, for clay, $\gamma_{\text{sat}} = 19.2 \text{ kN/m}^3$ and $c = 45 \text{ kN/m}^2$. Determine the theoretical value of D and the maximum moment.
- 9.6** An anchored sheet pile bulkhead is shown in Figure P9.6. Let $L_1 = 4 \text{ m}$, $L_2 = 9 \text{ m}$, $l_1 = 2 \text{ m}$, $\gamma = 17 \text{ kN/m}^3$, $\gamma_{\text{sat}} = 19 \text{ kN/m}^3$, and $\phi' = 34^\circ$.
- Calculate the theoretical value of the depth of embedment, D .
 - Draw the pressure distribution diagram.
 - Determine the anchor force per unit length of the wall.
- Use the free earth-support method.

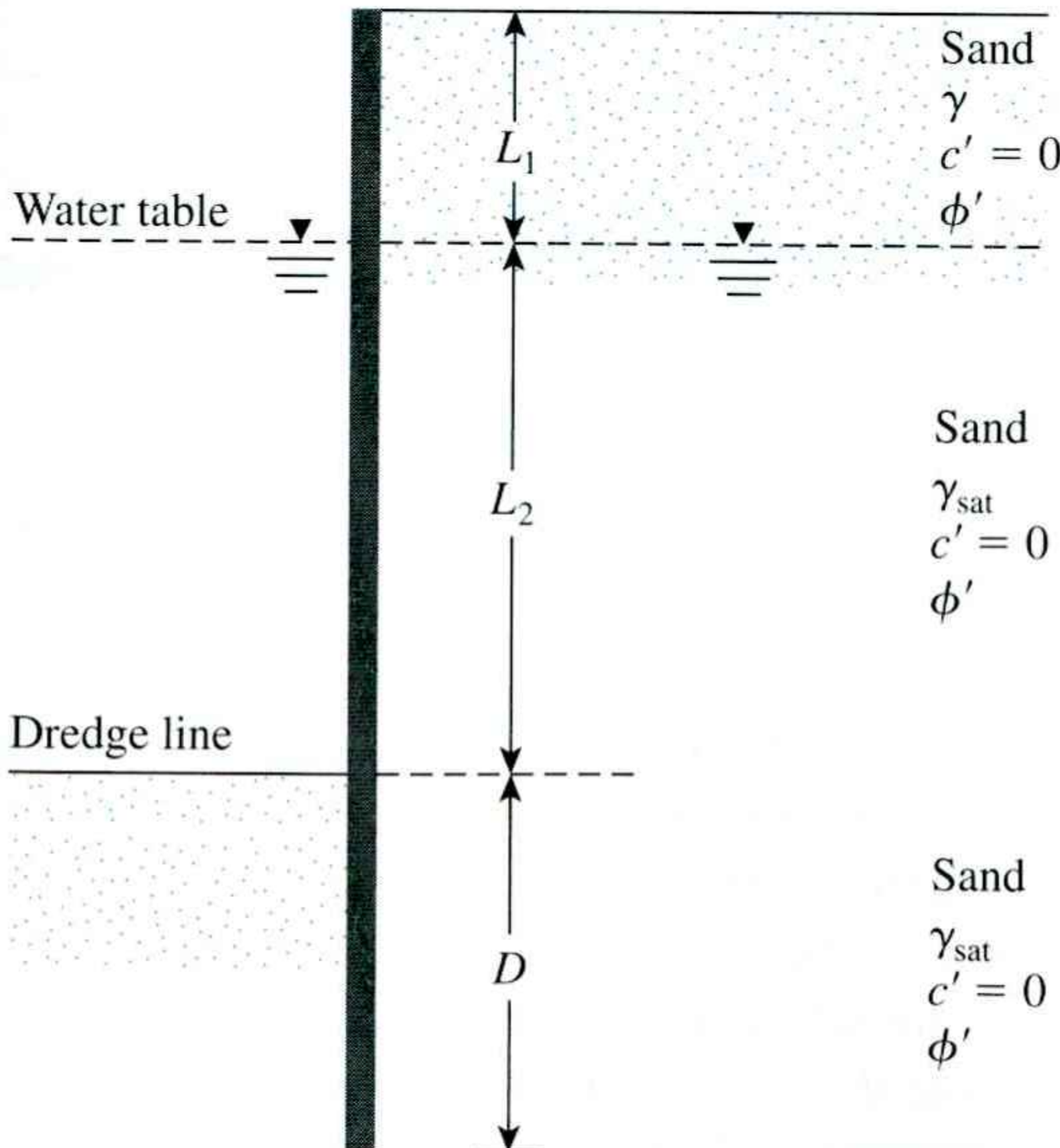


Figure P9.1

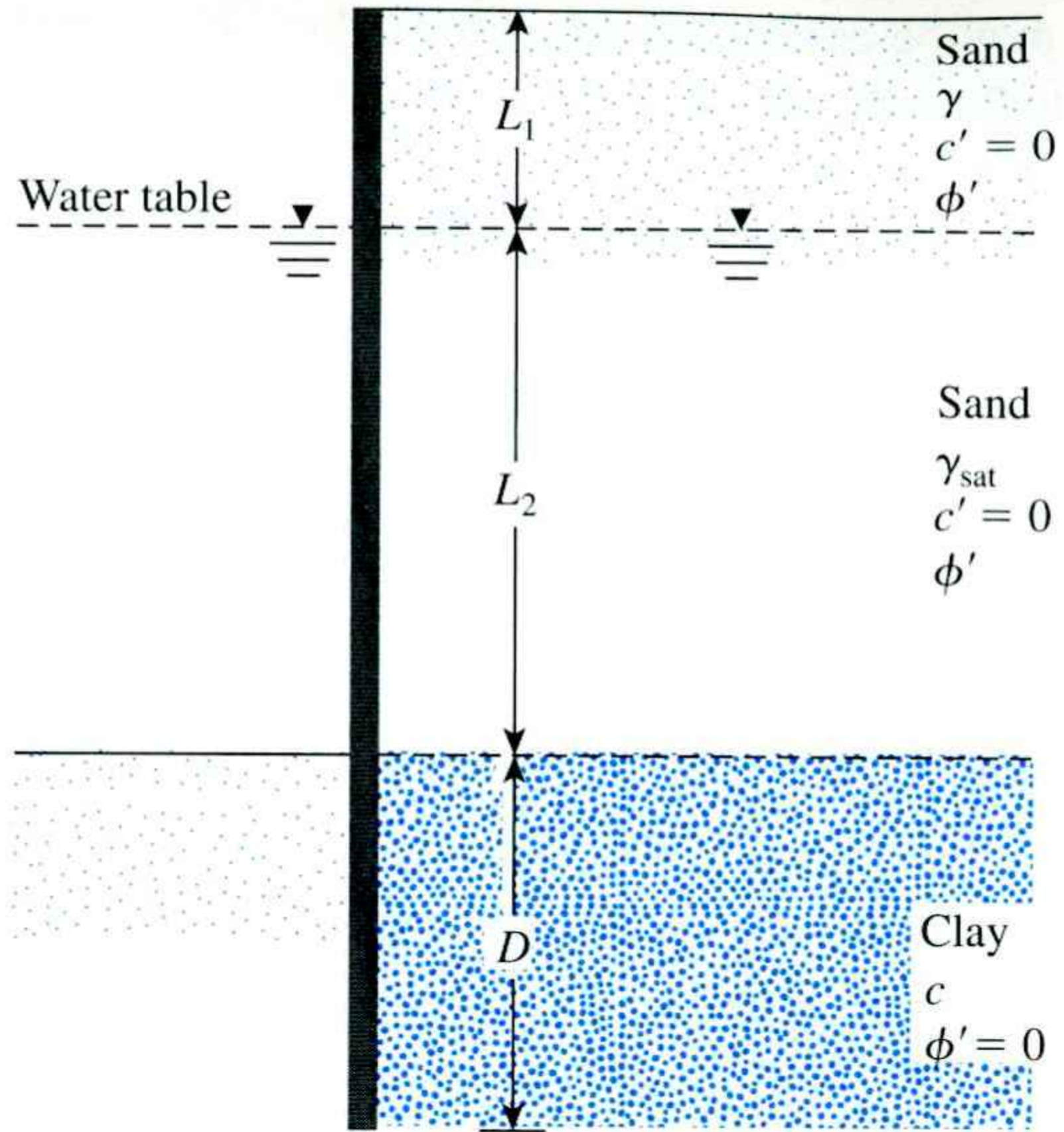


Figure P9.4

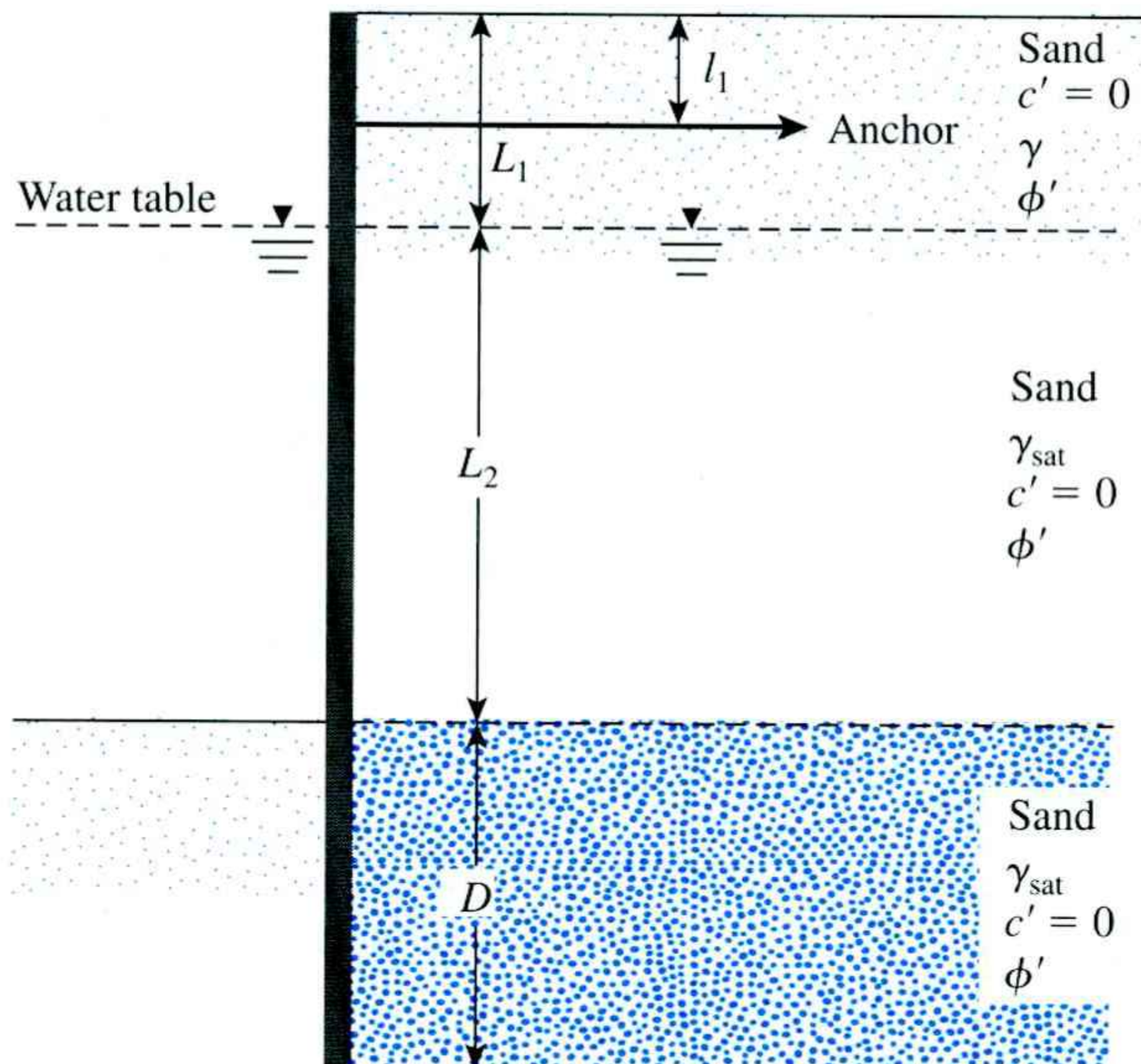


Figure P9.6

- 9.7** In Problem 9.6, assume that $D_{\text{actual}} = 1.3D_{\text{theory}}$.
- Determining the theoretical maximum moment.
 - Using Rowe's moment reduction technique, choose a sheet pile section. Take $E = 210 \times 10^3 \text{ MN/m}^2$ and $\sigma_{\text{all}} = 210,000 \text{ kN/m}^2$.
- 9.8** Refer to Figure P9.6. Given: $L_1 = 4 \text{ m}$, $L_2 = 8 \text{ m}$, $l_1 = l_2 = 2 \text{ m}$, $\gamma = 16 \text{ kN/m}^3$, $\gamma_{\text{sat}} = 18.5 \text{ kN/m}^3$, and $\phi' = 35^\circ$. Use the charts presented in Section 9.10 and determine:
- Theoretical depth of penetration
 - Anchor force per unit length
 - Maximum moment in the sheet pile.
- 9.9** Refer to Figure P9.6, for which $L_1 = 4 \text{ m}$, $L_2 = 7 \text{ m}$, $l_1 = 1.5 \text{ m}$, $\gamma = 18 \text{ kN/m}^3$, $\gamma_{\text{sat}} = 19.5 \text{ kN/m}^3$, and $\phi' = 30^\circ$. Use the computational diagram method (Section 9.12) to determine D , F , and M_{max} . Assume that $C = 0.68$ and $R = 0.6$.

- 9.10** An anchored sheet-pile bulkhead is shown in Figure P9.10. Let $L_1 = 2 \text{ m}$, $L_2 = 6 \text{ m}$, $l_1 = 1 \text{ m}$, $\gamma = 16 \text{ kN/m}^3$, $\gamma_{\text{sat}} = 18.86 \text{ kN/m}^3$, $\phi' = 32^\circ$, and $c = 27 \text{ kN/m}^2$.
- Determine the theoretical depth of embedment, D .
 - Calculate the anchor force per unit length of the sheet-pile wall.
- Use the free earth support method.
- 9.11** In Figure 9.41a, for the anchor slab in sand, $H = 1.52 \text{ m}$, $h = 0.91 \text{ m}$, $B = 1.22 \text{ m}$, $S' = 2.13 \text{ m}$, $\phi' = 30^\circ$, and $\gamma = 17.3 \text{ kN/m}^3$. The anchor plates are made of concrete and have a thickness of 76 mm. Using Ovesen and Stromann's method, calculate the ultimate holding capacity of each anchor. Take $\gamma_{\text{concrete}} = 23.58 \text{ kN/m}^3$.
- 9.12** A single anchor slab is shown in Figure P9.12. Here, $H = 0.9 \text{ m}$, $h = 0.3 \text{ m}$, $\gamma = 17 \text{ kN/m}^3$, and $\phi' = 32^\circ$. Calculate the ultimate holding capacity of the anchor slab if the width B is (a) 0.3 m, (b) 0.6 m, and (c) = 0.9 m.
(Note: center-to-center spacing, $S' = \infty$.) Use the empirical correlation given in Section 9.17 [Eq. (9.94)].
- 9.13** Repeat Problem 9.12 using Eq. (9.93). Use $m = 0$ in Figure 9.43.

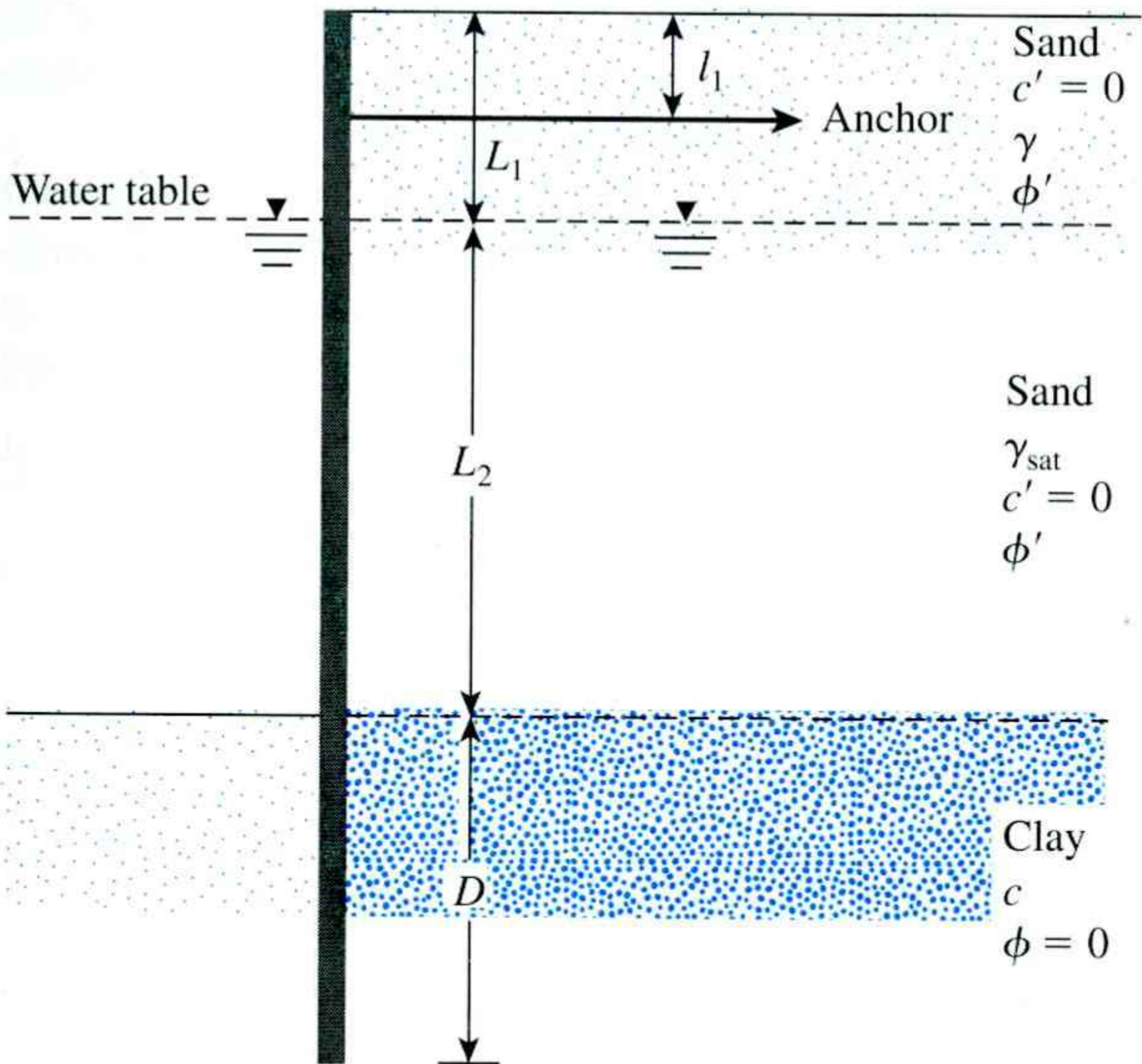


Figure P9.10

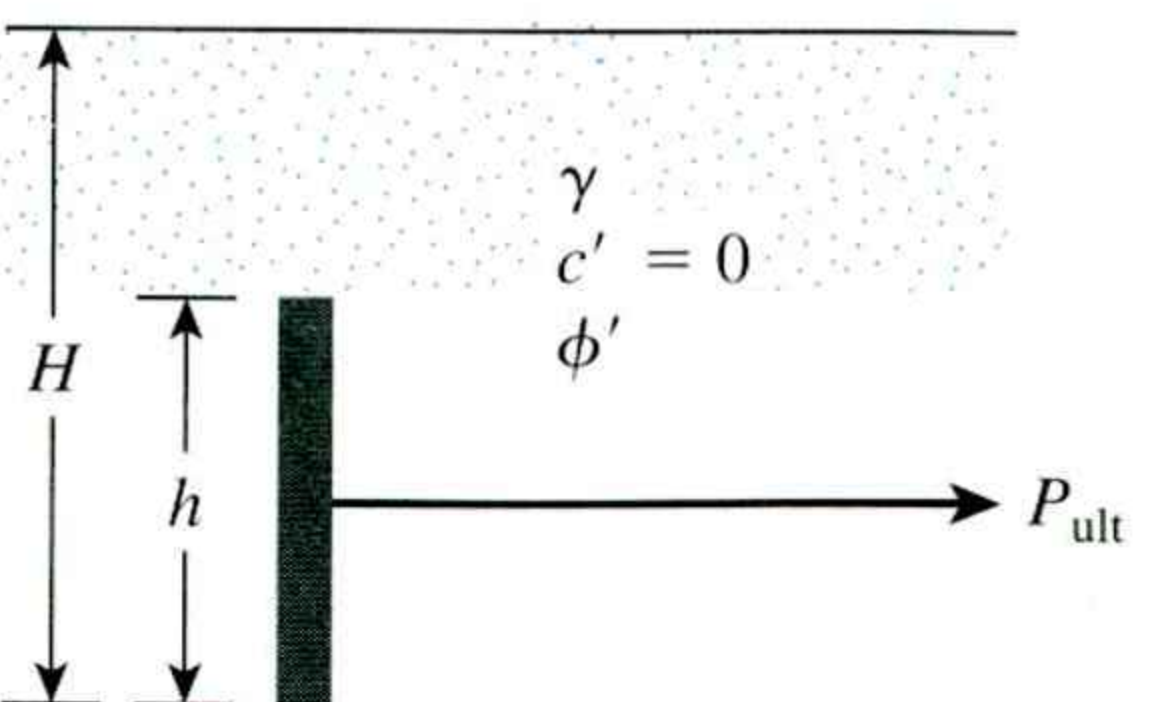


Figure P9.12

10 Braced Cuts

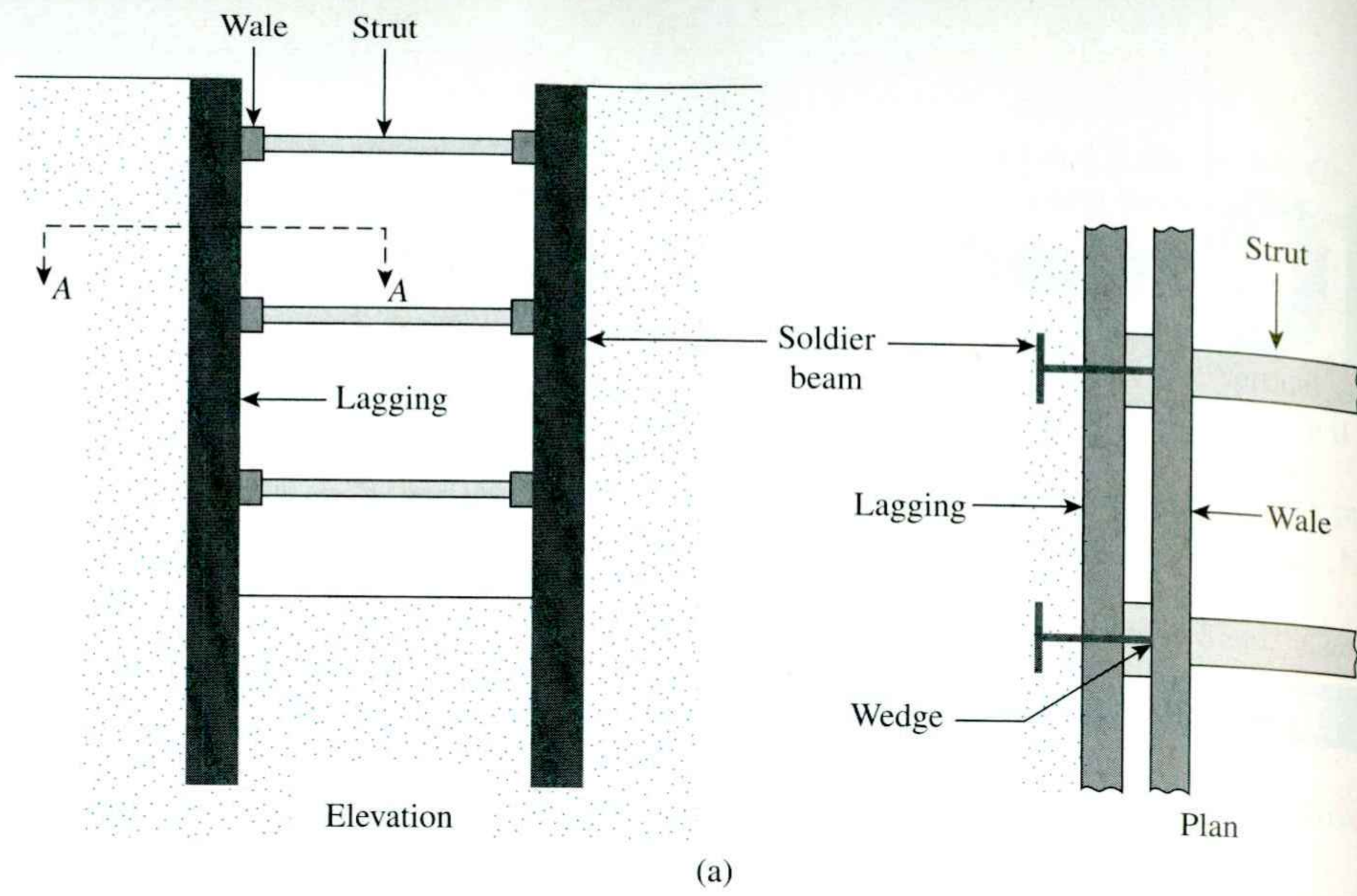
10.1 Introduction

Sometimes construction work requires ground excavations with vertical or near-vertical faces—for example, basements of buildings in developed areas or underground transportation facilities at shallow depths below the ground surface (a cut-and-cover type of construction). The vertical faces of the cuts need to be protected by temporary bracing systems to avoid failure that may be accompanied by considerable settlement or by bearing capacity failure of nearby foundations.

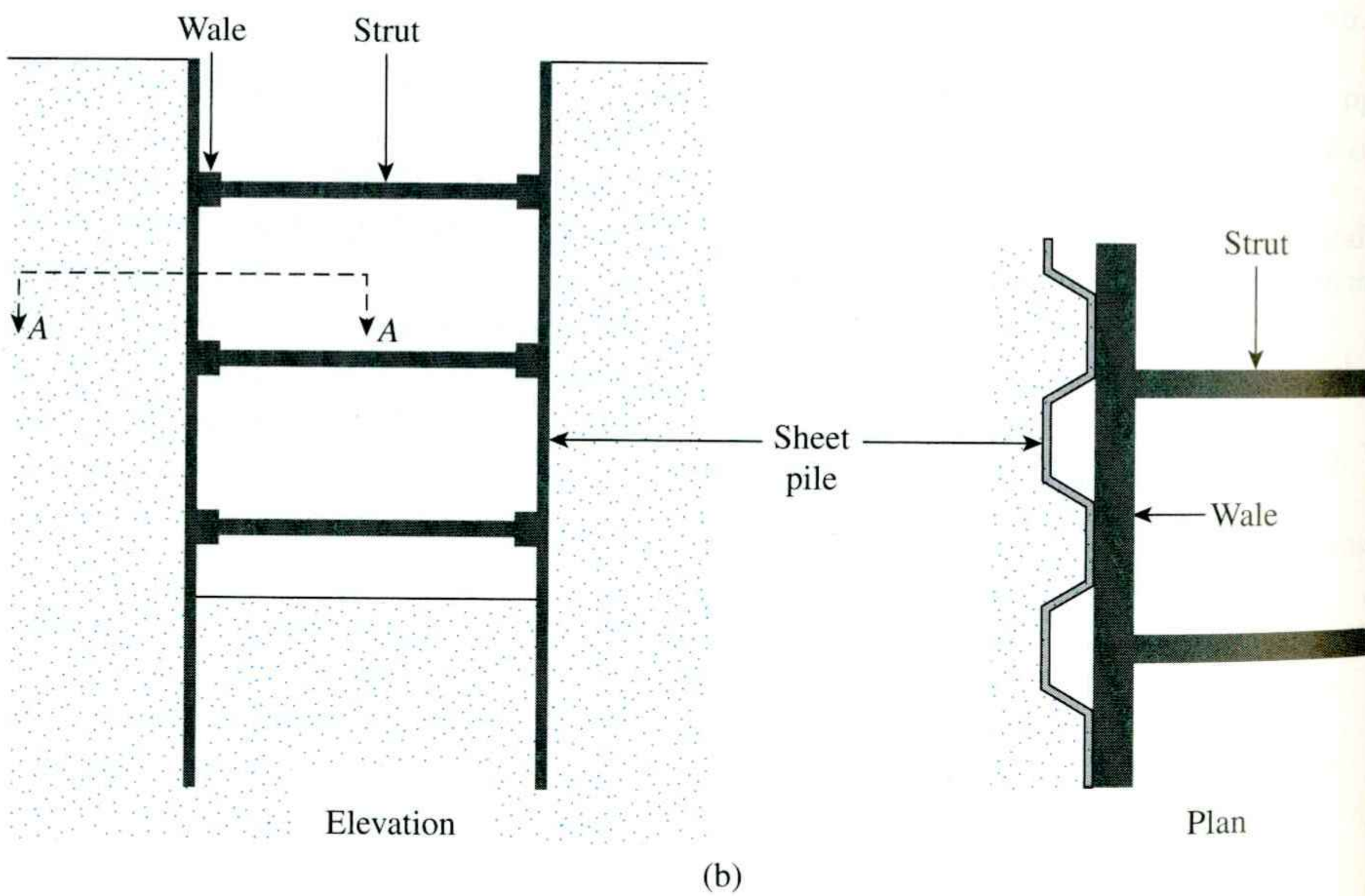
Figure 10.1 shows two types of braced cut commonly used in construction work. One type uses the *soldier beam* (Figure 10.1a), which is driven into the ground before excavation and is a vertical steel or timber beam. *Laggings*, which are horizontal timber planks, are placed between soldier beams as the excavation proceeds. When the excavation reaches the desired depth, *wales* and *struts* (horizontal steel beams) are installed. The struts are compression members. Figure 10.1b shows another type of braced excavation. In this case, interlocking *sheet piles* are driven into the soil before excavation. Wales and struts are inserted immediately after excavation reaches the appropriate depth.

Figure 10.2 shows the braced-cut construction used for the Chicago subway in 1940. Timber lagging, timber struts, and steel wales were used. Figure 10.3 shows a braced cut made during the construction of the Washington, DC, metro in 1974. In this cut, timber lagging, steel H-soldier piles, steel wales, and pipe struts were used.

To design braced excavations (i.e., to select wales, struts, sheet piles, and soldier beams), an engineer must estimate the lateral earth pressure to which the braced cuts will be subjected. The theoretical aspects of the lateral earth pressure on a braced cut were discussed in Section 7.8. The total active force per unit length of the wall (P_a) was calculated using the general wedge theory. However, that analysis does not provide the relationships required for estimating the variation of lateral pressure with depth, which is a function of several factors, such as the type of soil, the experience of the construction crew, the type of construction equipment used, and so forth. For that reason, empirical pressure envelopes developed from field observations are used for the design of braced cuts. This procedure is discussed in the next section.



(a)



(b)

Figure 10.1 Types of braced cut: (a) use of soldier beams; (b) use of sheet piles

10.2

Pressure Envelope for Braced-Cut Design

As mentioned in Section 10.1, the lateral earth pressure in a braced cut is dependent on the type of soil, construction method, and type of equipment used. The lateral earth pressure changes from place to place. Each strut should also be designed for the maximum load to

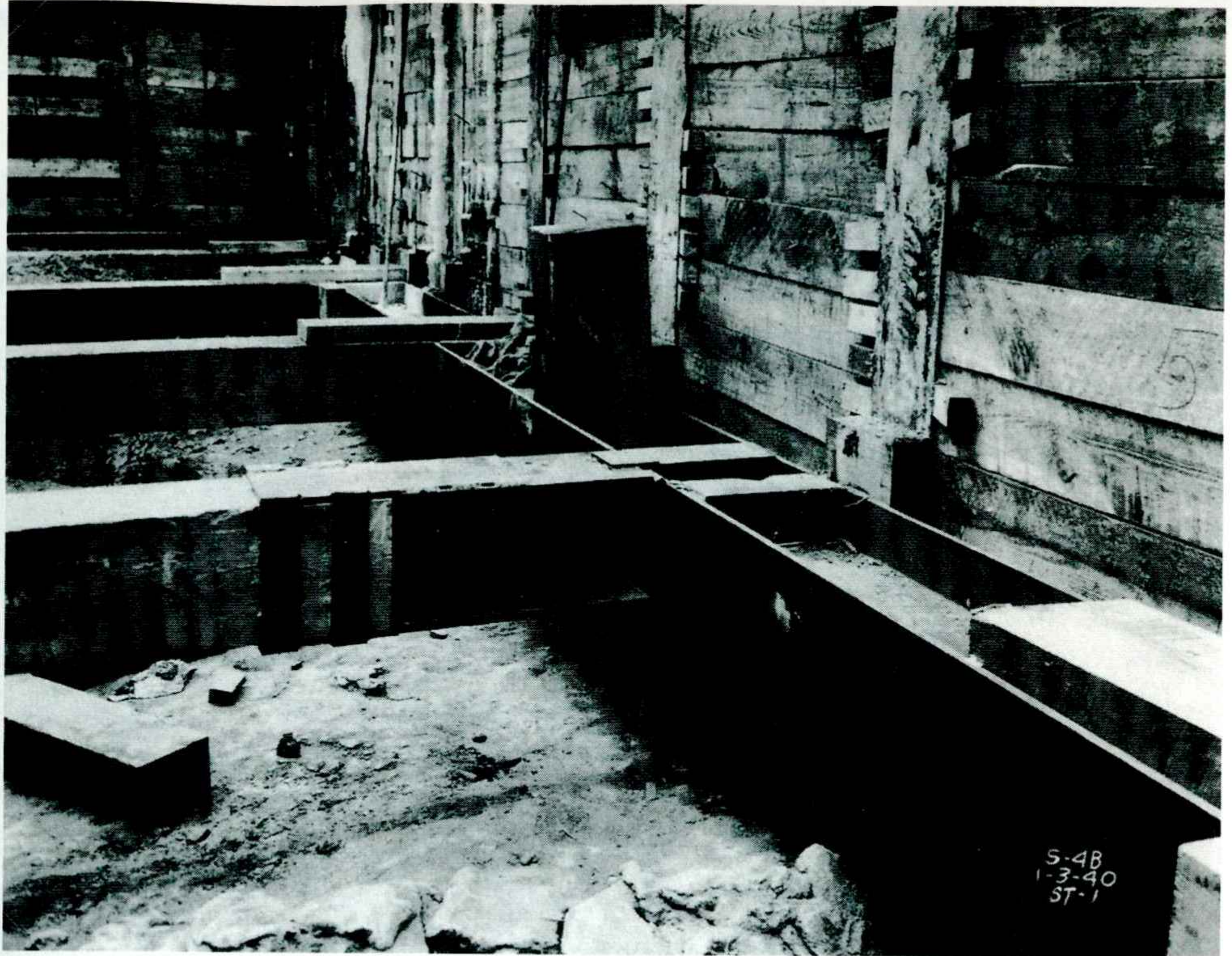


Figure 10.2 Braced cut in Chicago Subway construction, January 1940 (Courtesy of Ralph B. Peck)

which it may be subjected. Therefore, the braced cuts should be designed using apparent-pressure diagrams that are envelopes of all the pressure diagrams determined from measured strut loads in the field. Figure 10.4 shows the method for obtaining the apparent-pressure diagram at a section from strut loads. In this figure, let $P_1, P_2, P_3, P_4, \dots$ be the measured strut loads. The apparent horizontal pressure can then be calculated as

$$\sigma_1 = \frac{P_1}{(s) \left(d_1 + \frac{d_2}{2} \right)}$$

$$\sigma_2 = \frac{P_2}{(s) \left(\frac{d_2}{2} + \frac{d_3}{2} \right)}$$

$$\sigma_3 = \frac{P_3}{(s) \left(\frac{d_3}{2} + \frac{d_4}{2} \right)}$$

$$\sigma_4 = \frac{P_4}{(s) \left(\frac{d_4}{2} + \frac{d_5}{2} \right)}$$

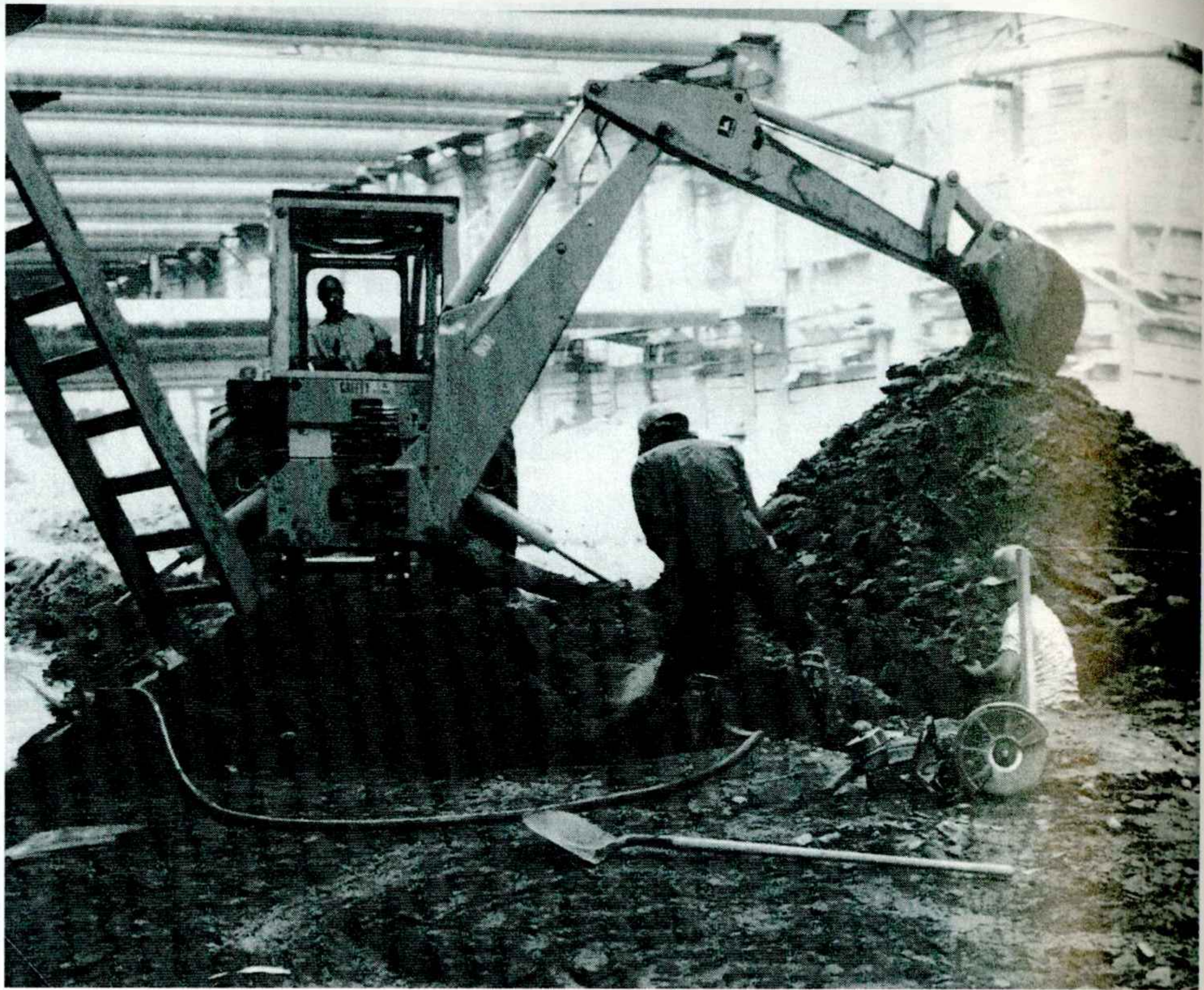


Figure 10.3 Braced cut in the construction of Washington, DC Metro, May 1974 (Courtesy of Ralph B. Peck)

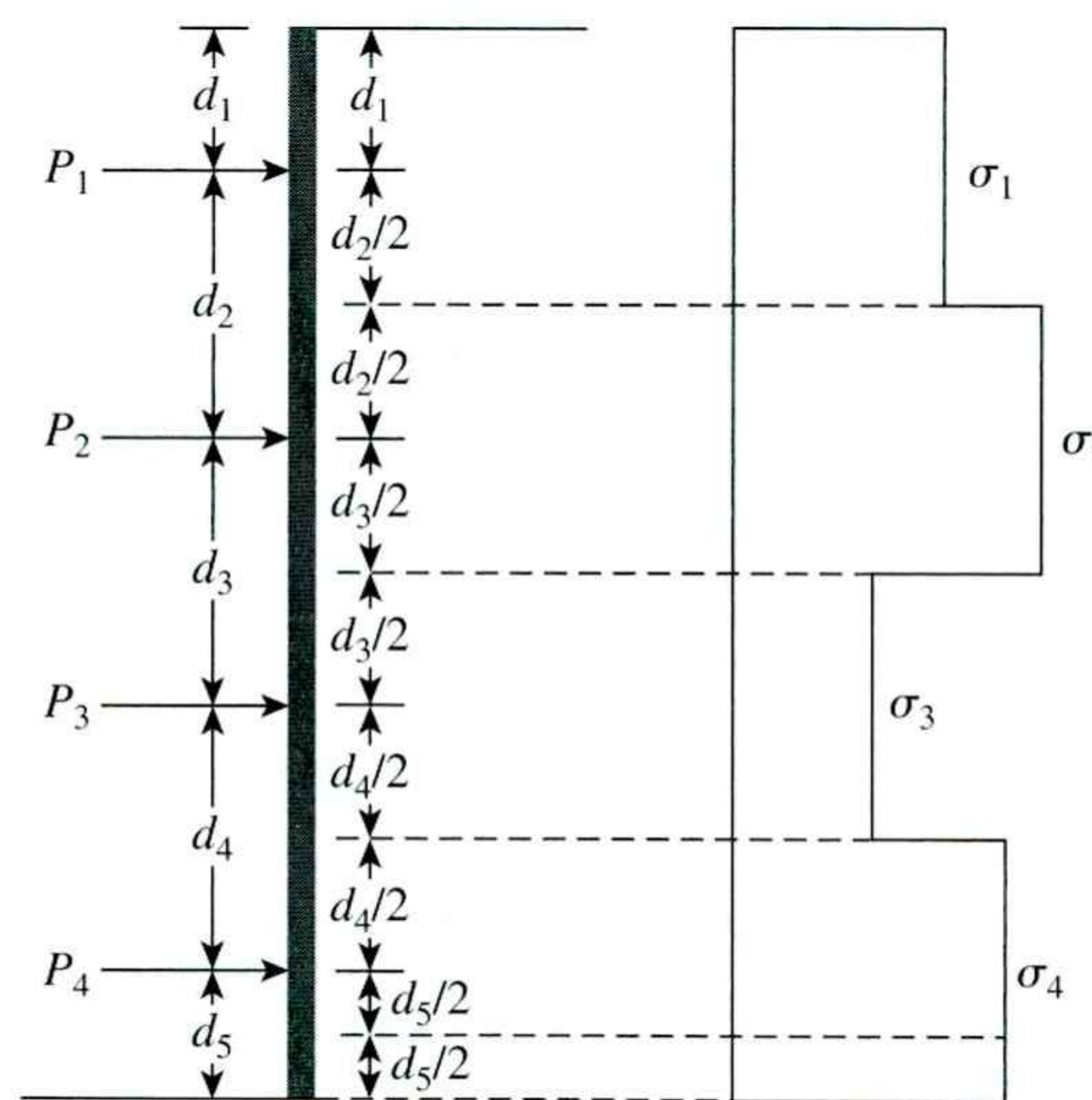


Figure 10.4 Procedure for calculating apparent-pressure diagram from measured strut loads

where

$\sigma_1, \sigma_2, \sigma_3, \sigma_4$ = apparent pressures

s = center-to-center spacing of the struts

Using the procedure just described for strut loads observed from the Berlin subway cut, Munich subway cut, and New York subway cut, Peck (1969) provided the envelope of apparent-lateral-pressure diagrams for design of cuts in *sand*. This envelope is illustrated in Figure 10.5, in which

$$\sigma_a = 0.65\gamma HK_a \quad (10.1)$$

where

γ = unit weight

H = height of the cut

K_a = Rankine active pressure coefficient = $\tan^2(45 - \phi'/2)$

ϕ' = effective friction angle of sand

Cuts in Clay

In a similar manner, Peck (1969) also provided the envelopes of apparent-lateral-pressure diagrams for cuts in *soft to medium clay* and in *stiff clay*. The pressure envelope for soft to medium clay is shown in Figure 10.6 and is applicable to the condition

$$\frac{\gamma H}{c} > 4$$

where c = undrained cohesion ($\phi = 0$).

The pressure, σ_a , is the larger of

$$\sigma_a = \gamma H \left[1 - \left(\frac{4c}{\gamma H} \right) \right] \quad \text{and} \quad \sigma_a = 0.3\gamma H \quad (10.2)$$

where γ = unit weight of clay.

The pressure envelope for cuts in stiff clay is shown in Figure 10.7, in which

$$\sigma_a = 0.2\gamma H \text{ to } 0.4\gamma H \quad (\text{with an average of } 0.3\gamma H) \quad (10.3)$$

is applicable to the condition $\gamma H/c \leq 4$.

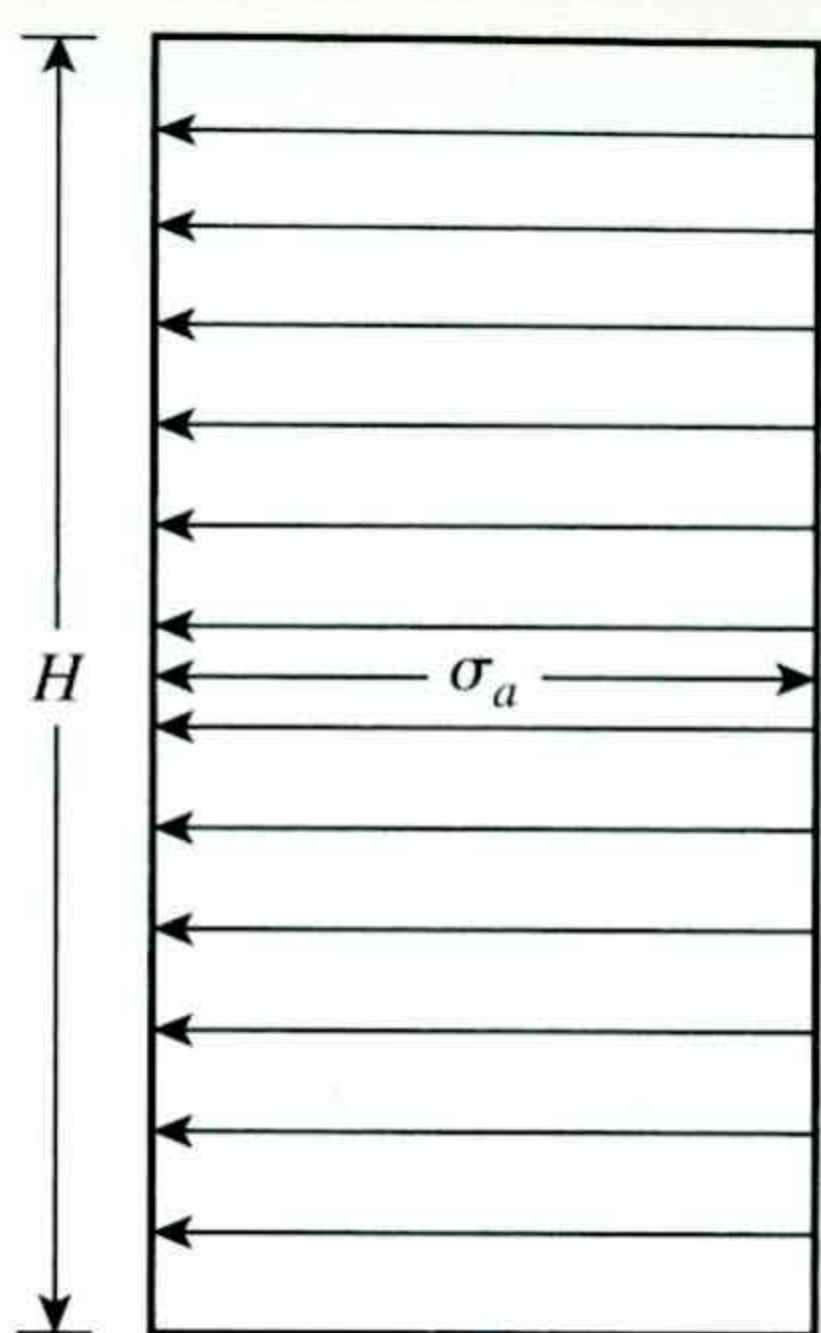


Figure 10.5 Peck's (1969) apparent-pressure envelope for cuts in sand

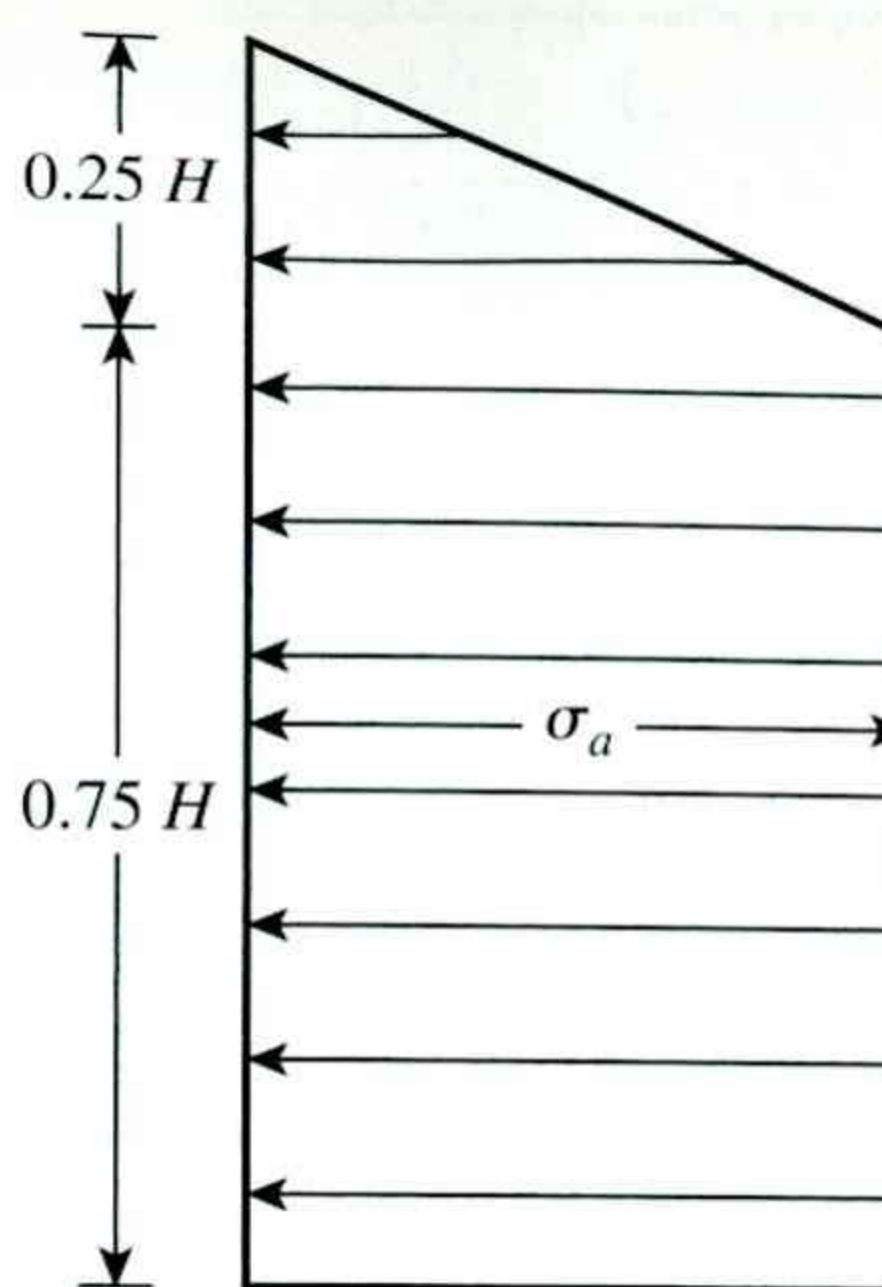


Figure 10.6 Peck's (1969) apparent-pressure envelope for cuts in soft to medium clay

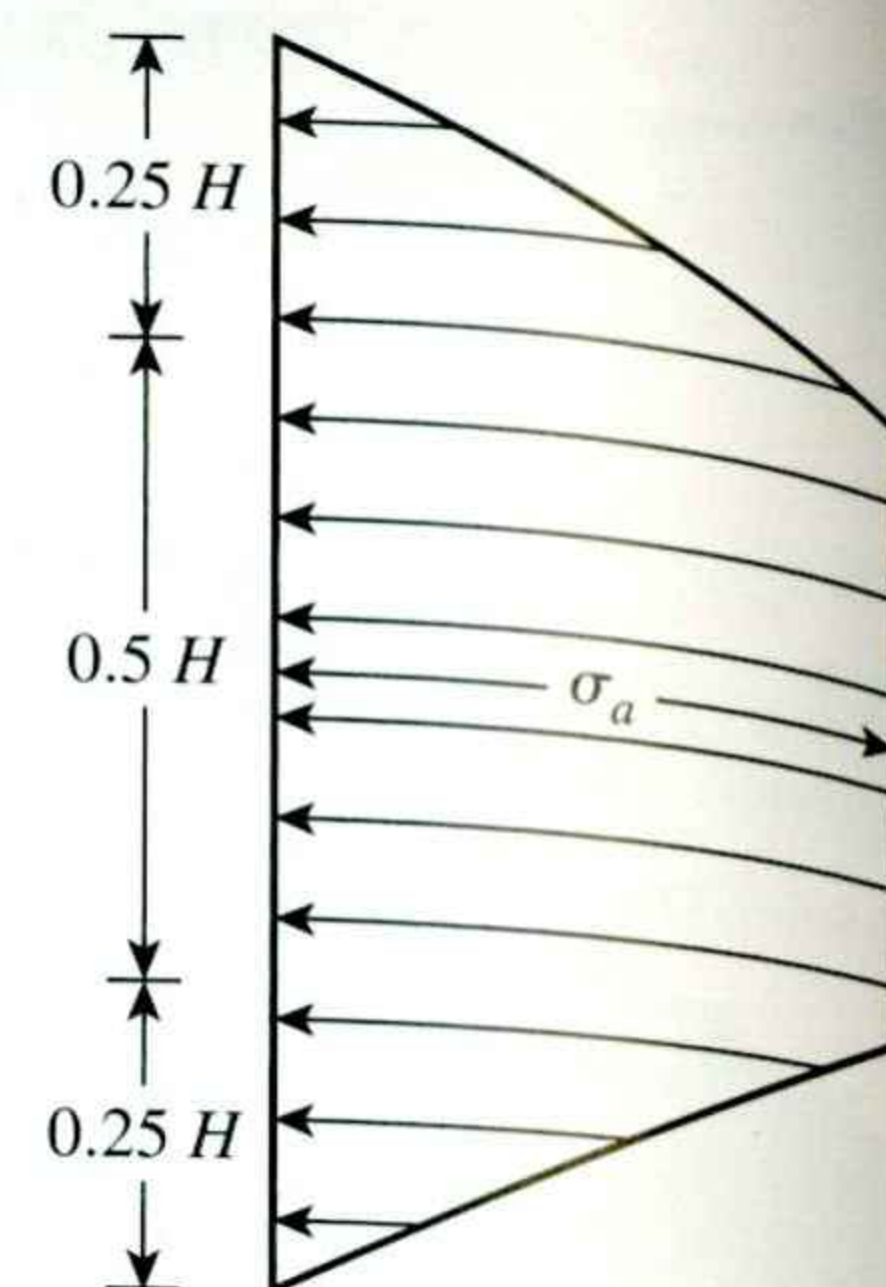


Figure 10.7 Peck's (1969) apparent-pressure envelope for cuts in stiff clay

When using the pressure envelopes just described, keep the following points in mind:

1. They apply to excavations having depths greater than about 6 m (≈ 20 ft).
2. They are based on the assumption that the water table is below the bottom of the cut.
3. Sand is assumed to be drained with zero pore water pressure.
4. Clay is assumed to be undrained and pore water pressure is not considered.

10.3

Pressure Envelope for Cuts in Layered Soil

Sometimes, layers of both sand and clay are encountered when a braced cut is being constructed. In this case, Peck (1943) proposed that an equivalent value of cohesion ($\phi = 0$) should be determined according to the formula (see Figure 10.8a).

$$c_{av} = \frac{1}{2H} [\gamma_s K_s H_s^2 \tan \phi'_s + (H - H_s) n' q_u] \quad (10.4)$$

where

H = total height of the cut

γ_s = unit weight of sand

H_s = height of the sand layer

K_s = a lateral earth pressure coefficient for the sand layer (≈ 1)

ϕ'_s = effective angle of friction of sand

q_u = unconfined compression strength of clay

n' = a coefficient of progressive failure (ranging from 0.5 to 1.0; average value 0.75)

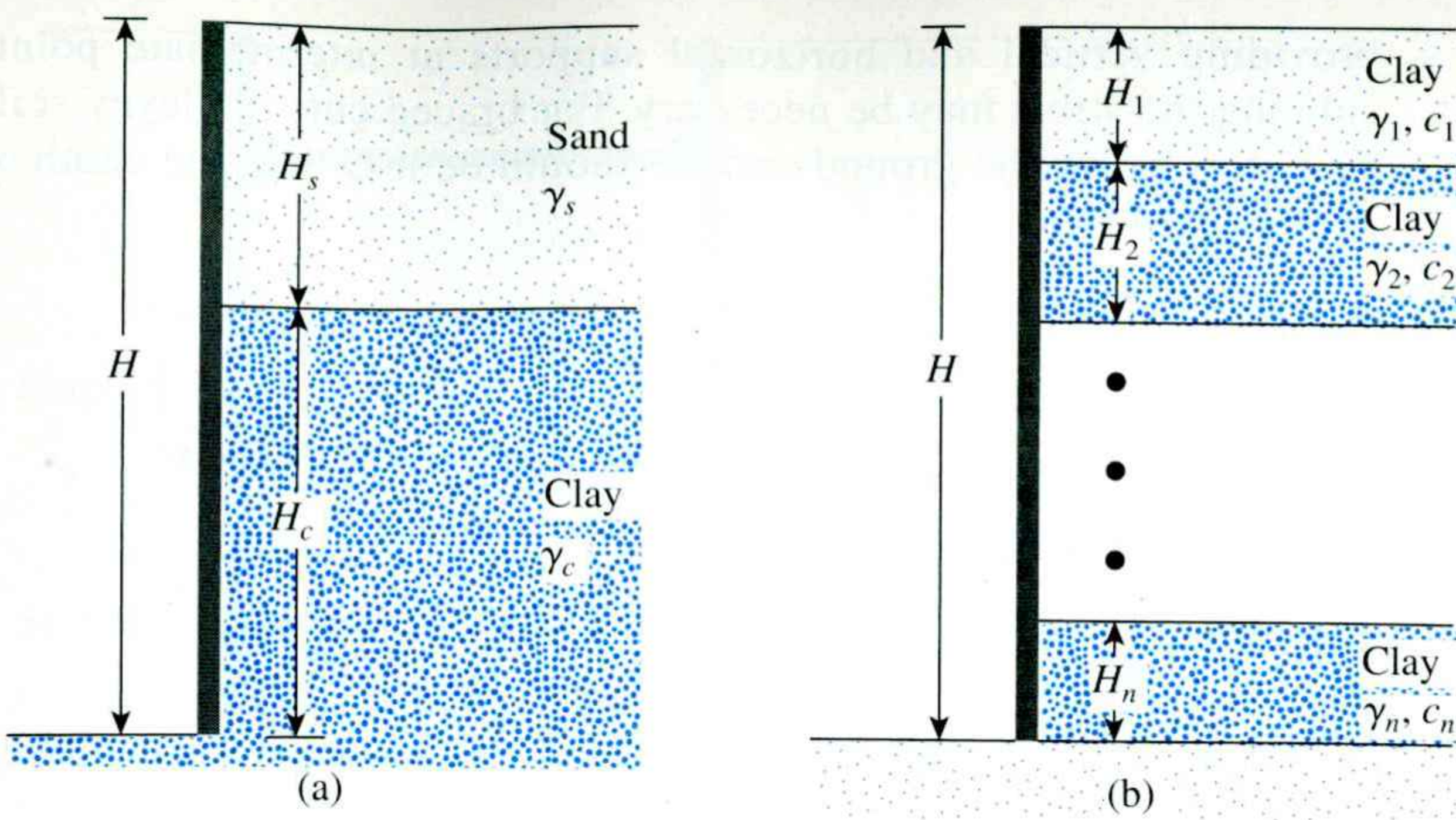


Figure 10.8 Layered soils in braced cuts

The average unit weight of the layers may be expressed as

$$\gamma_a = \frac{1}{H} [\gamma_s H_s + (H - H_s) \gamma_c] \quad (10.5)$$

where γ_c = saturated unit weight of clay layer.

Once the average values of cohesion and unit weight are determined, the pressure envelopes in clay can be used to design the cuts.

Similarly, when several clay layers are encountered in the cut (Figure 10.8b), the average undrained cohesion becomes

$$c_{av} = \frac{1}{H} (c_1 H_1 + c_2 H_2 + \dots + c_n H_n) \quad (10.6)$$

where

c_1, c_2, \dots, c_n = undrained cohesion in layers 1, 2, ..., n

H_1, H_2, \dots, H_n = thickness of layers 1, 2, ..., n

The average unit weight is now

$$\gamma_a = \frac{1}{H} (\gamma_1 H_1 + \gamma_2 H_2 + \gamma_3 H_3 + \dots + \gamma_n H_n) \quad (10.7)$$

10.4

Design of Various Components of a Braced Cut

Struts

In construction work, struts should have a minimum vertical spacing of about 2.75 m (9 ft) or more. Struts are horizontal columns subject to bending. The load-carrying capacity of columns depends on their *slenderness ratio*, which can be reduced by

providing vertical and horizontal supports at intermediate points. For wide cuts, splicing the struts may be necessary. For braced cuts in clayey soils, the depth of the first strut below the ground surface should be less than the depth of tensile crack, z_c . From Eq. (7.8),

$$\sigma'_a = \gamma z K_a - 2c' \sqrt{K_a}$$

where K_a = coefficient of Rankine active pressure.

For determining the depth of tensile crack,

$$\sigma'_a = 0 = \gamma z_c K_a - 2c' \sqrt{K_a}$$

or

$$z_c = \frac{2c'}{\sqrt{K_a \gamma}}$$

With $\phi = 0$, $K_a = \tan^2(45 - \phi/2) = 1$, so

$$z_c = \frac{2c}{\gamma}$$

A simplified conservative procedure may be used to determine the strut loads. Although this procedure will vary, depending on the engineers involved in the project, the following is a step-by-step outline of the general methodology (see Figure 10.9):

- Step 1.* Draw the pressure envelope for the braced cut. (See Figures 10.5, 10.6, and 10.7.) Also, show the proposed strut levels. Figure 10.9a shows a pressure envelope for a sandy soil; however, it could also be for a clay. The strut levels are marked *A*, *B*, *C*, and *D*. The sheet piles (or soldier beams) are assumed to be hinged at the strut levels, except for the top and bottom ones. In Figure 10.9a, the hinges are at the level of struts *B* and *C*. (Many designers also assume the sheet piles or soldier beams to be hinged at all strut levels except for the top.)
- Step 2.* Determine the reactions for the two simple cantilever beams (top and bottom) and all the simple beams between. In Figure 10.9b, these reactions are *A*, B_1 , B_2 , C_1 , C_2 , and *D*.
- Step 3.* The strut loads in the figure may be calculated via the formulas

$$\begin{aligned} P_A &= (A)(s) \\ P_B &= (B_1 + B_2)(s) \\ P_C &= (C_1 + C_2)(s) \end{aligned} \tag{10.8}$$

and

$$P_D = (D)(s)$$

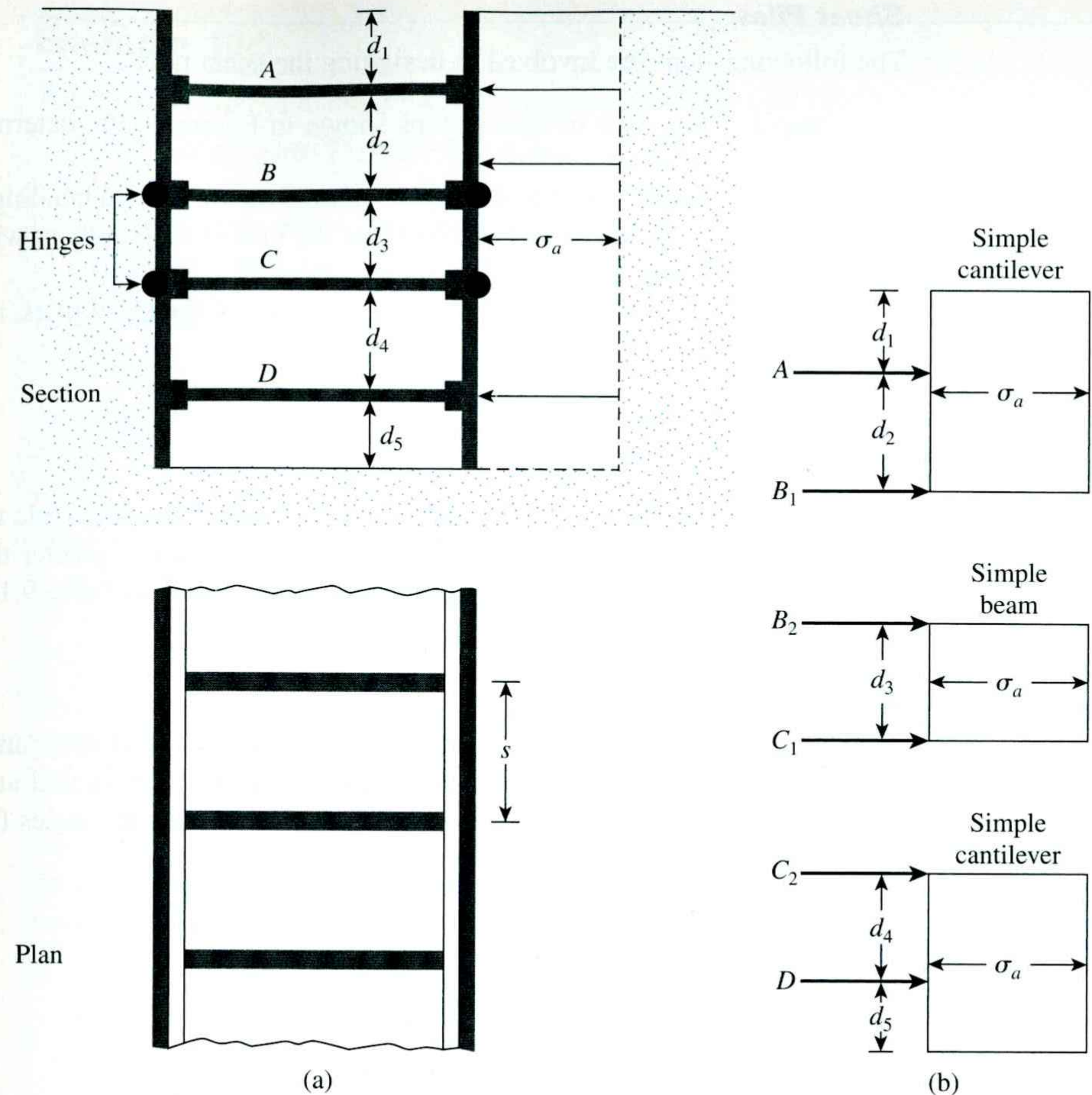


Figure 10.9 Determination of strut loads: (a) section and plan of the cut; (b) method for determining strut loads

where

P_A, P_B, P_C, P_D = loads to be taken by the individual struts at levels A, B, C, and D, respectively

A, B_1, B_2, C_1, C_2, D = reactions calculated in Step 2 (note the unit: force/unit length of the braced cut)

s = horizontal spacing of the struts (see plan in Figure 10.9a)

Step 4. Knowing the strut loads at each level and the intermediate bracing conditions allows selection of the proper sections from the steel construction manual.

Sheet Piles

The following steps are involved in designing the sheet piles:

- Step 1.* For each of the sections shown in Figure 10.9b, determine the maximum bending moment.
- Step 2.* Determine the maximum value of the maximum bending moments (M_{\max}) obtained in Step 1. Note that the unit of this moment will be, for example, kN-m/m (lb-ft/ft) length of the wall.
- Step 3.* Obtain the required section modulus of the sheet piles, namely,

$$S = \frac{M_{\max}}{\sigma_{\text{all}}} \quad (10.9)$$

where σ_{all} = allowable flexural stress of the sheet pile material.

- Step 4.* Choose a sheet pile having a section modulus greater than or equal to the required section modulus from a table such as Table 9.1.

Wales

Wales may be treated as continuous horizontal members if they are spliced properly. Conservatively, they may also be treated as though they are pinned at the struts. For the section shown in Figure 10.9a, the maximum moments for the wales (assuming that they are pinned at the struts) are,

$$\text{At level } A, \quad M_{\max} = \frac{(A)(s^2)}{8}$$

$$\text{At level } B, \quad M_{\max} = \frac{(B_1 + B_2)s^2}{8}$$

$$\text{At level } C, \quad M_{\max} = \frac{(C_1 + C_2)s^2}{8}$$

and

$$\text{At level } D, \quad M_{\max} = \frac{(D)(s^2)}{8}$$

where A, B_1, B_2, C_1, C_2 , and D are the reactions under the struts per unit length of the wall (see Step 2 of strut design).

Now determine the section modulus of the wales:

$$S = \frac{M_{\max}}{\sigma_{\text{all}}}$$

The wales are sometimes fastened to the sheet piles at points that satisfy the lateral support requirements.

Example 10.1

The cross section of a long braced cut is shown in Figure 10.10a.

- a. Draw the earth-pressure envelope.
- b. Determine the strut loads at levels A, B, and C.
- c. Determine the section modulus of the sheet pile section required.
- d. Determine a design section modulus for the wales at level B.

(Note: The struts are placed at 3 m, center to center, in the plan.) Use

$$\sigma_{\text{all}} = 170 \times 10^3 \text{ kN/m}^2$$

Solution

Part a

We are given that $\gamma = 18 \text{ kN/m}^2$, $c = 35 \text{ kN/m}^2$, and $H = 7 \text{ m}$. So,

$$\frac{\gamma H}{c} = \frac{(18)(7)}{35} = 3.6 < 4$$

Thus, the pressure envelope will be like the one in Figure 10.7. The envelope is plotted in Figure 10.10a with maximum pressure intensity, σ_a , equal to $0.3\gamma H = 0.3(18)(7) = 37.8 \text{ kN/m}^2$.

Part b

To calculate the strut loads, examine Figure 10.10b. Taking the moment about B_1 , we have $\Sigma M_{B_1} = 0$, and

$$A(2.5) - \left(\frac{1}{2}\right)(37.8)(1.75)\left(1.75 + \frac{1.75}{3}\right) - (1.75)(37.8)\left(\frac{1.75}{2}\right) = 0$$

or

$$A = 54.02 \text{ kN/m}$$

Also, Σ vertical forces = 0. Thus,

$$\frac{1}{2}(1.75)(37.8) + (37.8)(1.75) = A + B_1$$

or

$$33.08 + 66.15 - A = B_1$$

So,

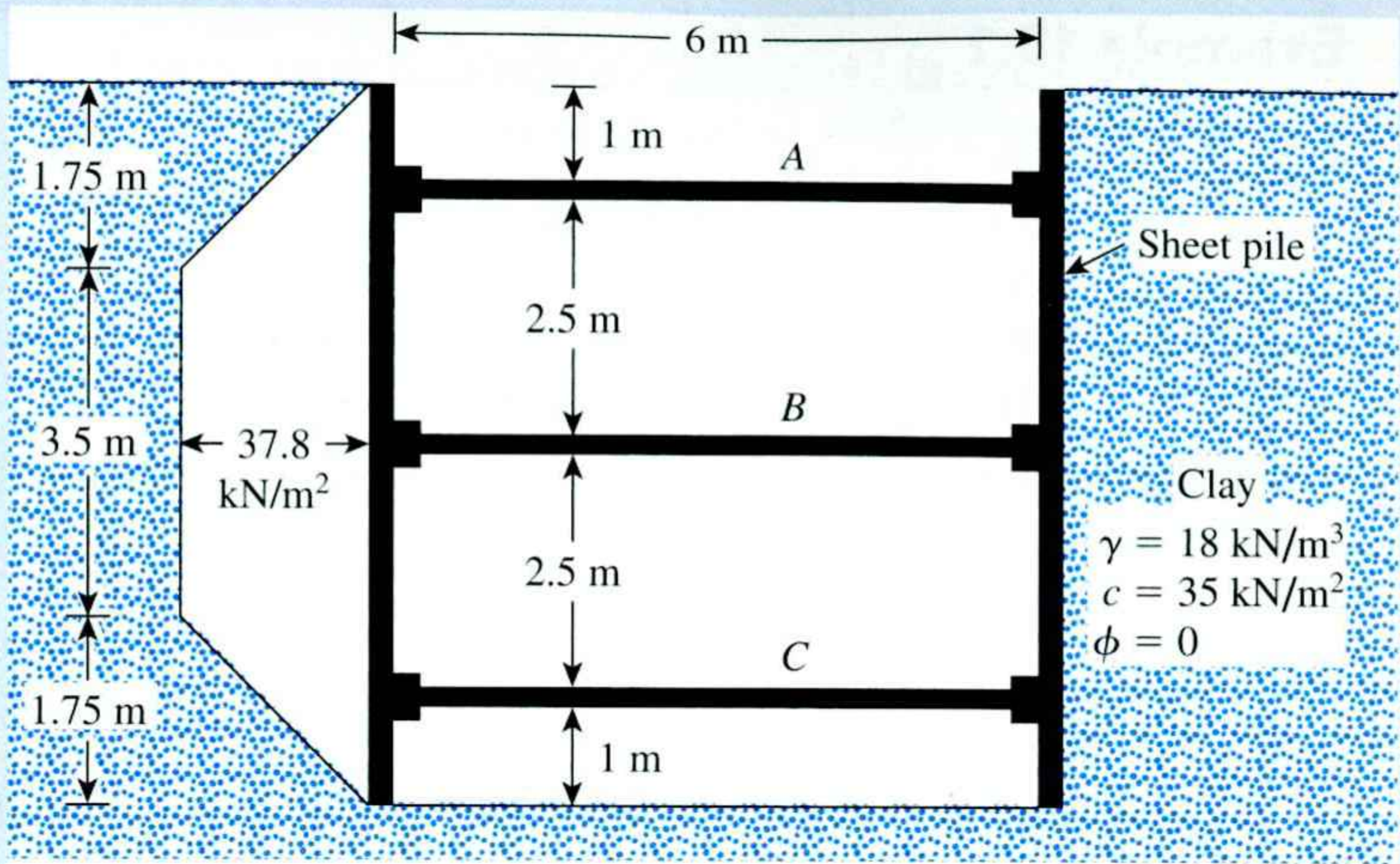
$$B_1 = 45.2 \text{ kN/m}$$

Due to symmetry,

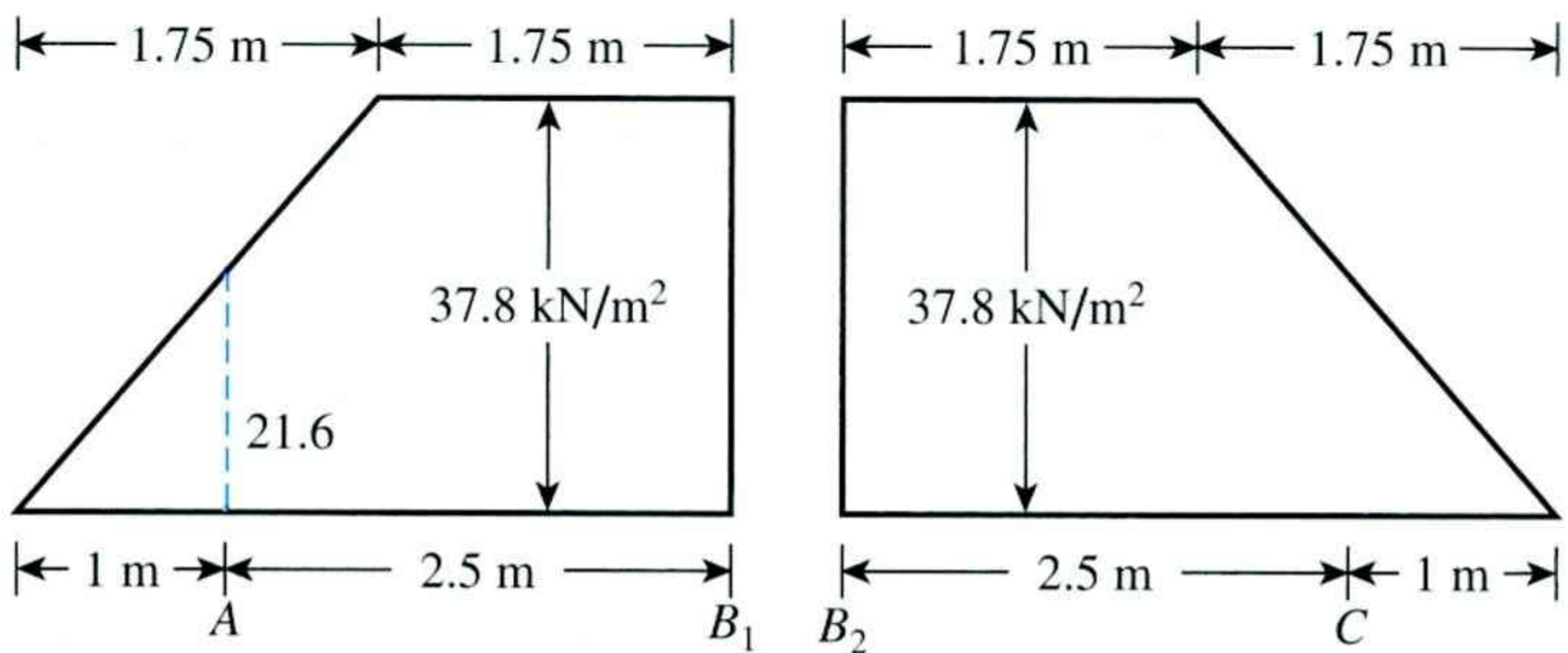
$$B_2 = 45.2 \text{ kN/m}$$

and

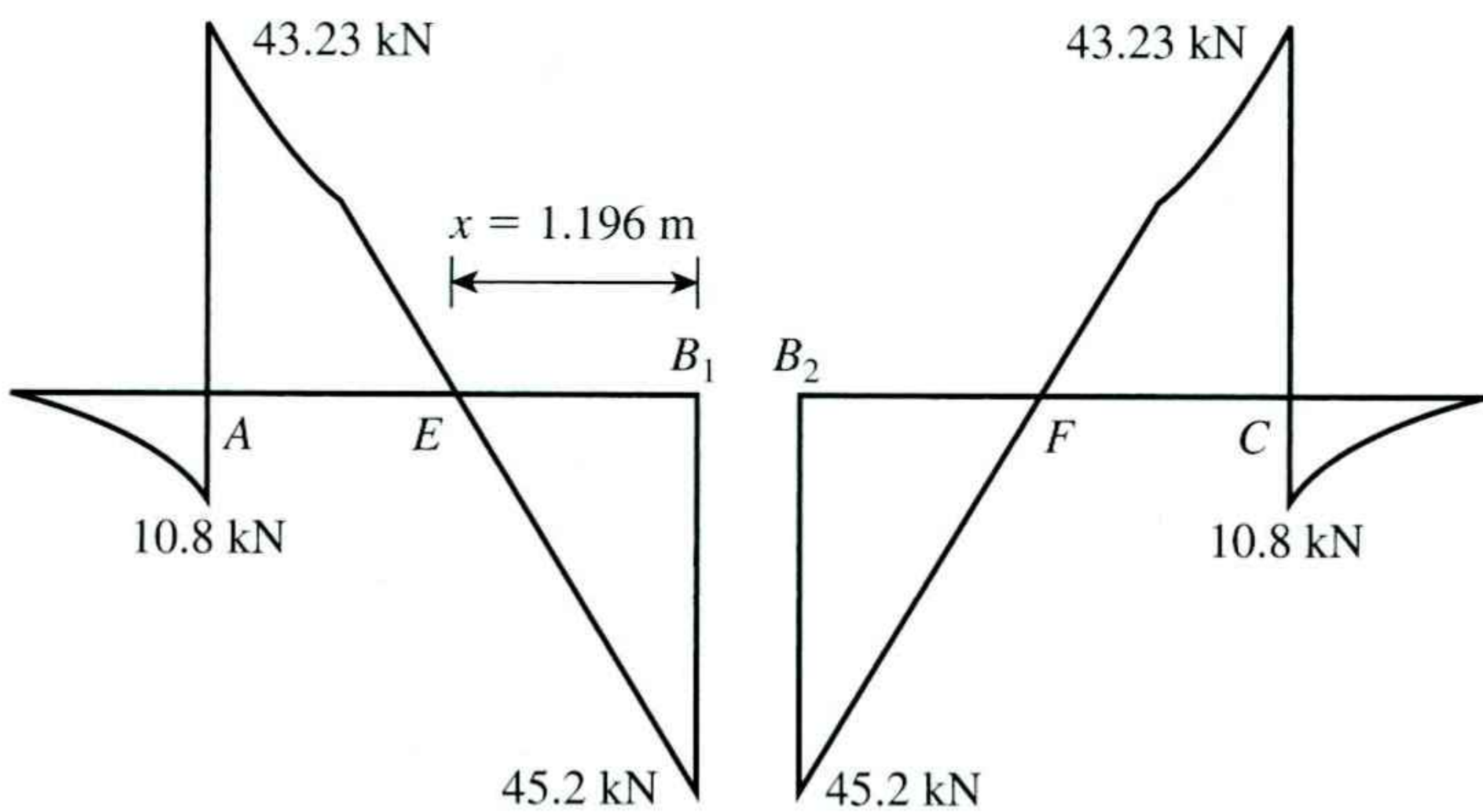
$$C = 54.02 \text{ kN/m}$$



(a) Cross section



(b) Determination of reaction



(c) Shear force diagram

Figure 10.10 Analysis of a braced cut

Hence, the strut loads at the levels indicated by the subscripts are

$$P_A = 54.02 \times \text{horizontal spacing}, s = 54.02 \times 3 = \mathbf{162.06 \text{ kN}}$$

$$P_B = (B_1 + B_2)3 = (45.2 + 45.2)3 = \mathbf{271.2 \text{ kN}}$$

and

$$P_C = 54.02 \times 3 = \mathbf{162.06 \text{ kN}}$$

Part c

At the left side of Figure 10.10b, for the maximum moment, the shear force should be zero. The nature of the variation of the shear force is shown in Figure 10.10c. The location of point E can be given as

$$x = \frac{\text{reaction at } B_1}{37.8} = \frac{45.2}{37.8} = 1.196 \text{ m}$$

Also,

$$\begin{aligned} \text{Magnitude of moment at } A &= \frac{1}{2}(1)\left(\frac{37.8}{1.75} \times 1\right)\left(\frac{1}{3}\right) \\ &= 3.6 \text{ kN-m/meter of wall} \end{aligned}$$

and

$$\begin{aligned} \text{Magnitude of moment at } E &= (45.2 \times 1.196) - (37.8 \times 1.196)\left(\frac{1.196}{2}\right) \\ &= 54.06 - 27.03 = 27.03 \text{ kN-m/meter of wall} \end{aligned}$$

Because the loading on the left and right sections of Figure 10.10b are the same, the magnitudes of the moments at F and C (see Figure 10.10c) will be the same as those at E and A, respectively. Hence, the maximum moment is 27.03 kN-m/meter of wall.

The section modulus of the sheet piles is thus

$$S = \frac{M_{\max}}{\sigma_{\text{all}}} = \frac{27.03 \text{ kN-m}}{170 \times 10^3 \text{ kN/m}^2} = \mathbf{15.9 \times 10^{-5} \text{ m}^3/\text{m of the wall}}$$

Part d

The reaction at level B has been calculated in part b. Hence,

$$M_{\max} = \frac{(B_1 + B_2)s^2}{8} = \frac{(45.2 + 45.2)3^2}{8} = 101.7 \text{ kN-m}$$

and

$$\begin{aligned} \text{Section modulus, } S &= \frac{101.7}{\sigma_{\text{all}}} = \frac{101.7}{(170 \times 1000)} \\ &= \mathbf{0.598 \times 10^{-3} \text{ m}^3} \end{aligned}$$

Example 10.2

Refer to the braced cut shown in Figure 10.11, for which $\gamma = 17 \text{ kN/m}^3$, $\phi' = 35^\circ$, and $c' = 0$. The struts are located 4 m on center in the plan. Draw the earth-pressure envelope and determine the strut loads at levels A, B, and C.

Solution

For this case, the earth-pressure envelope shown in Figure 10.5 is applicable. Hence,

$$K_a = \tan^2 \left(45 - \frac{\phi'}{2} \right) = \tan^2 \left(45 - \frac{35}{2} \right) = 0.271$$

From Equation (10.1)

$$\sigma_a = 0.65 \gamma H K_a = (0.65)(17)(9)(0.271) = 26.95 \text{ kN/m}^2$$

Figure 10.12a shows the pressure envelope. Refer to Figure 10.12b and calculate B_1 :

$$\sum M_{B_1} = 0$$

$$A = \frac{(26.95)(5)\left(\frac{5}{2}\right)}{3} = 112.29 \text{ kN/m}$$

$$B_1 = (26.95)(5) - 112.29 = 22.46 \text{ kN/m}$$

Now, refer to Figure 10.12c and calculate B_2 :

$$\sum M_{B_2} = 0$$

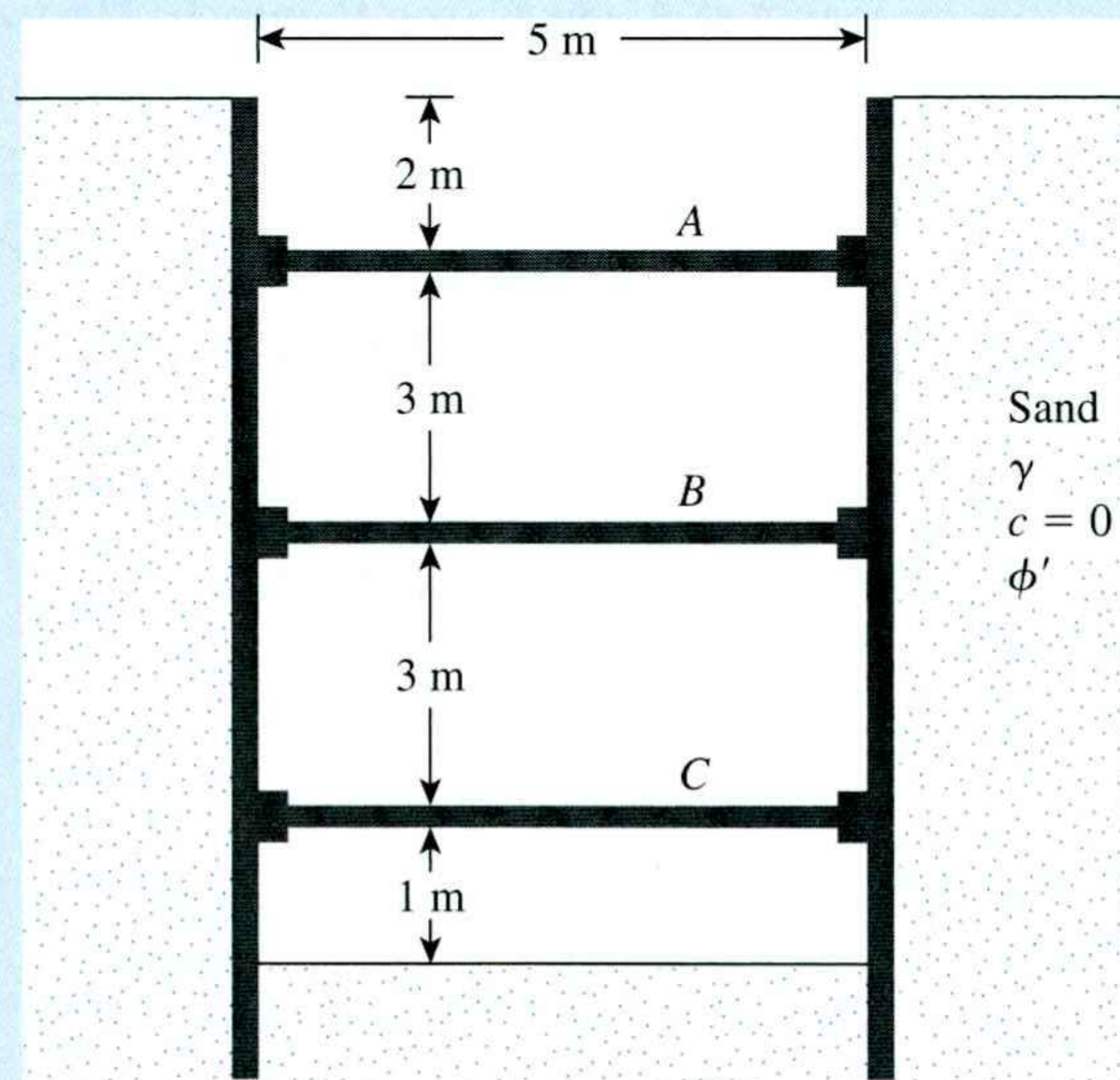


Figure 10.11

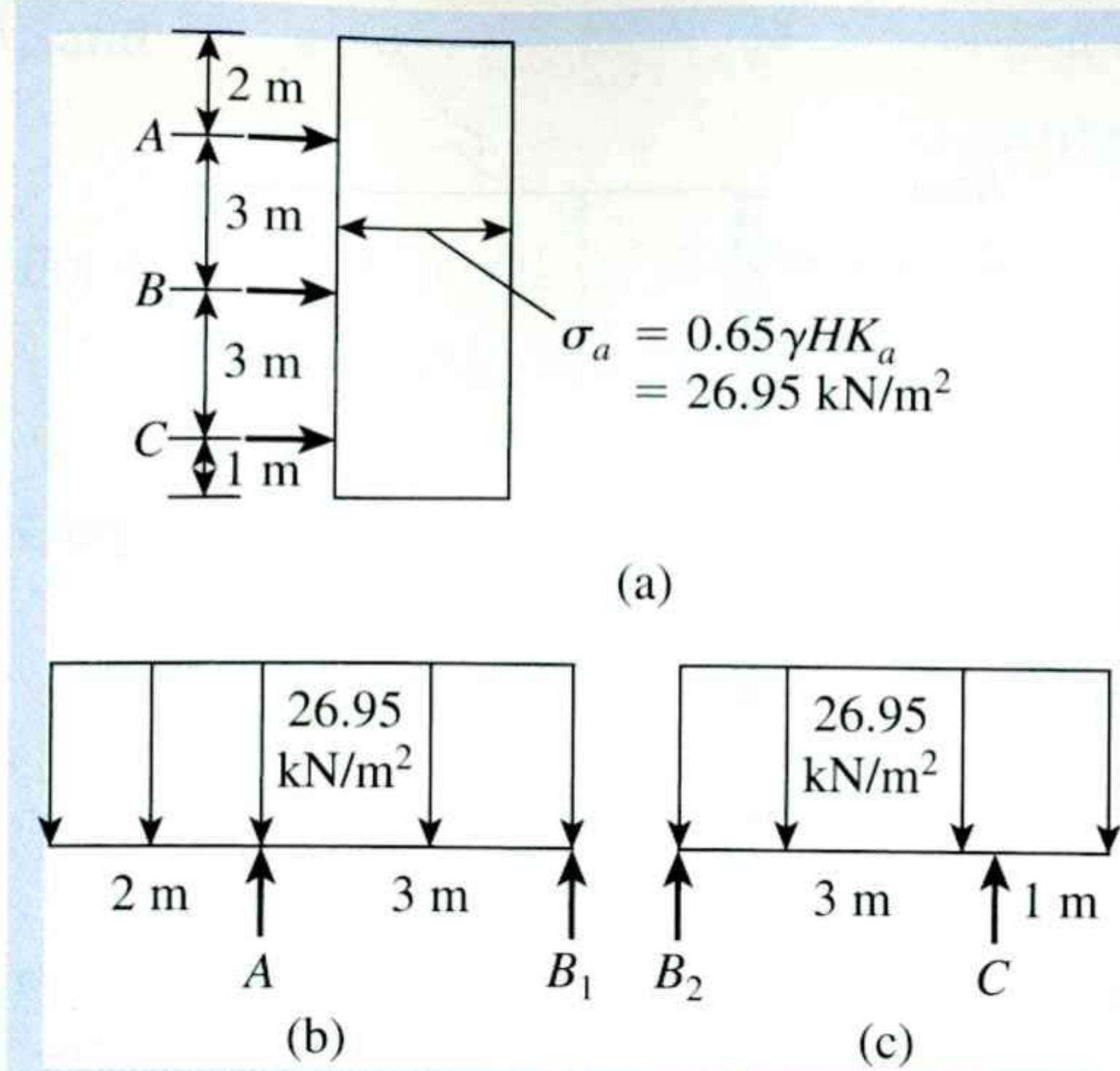


Figure 10.12 Load diagrams

$$C = \frac{(26.95)(4)\left(\frac{4}{2}\right)}{3} = 71.87 \text{ kN/m}$$

$$B_2 = (26.95)(4) - 71.87 = 35.93 \text{ kN/m}$$

The strut loads are

$$\text{At } A, (112.29)(\text{spacing}) = (112.29)(4) = \mathbf{449.16 \text{ kN}}$$

$$\text{At } B, (B_1 + B_2)(\text{spacing}) = (22.46 + 35.93)(4) = \mathbf{233.56 \text{ kN}}$$

$$\text{At } C, (71.87)(\text{spacing}) = (71.87)(4) = \mathbf{287.48 \text{ kN}}$$

10.5

Case Studies of Braced Cuts

The procedure for determining strut loads and the design of sheet piles and wales presented in the preceding sections appears to be fairly straightforward. It is, however, only possible if a proper pressure envelope is chosen for the design, which is difficult. This section describes some case studies of braced cuts and highlights the difficulties and degree of judgment needed for successful completion of various projects.

Subway Extension of the Massachusetts Bay Transportation Authority (MBTA)

Lambe (1970) provided data on the performance of three excavations for the subway extension of the MBTA in Boston (test sections A, B, and D), all of which were well instrumented. Figure 10.13 gives the details of test section B, where the cut was 58 ft, including subsoil conditions. The subsoil consisted of gravel, sand, silt, and clay (fill) to a depth of about 26 ft, followed by a light gray, slightly organic silt to a depth of 46 ft. A layer of coarse sand and gravel with some clay was present from 46 ft to 54 ft below the ground surface. Rock was encountered below 54 ft. The horizontal spacing of the struts was 12 ft center-to-center.

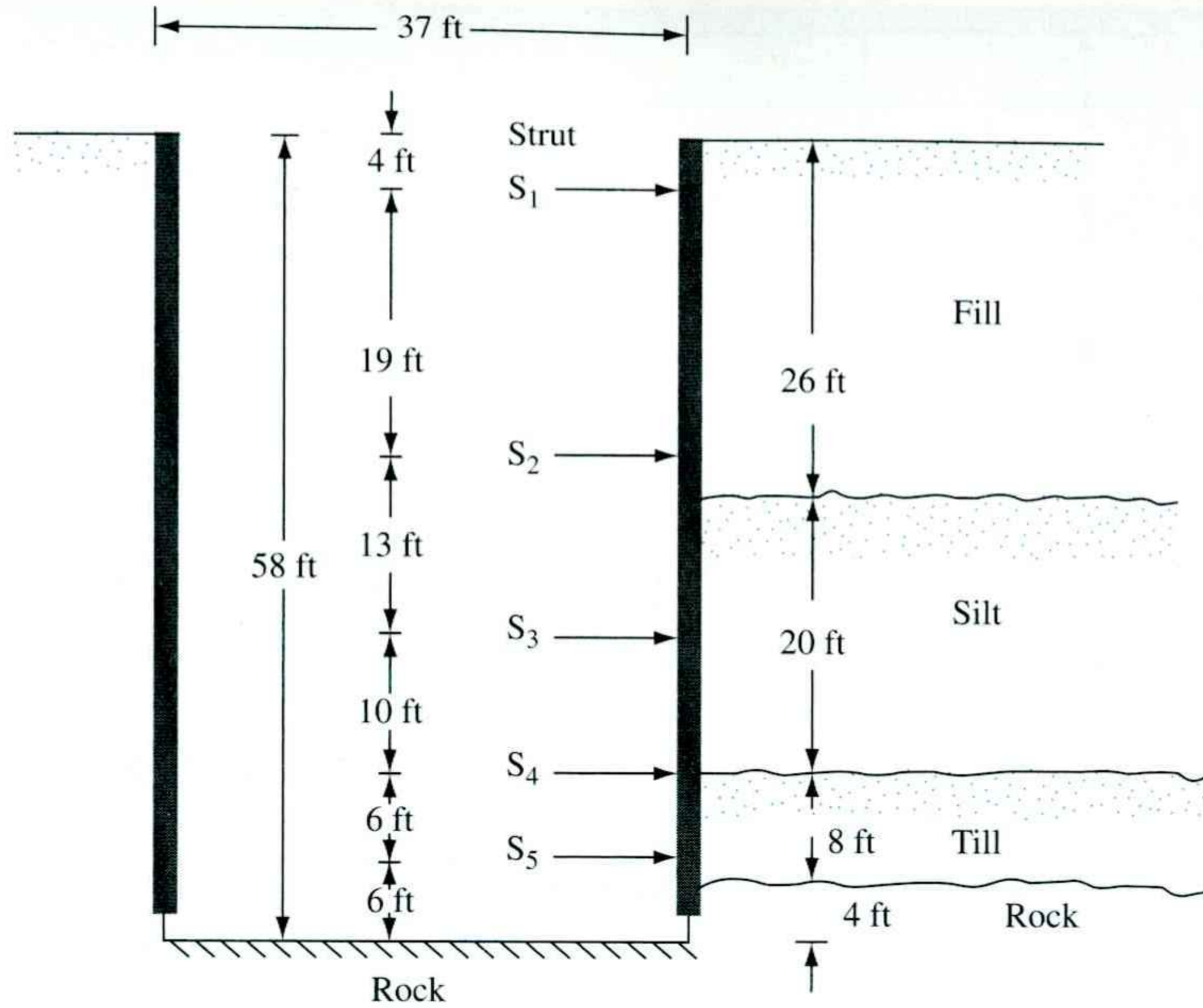


Figure 10.13 Schematic diagram of test section B for subway extension, MTBA

Because the apparent pressure envelopes available (Section 10.2) are for *sand* and *clay* only, questions may arise about how to treat the fill, silt, and till. Figure 10.14 shows the apparent pressure envelopes proposed by Peck (1969), considering the soil as *sand* and also as *clay*, to overcome that problem. For the average soil parameters of the profile, the following values of σ_a were used to develop the pressure envelopes shown in Figure 10.14.

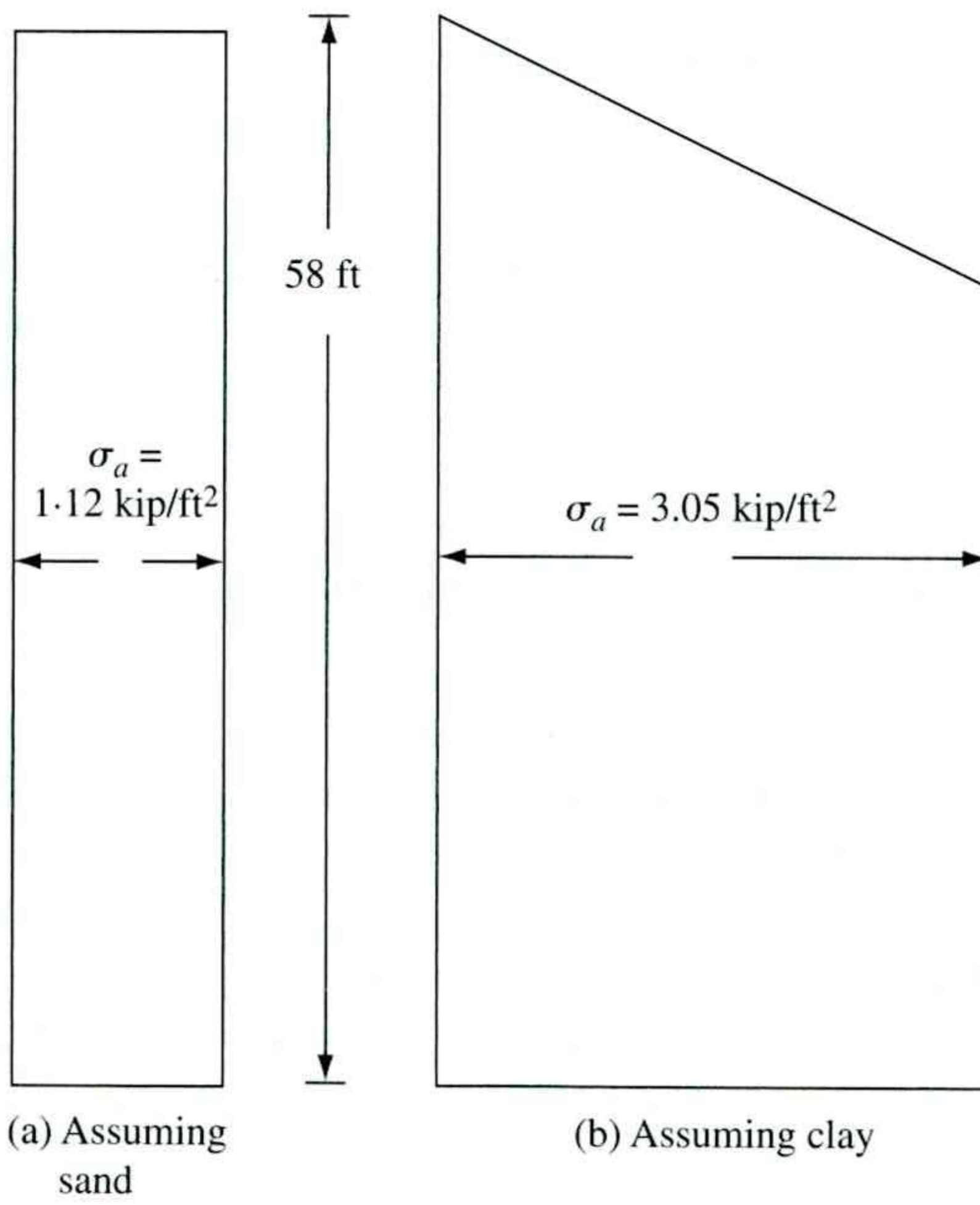


Figure 10.14 Pressure envelopes
(a) assuming sand; (b) assuming clay

Sand

$$\sigma_a = 0.65\gamma HK_a \quad (10.10)$$

For $\gamma = 114 \text{ lb/ft}^3$, $H = 58 \text{ ft}$, and $K_a = 0.26$,

$$\sigma_a = (0.65)(114)(58)(0.26) = 1117 \text{ lb/ft}^2 \approx 1.12 \text{ kip/ft}^2$$

Clay

$$\sigma_a = \gamma H \left[1 - \left(\frac{4c}{\gamma H} \right) \right] \quad (10.11)$$

For $c = 890 \text{ lb/ft}^2$,

$$\sigma_a = (114)(58) \left[1 - \frac{(4)(890)}{(114)(58)} \right] = 3052 \text{ lb/ft}^2 \approx 3.05 \text{ kip/ft}^2$$

Table 10.1 shows the variations of the strut load, based on the assumed pressure envelopes shown in Figure 10.14. Also shown in Table 10.1 are the measured strut loads in the field and the design strut loads. This comparison indicates that

1. In most cases the measured strut loads differed widely from those predicted. This result is due primarily to the uncertainties involved in the assumption of the soil parameters.
2. The actual design strut loads were substantially higher than those measured.

B. Construction of National Plaza (South Half) in Chicago

The construction of the south half of the National Plaza in Chicago required a braced cut 70 ft deep. Swatek et al. (1972) reported the case history for this construction. Figure 10.15 shows a schematic diagram for the braced cut and the subsoil profile. There were six levels of struts. Table 10.2 gives the actual maximum wale and strut loads.

Table 10.1 Computed and Measured Strut Loads at Test Section B

Strut number	Computed load (kip)		Measured strut load (kip)
	Envelope based on sand	Envelope based on clay	
S-1	182	230	70.4
S-2	215	580	215
S-3	154	420	304
S-4	108	292	230
S-5	75	219	274

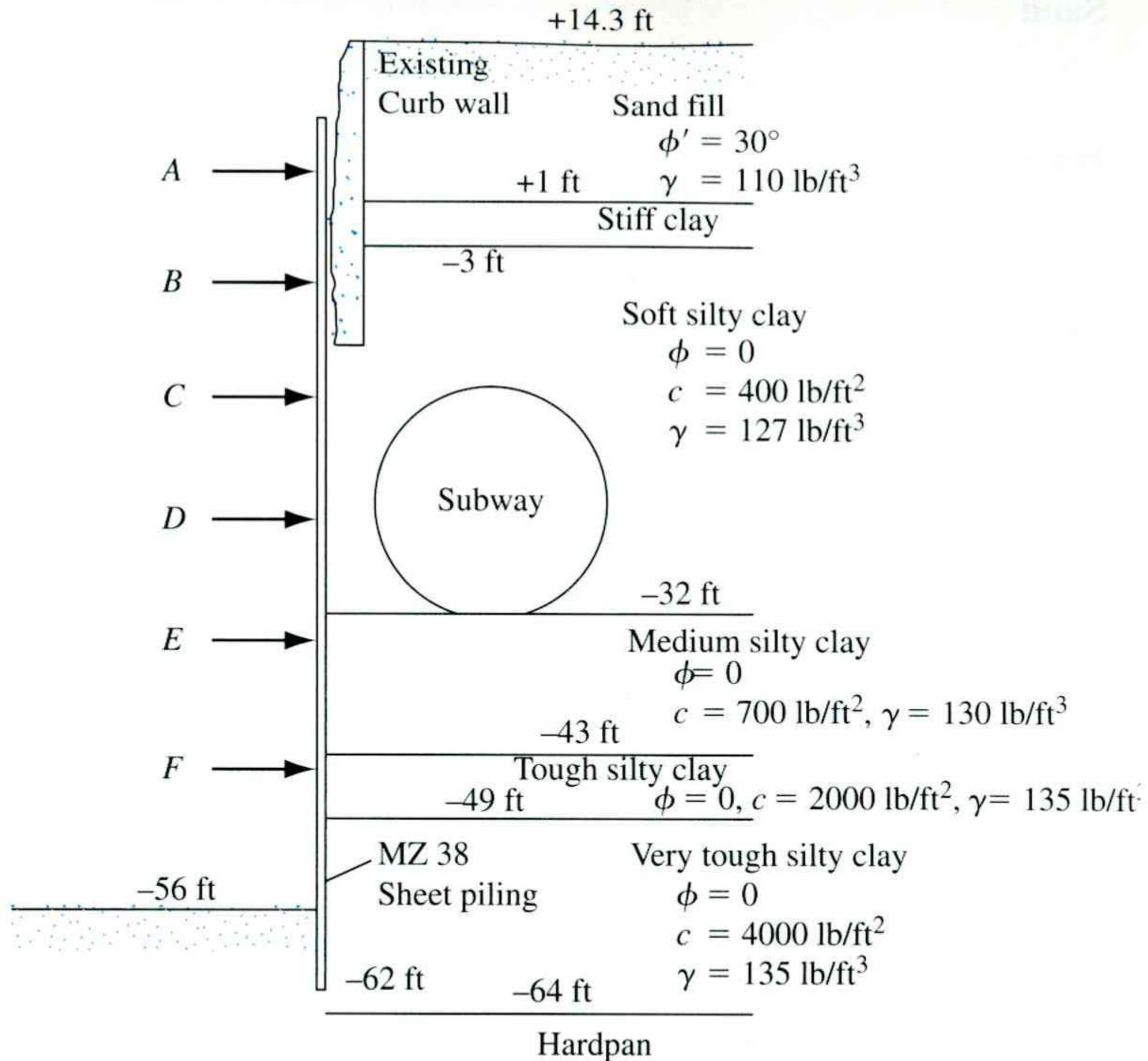


Figure 10.15 Schematic diagram of braced cut—National Plaza of Chicago

Table 10.2 National Plaza Wale and Strut Loads

Strut level	Elevation (ft)	Load measured (kip/ft)
A	+3	16.0
B	-6	26.5
C	-15	29.0
D	-24.5	29.0
E	-34	29.0
F	-44.5	30.7
		$\Sigma 160.2$

Figure 10.16 presents a lateral earth-pressure envelope based on the maximum wale loads measured. To compare the theoretical prediction to the actual observation requires making an approximate calculation. To do so, we convert the clayey soil layers from Elevation +1 ft to -56 ft to a single equivalent layer in Table 10.3 by using Eq. (10.6).

Now, using Eq. (10.4), we can convert the sand layer located between elevations +14 ft and +1 ft and the equivalent clay layer of 57 ft to one equivalent clay layer with a thickness of 70 ft:

$$\begin{aligned}
 c_{av} &= \frac{1}{2H} [\gamma_s K_s H_s^2 \tan \phi'_s + (H - H_s) n' q_u] \\
 &= \left[\frac{1}{(2)(70)} \right] [(110)(1)(13)^2 \tan 30 + (57)(0.75)(2 \times 1068)] \approx 730 \text{ lb/ft}^2
 \end{aligned}$$

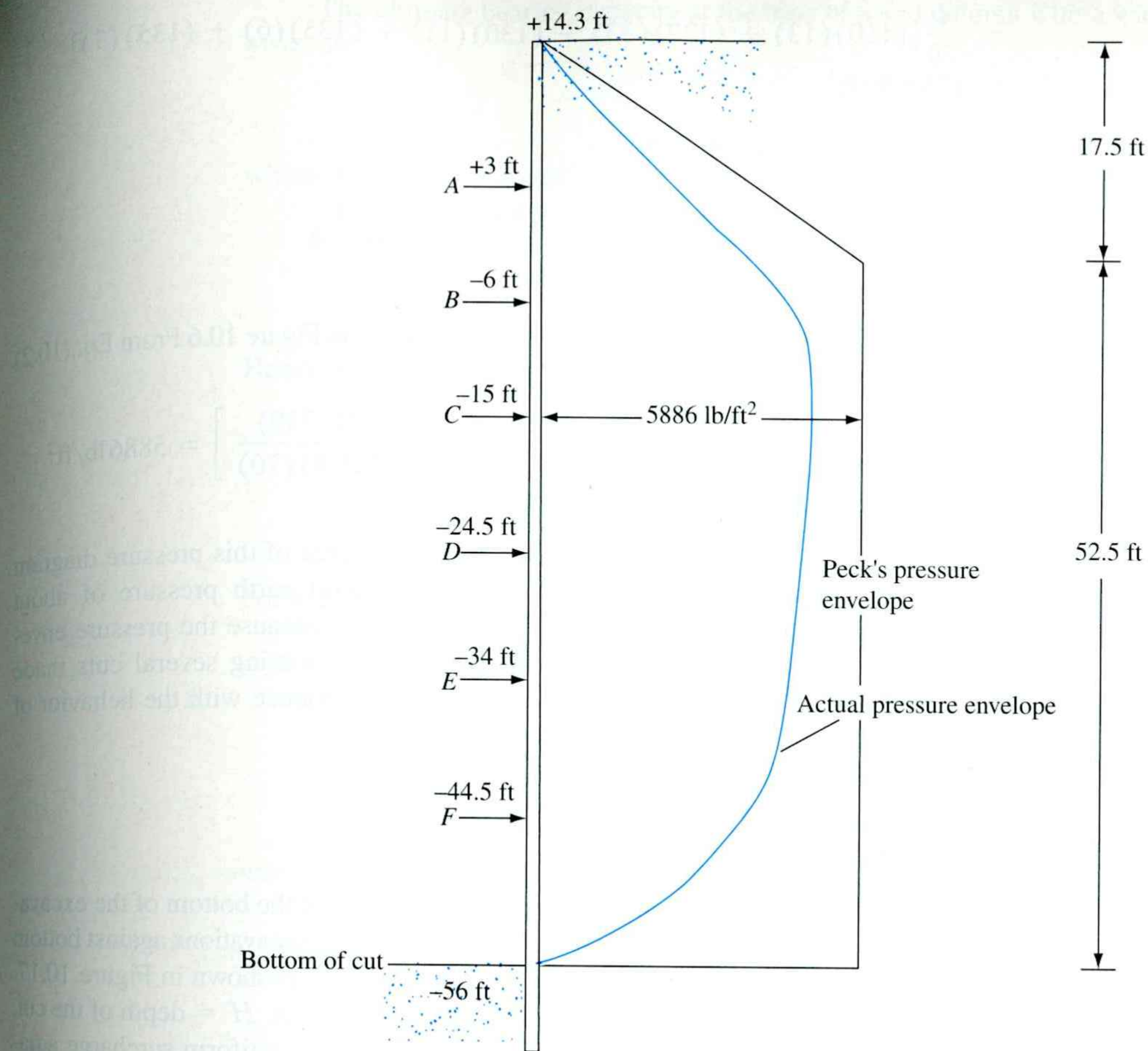


Figure 10.16 Comparison of actual and Peck's pressure envelopes

Table 10.3 Conversion of Soil Layers using Eq. (10.6)

Elevation (ft)	Thickness, <i>H</i> (ft)	<i>c</i> (lb/ft ²)	Equivalent <i>c</i> (lb/ft ²)
+1 to -32 ft	33	400	$c_{av} = \frac{1}{57}[(33)(400) + (11)(700) + (6)(2000) + (7)(4000)] = 1068 \text{ lb/ft}^2$
-32 ft to -43 ft	11	700	
-43 ft to -49 ft	6	2000	
-49 ft to -56 ft	7	4000	
		$\Sigma 57$	

Equation (10.7) gives

$$\gamma_{av} = \frac{1}{H} [\gamma_1 H_1 + \gamma_2 H_2 + \dots + \gamma_n H_n]$$

$$\begin{aligned}
 &= \frac{1}{70} [(110)(13) + (127)(33) + (130)(11) + (135)(6) + (135)(7)] \\
 &= 125.8 \text{ lb/ft}^3
 \end{aligned}$$

For the equivalent clay layer of 70 ft,

$$\frac{\gamma_{av}H}{c_{av}} = \frac{(125.8)(70)}{730} = 12.06 > 4$$

Hence the apparent pressure envelope will be of the type shown in Figure 10.6 From Eq. (10.2)

$$\sigma_a = \gamma H \left[1 - \left(\frac{4c_{av}}{\gamma_{av}H} \right) \right] = (125.8)(70) \left[1 - \frac{(4)(730)}{(125.8)(70)} \right] = 5886 \text{ lb/ft}^2$$

The pressure envelope is shown in Figure 10.16. The area of this pressure diagram is 201 kip/ft. Thus Peck's pressure envelope gives a lateral earth pressure of about 1.8 times that actually observed. This result is not surprising because the pressure envelope provided by Figure 10.6 is an envelope developed considering several cuts made at different locations. Under actual field conditions, past experience with the behavior of similar soils can help reduce overdesigning substantially.

10.6 Bottom Heave of a Cut in Clay

Braced cuts in clay may become unstable as a result of heaving of the bottom of the excavation. Terzaghi (1943) analyzed the factor of safety of long braced excavations against bottom heave. The failure surface for such a case in a homogeneous soil is shown in Figure 10.17. In the figure, the following notations are used: B = width of the cut, H = depth of the cut, T = thickness of the clay below the base of excavation, and q = uniform surcharge adjacent to the excavation.

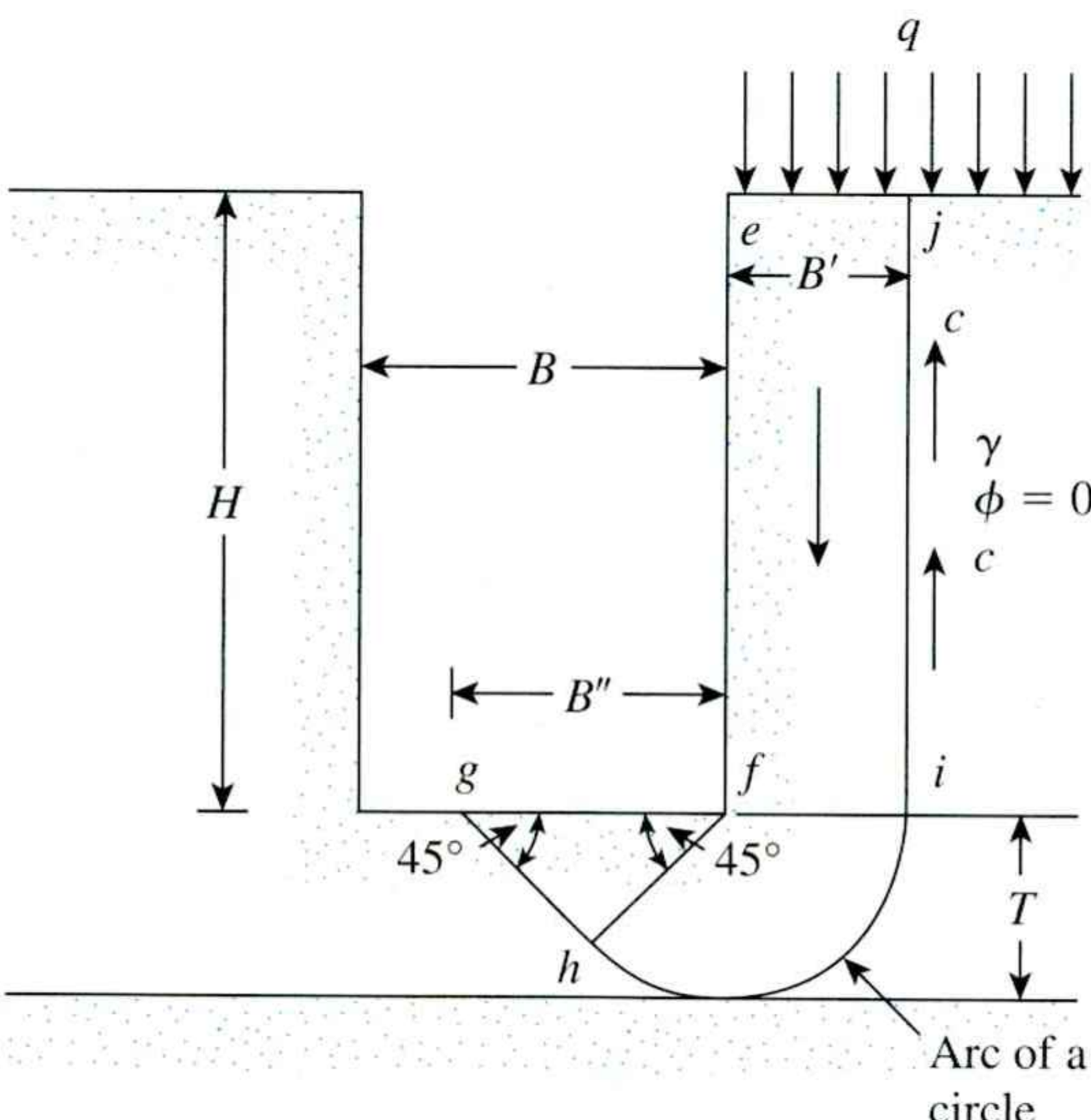


Figure 10.17 Heaving in braced cuts in clay

The ultimate bearing capacity at the base of a soil column with a width of B' can be given as

$$q_{\text{ult}} = cN_c \quad (10.12)$$

where $N_c = 5.7$ (for a perfectly rough foundation).

The vertical load per unit area along fi is

$$q = \gamma H + q - \frac{cH}{B'} \quad (10.13)$$

Hence, the factor of safety against bottom heave is

$$\text{FS} = \frac{q_{\text{ult}}}{q} = \frac{cN_c}{\gamma H + q - \frac{cH}{B'}} = \frac{cN_c}{\left(\gamma + \frac{q}{H} - \frac{c}{B'}\right)H} \quad (10.14)$$

For excavations of limited length L , the factor of safety can be modified to

$$\text{FS} = \frac{cN_c \left(1 + 0.2 \frac{B'}{L}\right)}{\left(\gamma + \frac{q}{H} - \frac{c}{B'}\right)H} \quad (10.15)$$

where $B' = T$ or $B/\sqrt{2}$ (whichever is smaller).

In 2000, Chang suggested a revision of Eq. (10.15) with the following changes:

1. The shearing resistance along ij may be considered as an increase in resistance rather than a reduction in loading.
2. In Figure 10.17, fg with a width of B'' at the base of the excavation may be treated as a negatively loaded footing.
3. The value of the bearing capacity factor N_c should be 5.14 (not 5.7) for a perfectly smooth footing, because of the restraint-free surface at the base of the excavation.

With the foregoing modifications, Eq. (10.15) takes the form

$$\text{FS} = \frac{5.14c \left(1 + \frac{0.2B''}{L}\right) + \frac{cH}{B'}}{\gamma H + q} \quad (10.16)$$

where

$$B' = T \text{ if } T \leq B/\sqrt{2}$$

$$B' = B/\sqrt{2} \text{ if } T > B/\sqrt{2}$$

$$B'' = \sqrt{2}B'$$

Bjerrum and Eide (1956) compiled a number of case records for the bottom heave of cuts in clay. Chang (2000) used those records to calculate FS by means of Eq. (10.16); his findings are summarized in Table 10.4. It can be seen from this table that the actual field observations agree well with the calculated factors of safety.

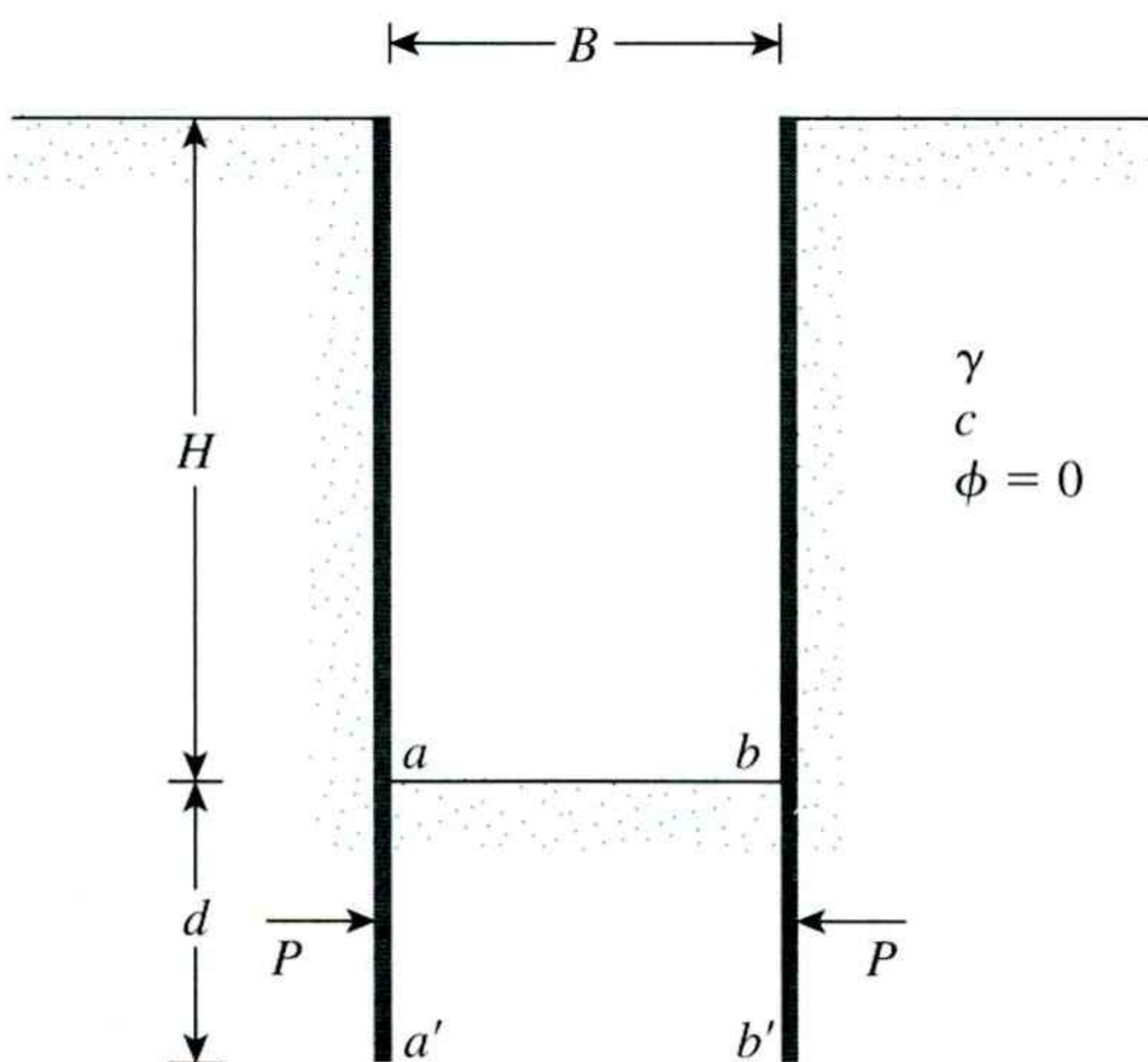
Table 10.4 Calculated Factors of Safety for Selected Case Records Compiled by Bjerrum and Eide (1956) and Calculated by Chang (2000)

Site	B (m)	B/L	H (m)	H/B	γ (kN/m ³)	c (kN/m ²)	q (kN/m ²)	FS [Eq. (10.16)]	Type of failure
Pumping station, Fornebu, Oslo	5.0	1.0	3.0	0.6	17.5	7.5	0	1.05	Total failure
Storehouse, Drammen	4.8	0	2.4	0.5	19.0	12	15	1.05	Total failure
Sewerage tank, Drammen	5.5	0.69	3.5	0.64	18.0	10	10	0.92	Total failure
Excavation, Grey Wedels Plass, Oslo	5.8	0.72	4.5	0.78	18.0	14	10	1.07	Total failure
Pumping station, Jernbanetorget, Oslo	8.5	0.70	6.3	0.74	19.0	22	0	1.26	Partial failure
Storehouse, Freia, Oslo	5.0	0	5.0	1.00	19.0	16	0	1.10	Partial failure
Subway, Chicago	16	0	11.3	0.70	19.0	35	0	1.00	Near failure

Equation (10.16) is recommended for use in this test. In most cases, a factor of safety of about 1.5 is recommended.

In homogeneous clay, if FS becomes less than 1.5, the sheet pile is driven deeper. (See Figure 10.18.) Usually, the depth d is kept less than or equal to $B/2$, in which case the force P per unit length of the buried sheet pile (aa' and bb') may be expressed as (U.S. Department of the Navy, 1971)

$$P = 0.7(\gamma HB - 1.4cH - \pi cB) \quad \text{for } d > 0.47B \quad (10.17)$$

**Figure 10.18** Force on the buried length of sheet pile

and

$$P = 1.5d \left(\gamma H - \frac{1.4cH}{B} - \pi c \right) \quad \text{for } d < 0.47B \quad (10.18)$$

Example 10.3

In Figure 10.19, for a braced cut in clay, $B = 3\text{m}$, $L = 20\text{m}$, $H = 5.5\text{m}$, $T = 1.5\text{m}$, $\gamma = 17\text{kN/m}^3$, $c = 30\text{kN/m}^2$, and $q = 0$. Calculate the factor of safety against heave. Use Eq. (10.16).

Solution

From Eq. (10.16),

$$\text{FS} = \frac{5.14c \left(1 + \frac{0.2B''}{L} \right) + \frac{cH}{B'}}{\gamma H + q}$$

with $T = 1.5\text{m}$,

$$\frac{B}{\sqrt{2}} = \frac{3}{\sqrt{2}} = 2.12\text{m}$$

So

$$T \leq \frac{B}{\sqrt{2}}$$

Hence, $B' = T = 1.5\text{m}$, and it follows that

$$B'' = \sqrt{2}B' = (\sqrt{2})(1.5) = 2.12\text{m}$$

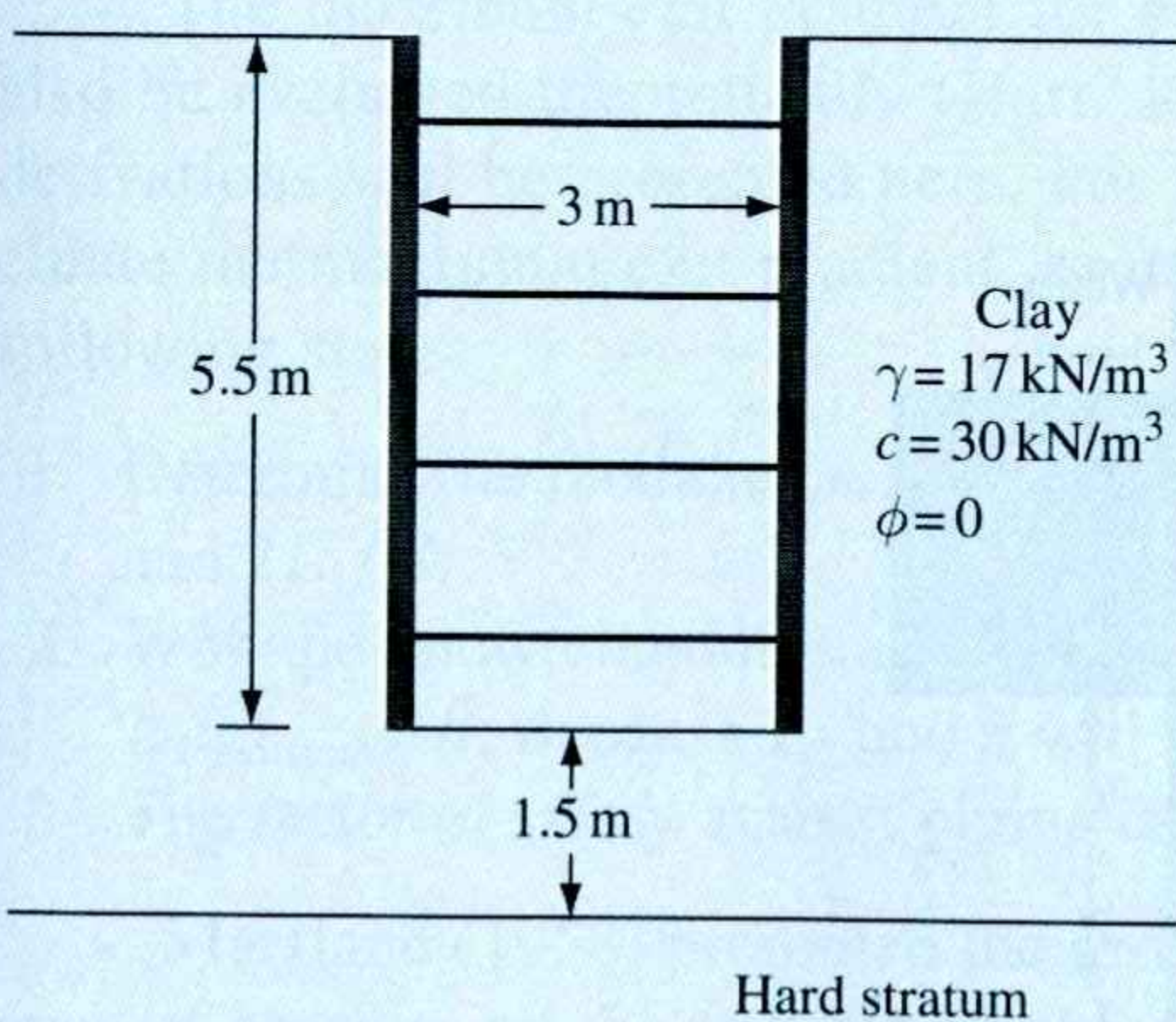


Figure 10.19 Factor of safety against heaving for a braced cut

and

$$\text{FS} = \frac{(5.14)(30) \left[1 + \frac{(0.2)(2.12)}{20} \right] + \frac{(30)(5.5)}{1.5}}{(17)(5.5)} = 2.86 \quad \blacksquare$$

The bottom of a cut in sand is generally stable. When the water table is encountered, the bottom of the cut is stable as long as the water level inside the excavation is higher than the groundwater level. In case dewatering is needed (see Figure 10.20), the factor of safety against piping should be checked. [Piping is another term for failure by heave, as defined in Section 1.12; see Eq. (1.45).] Piping may occur when a high hydraulic gradient is created by water flowing into the excavation. To check the factor of safety, draw flow nets and determine the maximum exit gradient [$i_{\max(\text{exit})}$] that will occur at points A and B. Figure 10.21 shows such a flow net, for which the maximum exit gradient is

$$i_{\max(\text{exit})} = \frac{h}{N_d} = \frac{h}{a} \quad (10.19)$$

where

a = length of the flow element at A (or B)
 N_d = number of drops (Note: in Figure 10.21, $N_d = 8$; see also Section 1.11)

The factor of safety against piping may be expressed as

$$\text{FS} = \frac{i_{\text{cr}}}{i_{\max(\text{exit})}} \quad (10.20)$$

where i_{cr} = critical hydraulic gradient.

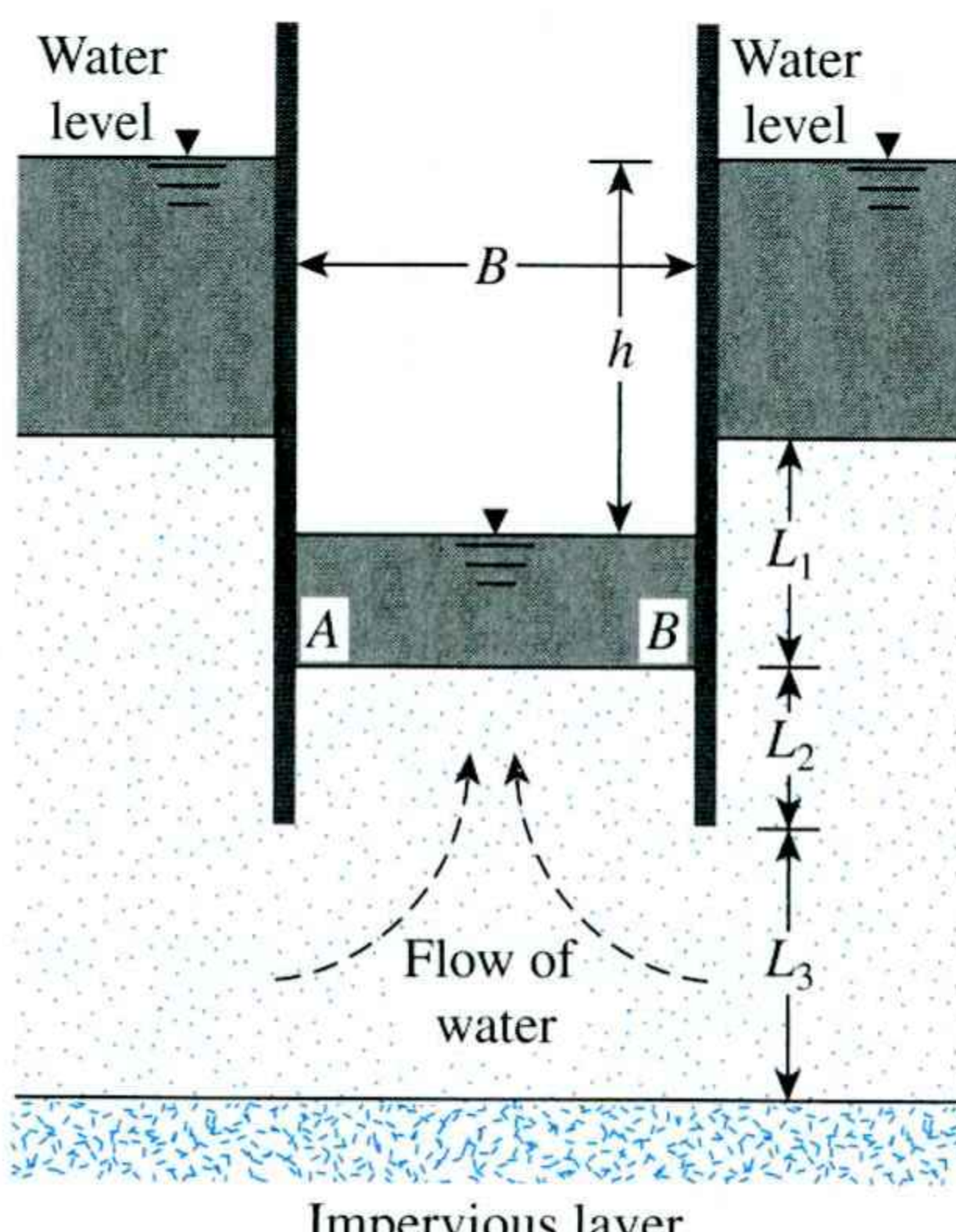


Figure 10.20 Stability of the bottom of a cut in sand

ered,
higher
factor
re by
high
factor
t will
mum

0.19)

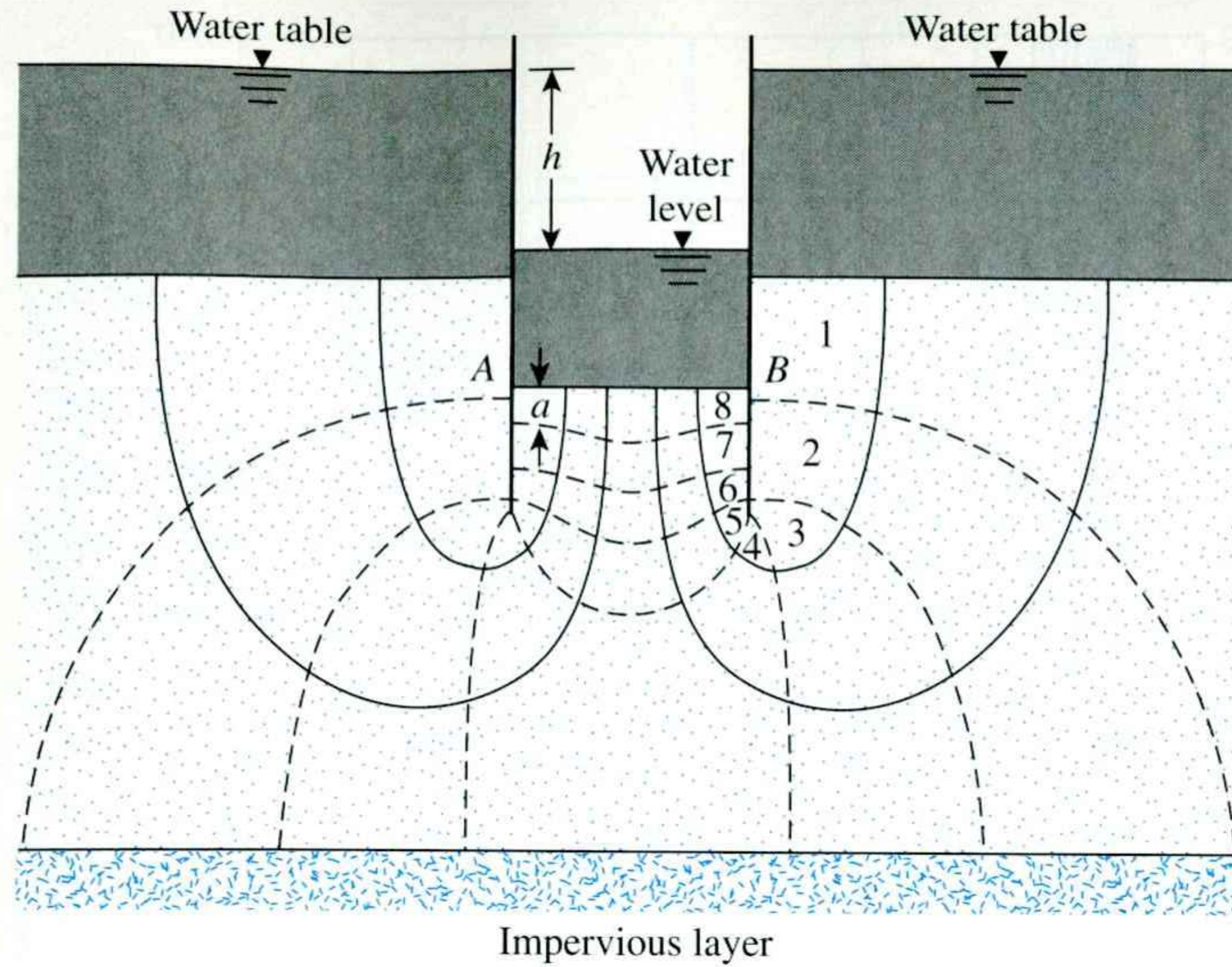


Figure 10.21 Determining the factor of safety against piping by drawing a flow net

The relationship for i_{cr} was given in Chapter 1 as

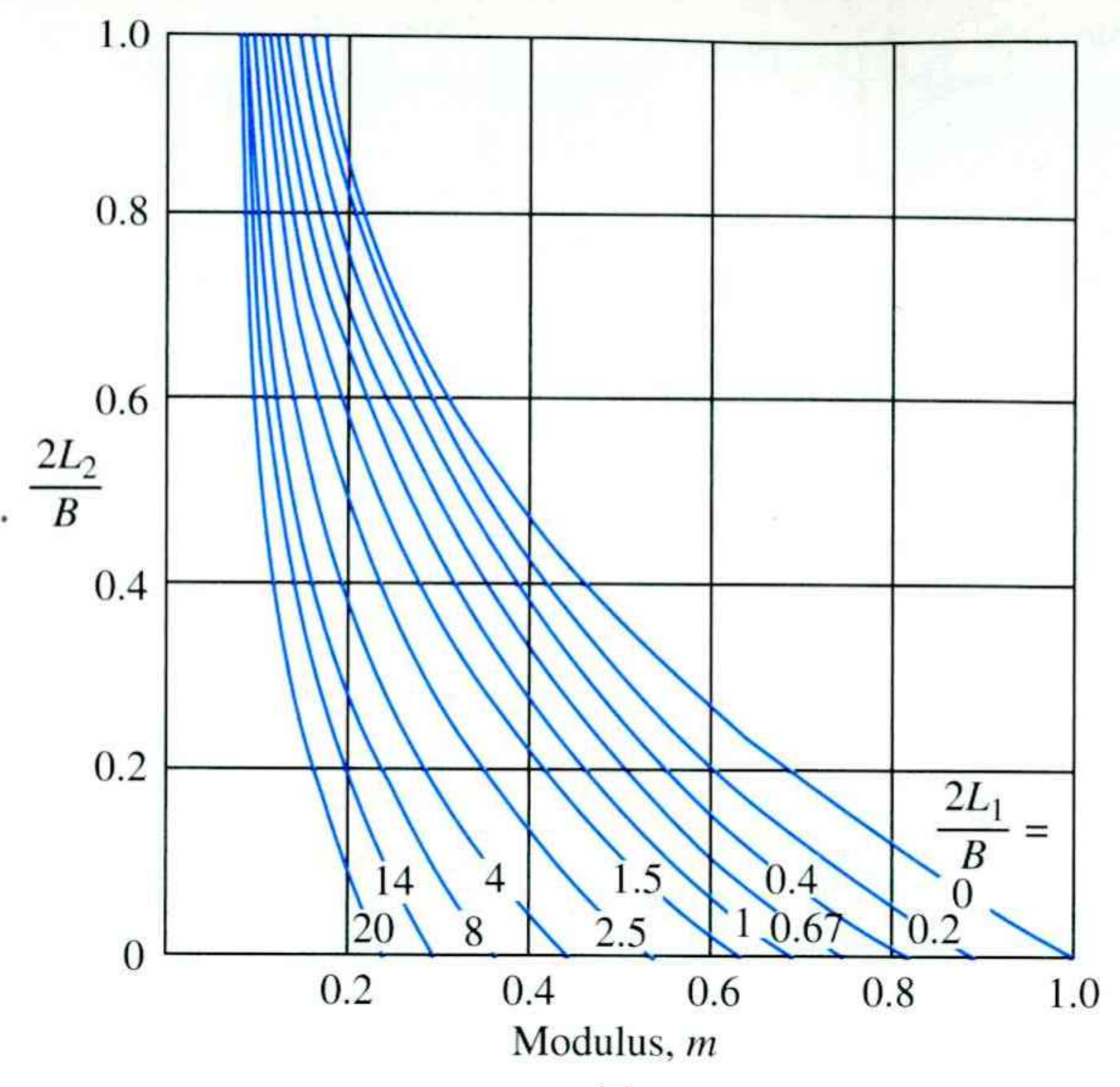
$$i_{cr} = \frac{G_s - 1}{e + 1}$$

The magnitude of i_{cr} varies between 0.9 and 1.1 in most soils, with an average of about 1.0. A factor of safety of about 1.5 is desirable.

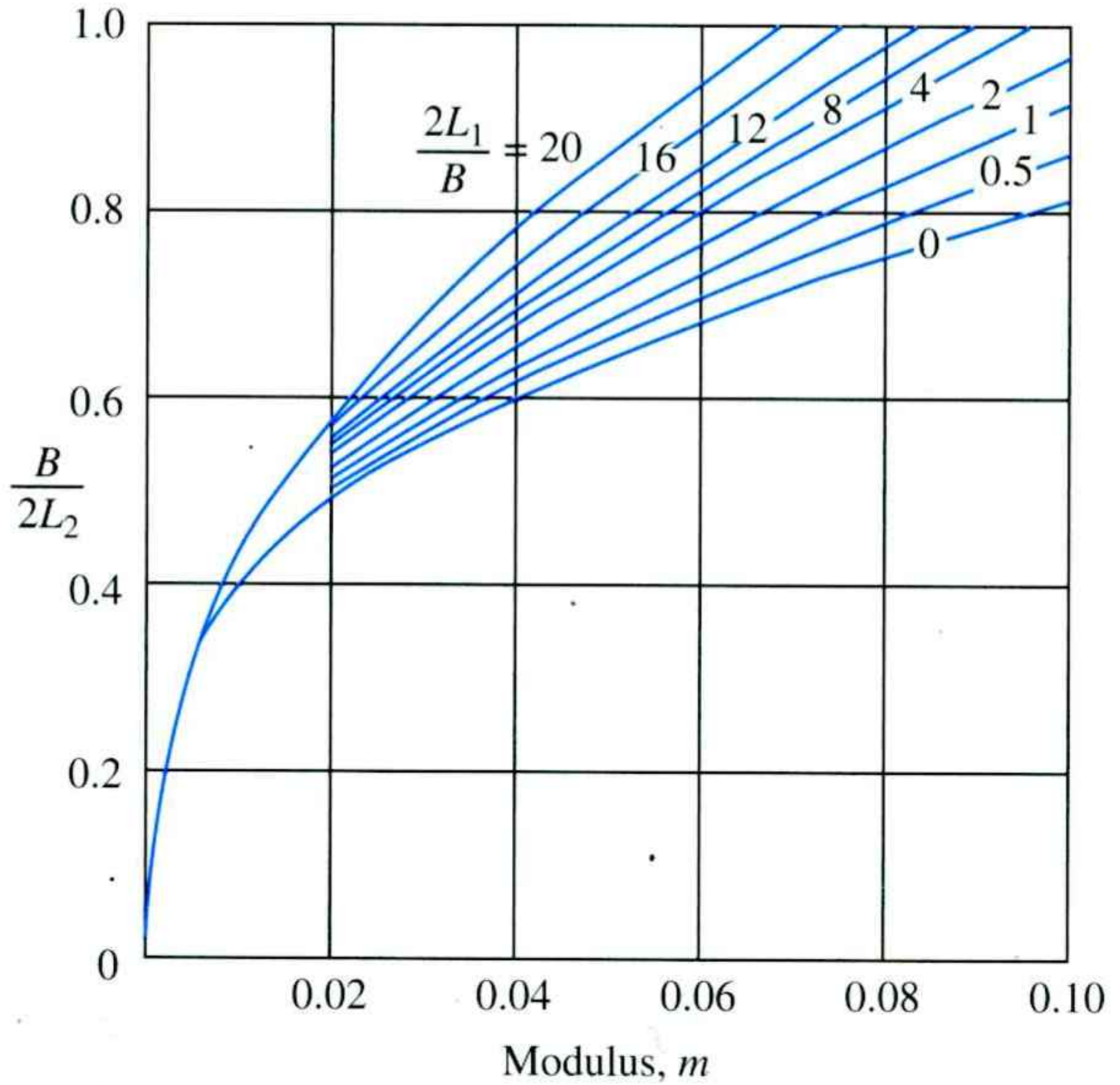
The maximum exit gradient for sheeted excavations in sands with $L_3 = \infty$ can also be evaluated theoretically (Harr, 1962). (Only the results of these mathematical derivations will be presented here. For further details, see the original work.) To calculate the maximum exit gradient, examine Figures 10.22 and 10.23 and perform the following steps:

1. Determine the modulus, m , from Figure 10.22 by obtaining $2L_2/B$ (or $B/2L_2$) and $2L_1/B$.
2. With the known modulus and $2L_1/B$, examine Figure 10.23 and determine $L_2 i_{exit(max)}/h$. Because L_2 and h will be known, $i_{exit(max)}$ can be calculated.
3. The factor of safety against piping can be evaluated by using Eq. (10.20).

Marsland (1958) presented the results of model tests conducted to study the influence of seepage on the stability of sheeted excavations in sand. The results were summarized by the U.S. Department of the Navy (1971) in NAVFAC DM-7 and are given in Figure 10.24a, b, and c. Note that Figure 10.24b is for the case of determining the sheet pile penetration L_2 needed for the required factor of safety against piping when the sand layer extends to a great depth below the excavation. By contrast, Figure 10.24c represents the case in which an impervious layer lies at a limited depth below the bottom of the excavation.

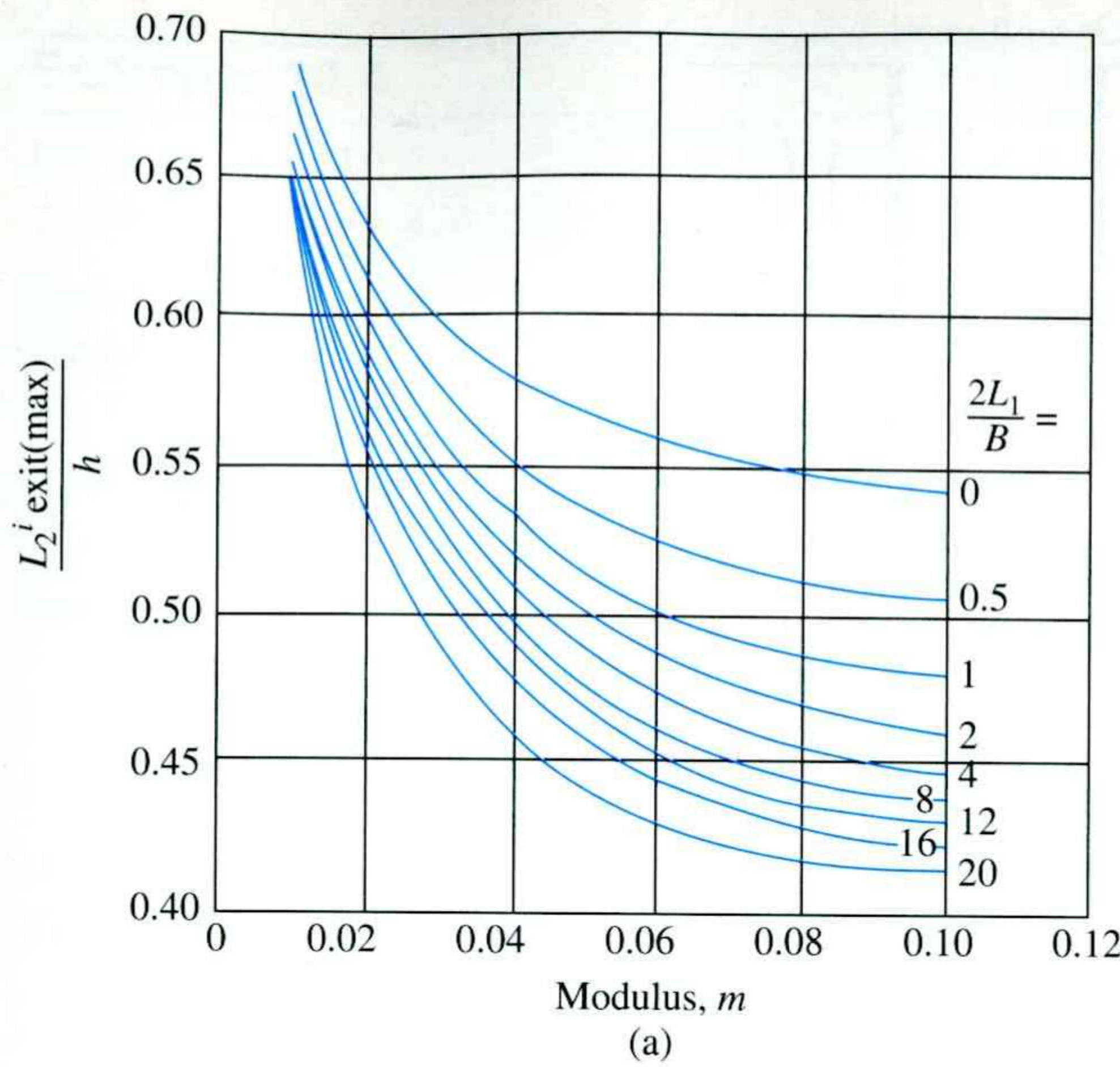


(a)

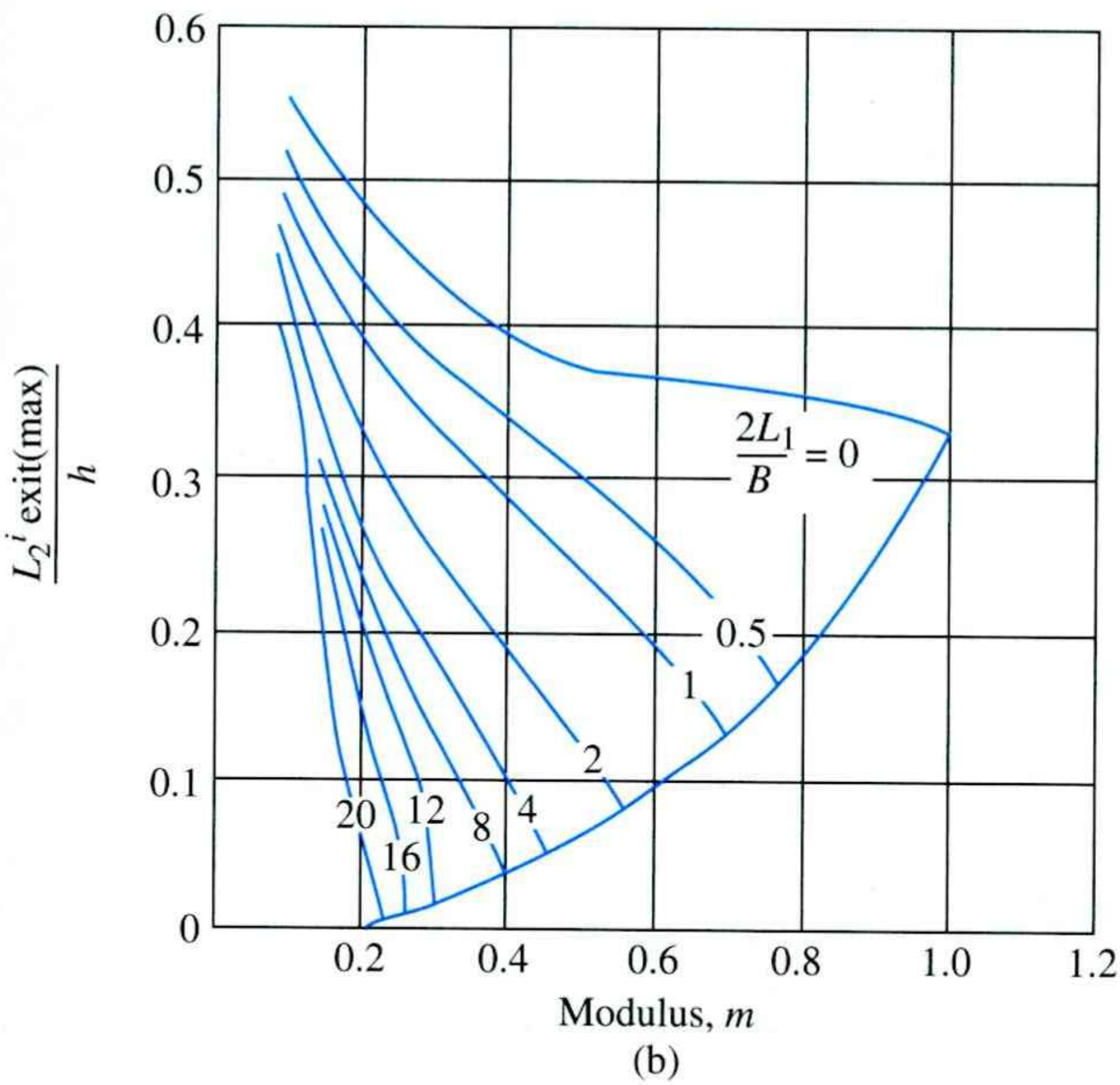


(b)

Figure 10.22 Variation of modulus (From *Groundwater and Seepage*, by M. E. Harr. Copyright 1962 by McGraw-Hill. Used with permission.)

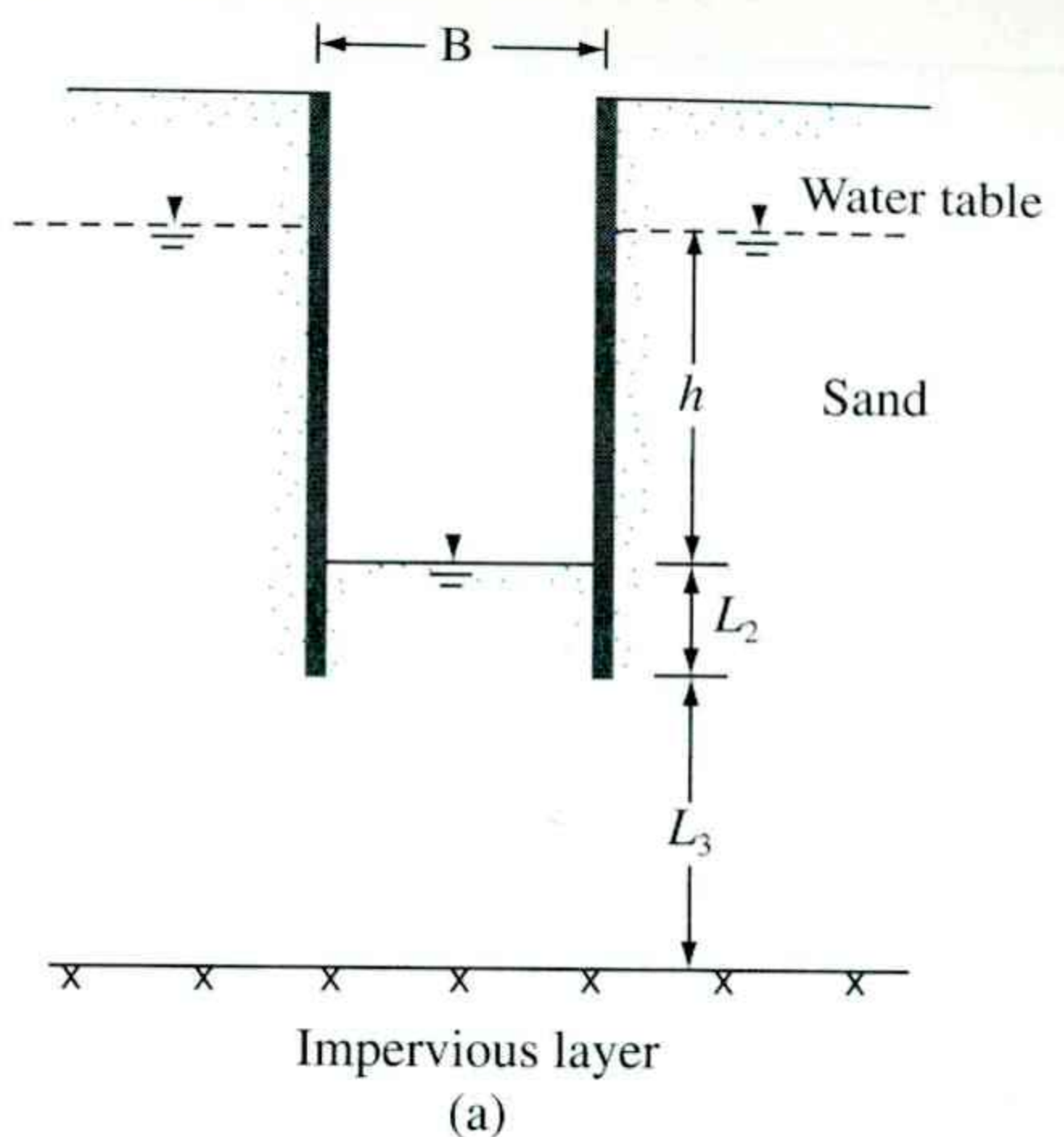


(a)

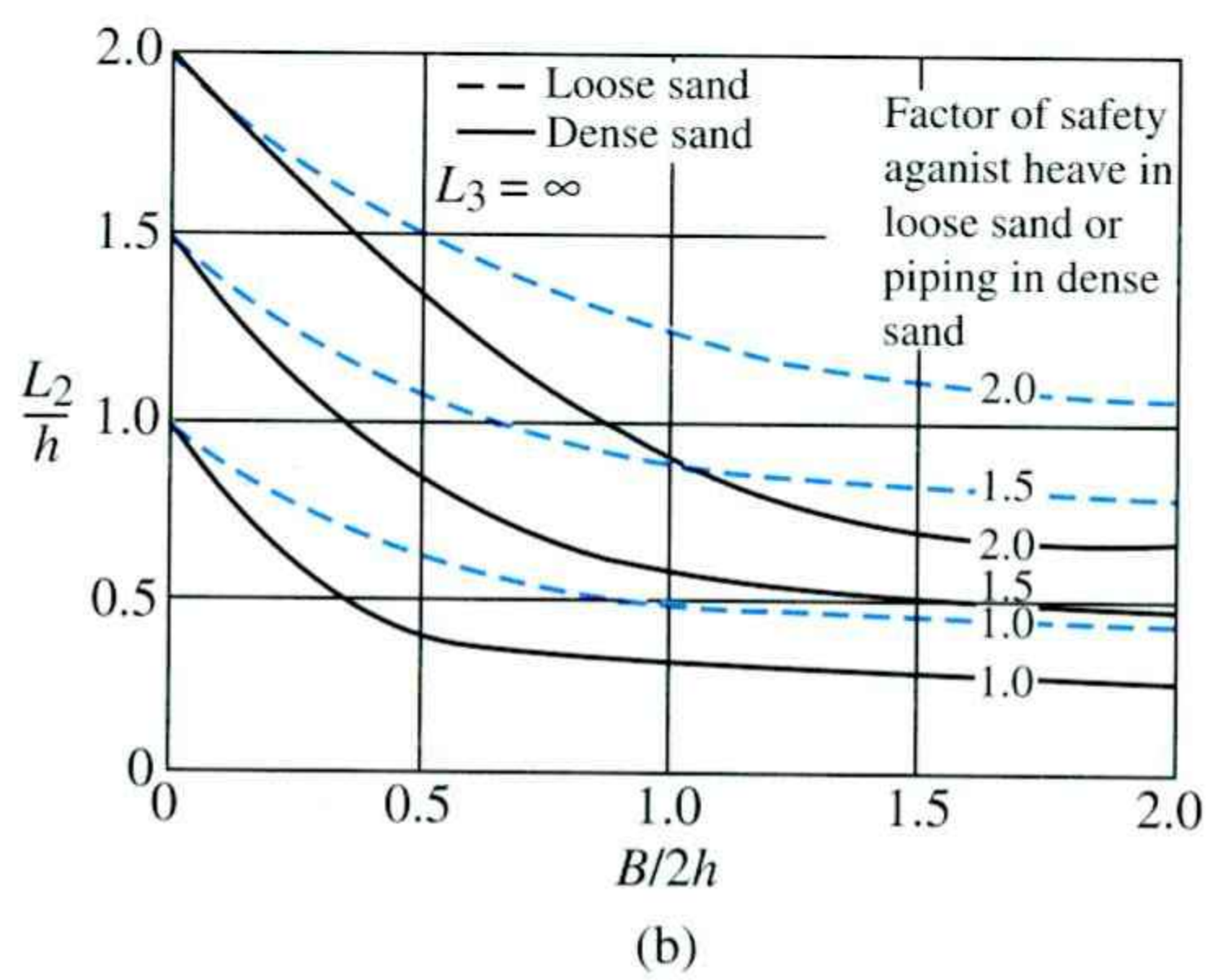


(b)

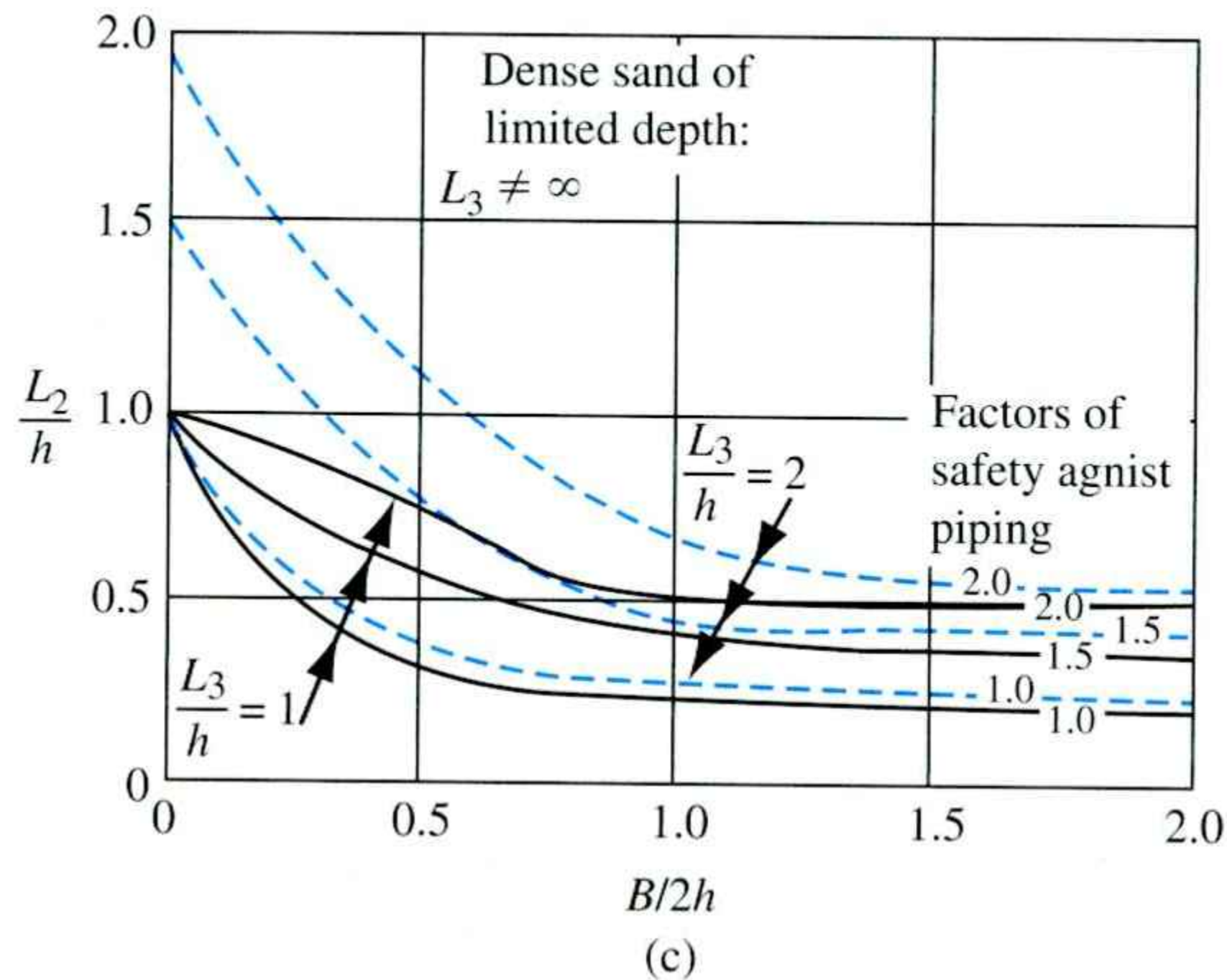
Figure 10.23 Variation of maximum exit gradient with modulus
(From *Groundwater and Seepage*, by M. E. Harr. Copyright 1962
by McGraw-Hill. Used with permission.)



(a)



(b)



(c)

Figure 10.24 Influence of seepage on the stability of sheeted excavation (US Department of Navy, 1971.)

Example 10.4

In Figure 10.20, let $h = 4.5\text{m}$, $L_1 = 5\text{m}$, $L_2 = 4\text{m}$, $B = 5\text{m}$, and $L_3 = \infty$. Determine the factor of safety against piping. Use Figures 10.22 and 10.23.

Solution

We have

$$\frac{2L_1}{B} = \frac{2(5)}{5} = 2$$

and

$$\frac{B}{2L_2} = \frac{5}{2(4)} = 0.625$$

According to Figure 10.22b, for $2L_1/B = 2$ and $B/2L_2 = 0.625$, $m \approx 0.033$. From Figure 10.23a, for $m = 0.033$ and $2L_1/B = 2$, $L_2 i_{\text{exit(max)}}/h = 0.54$. Hence,

$$i_{\text{exit(max)}} = \frac{0.54(h)}{L_2} = 0.54(4.5)/4 = 0.608$$

and

$$\text{FS} = \frac{i_{\text{cr}}}{i_{\text{max(exit)}}} = \frac{1}{0.608} = \mathbf{1.645}$$

■

10.8

Lateral Yielding of Sheet Piles and Ground Settlement

In braced cuts, some lateral movement of sheet pile walls may be expected. (See Figure 10.25.) The amount of lateral yield (δ_H) depends on several factors, the most important of which is the elapsed time between excavation and the placement of wales and struts. As discussed before, in several instances the sheet piles (or the soldier piles, as the case may be) are driven to a certain depth below the bottom of the excavation. The reason is to reduce the lateral yielding of the walls during the last stages of excavation. Lateral yielding of the walls will cause the ground surface surrounding the cut to settle. The degree of lateral yielding, however, depends mostly on the type of soil below the bottom of the cut. If clay below the cut extends to a great depth and $\gamma H/c$ is less than about 6, extension of the sheet piles or soldier piles below the bottom of the cut will help considerably in reducing the lateral yield of the walls.

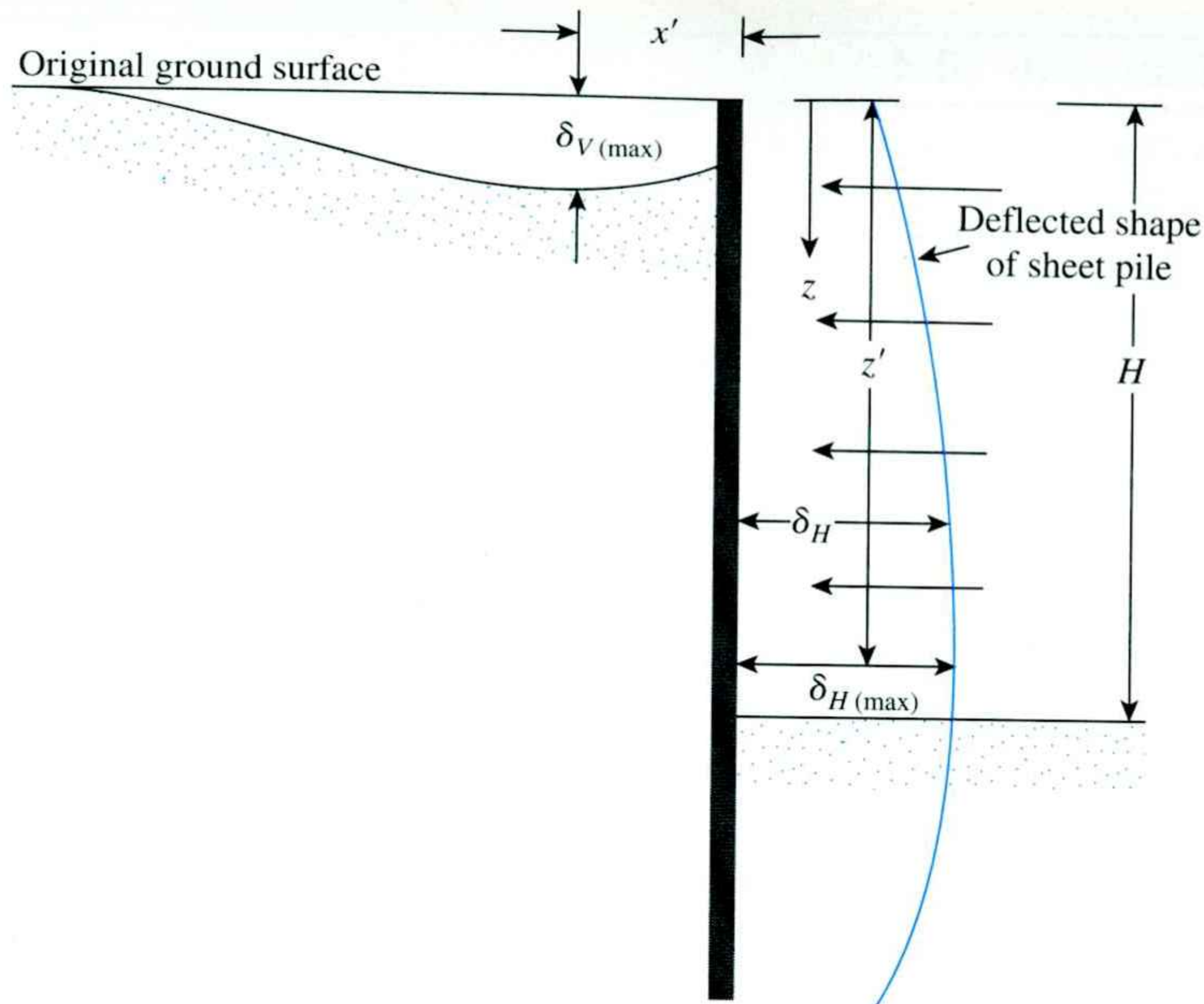


Figure 10.25 Lateral yielding of sheet pile and ground settlement

However, under similar circumstances, if $\gamma H/c$ is about 8, the extension of sheet piles into the clay below the cut does not help greatly. In such circumstances, we may expect a great degree of wall yielding that could result in the total collapse of the bracing systems. If a hard layer of soil lies below a clay layer at the bottom of the cut, the piles should be embedded in the stiffer layer. This action will greatly reduce lateral yield.

The lateral yielding of walls will generally induce ground settlement, δ_V , around a braced cut. Such settlement is generally referred to as *ground loss*. On the basis of several field observations, Peck (1969) provided curves for predicting ground settlement in various types of soil. (See Figure 10.26.) The magnitude of ground loss varies extensively; however, the figure may be used as a general guide.

Moormann (2004) analyzed about 153 case histories dealing mainly with the excavation in soft clay (that is, undrained shear strength, $c \leq 75 \text{ kN/m}^2$). Following is a summary of his analysis relating to $\delta_{V(\max)}$, x' , $\delta_{H(\max)}$, and z' (see Figure 10.25).

- Maximum Vertical Movement [$\delta_{V(\max)}$]
 - $\delta_{V(\max)}/H \approx 0.1$ to 10.1% with an average of 1.07% (soft clay)
 - $\delta_{V(\max)}/H \approx 0$ to 0.9% with an average of 0.18% (stiff clay)
 - $\delta_{V(\max)}/H \approx 0$ to 2.43% with an average of 0.33% (non-cohesive soils)
- Location of $\delta_{V(\max)}$, that is x' (Figure 10.25)
 - For 70% of all case histories considered, $x' \leq 0.5H$.
 - However, in soft clays, x' may be as much as $2H$.

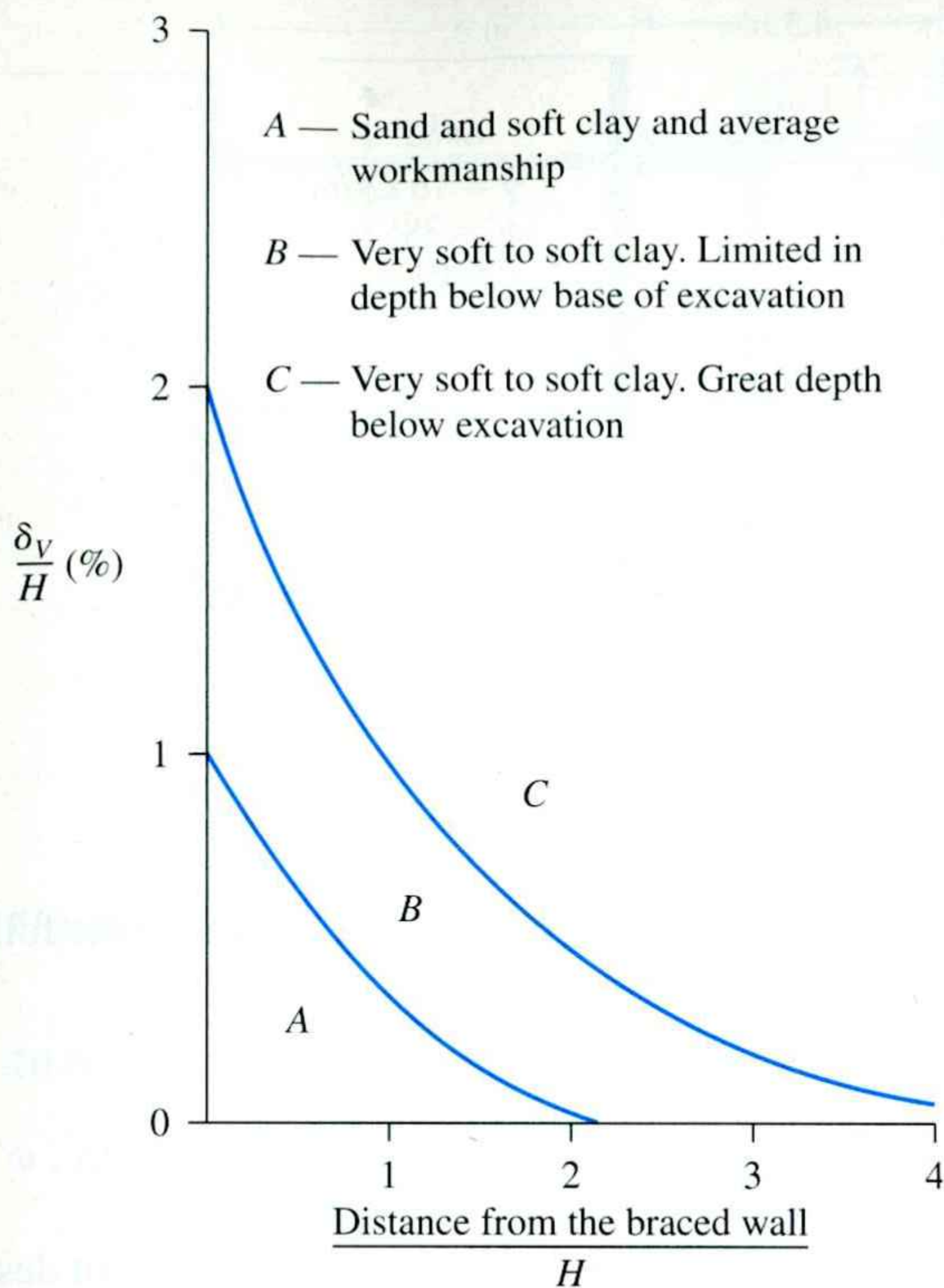


Figure 10.26 Variation of ground settlement with distance (From Peck, R. B. (1969). "Deep Excavation and Tunneling in Soft Ground," Proceedings Seventh International Conference on Soil Mechanics and Foundation Engineering, Mexico City, State-of-the-Art Volume, pp. 225–290. With permission from ASCE.)

- Maximum Horizontal Deflection of Sheet Piles, $\delta_{H(\max)}$
For 40% of excavation in soft clay, $0.5\% \leq \delta_{H(\max)}/H \leq 1\%$.
The average value of $\delta_{H(\max)}/H$ is about 0.87%.
In stiff clays, the average value of $\delta_{H(\max)}/H$ is about 0.25%.
In non-cohesive soils, $\delta_{H(\max)}/H$ is about 0.27% of the average.
- Location of $\delta_{H(\max)}$, that is z' (Figure 10.25)
For deep excavation of soft and stiff cohesive soils, z'/H is about 0.5 to 1.0.

Problems

- 10.1** Refer to the braced cut shown in Figure P10.1. Given: $\gamma = 16 \text{ kN/m}^3$, $\phi' = 38^\circ$, and $c' = 0$. The struts are located at 3.5 m center-to-center in the plan. Draw the earth-pressure envelope and determine the strut loads at levels A, B, and C.

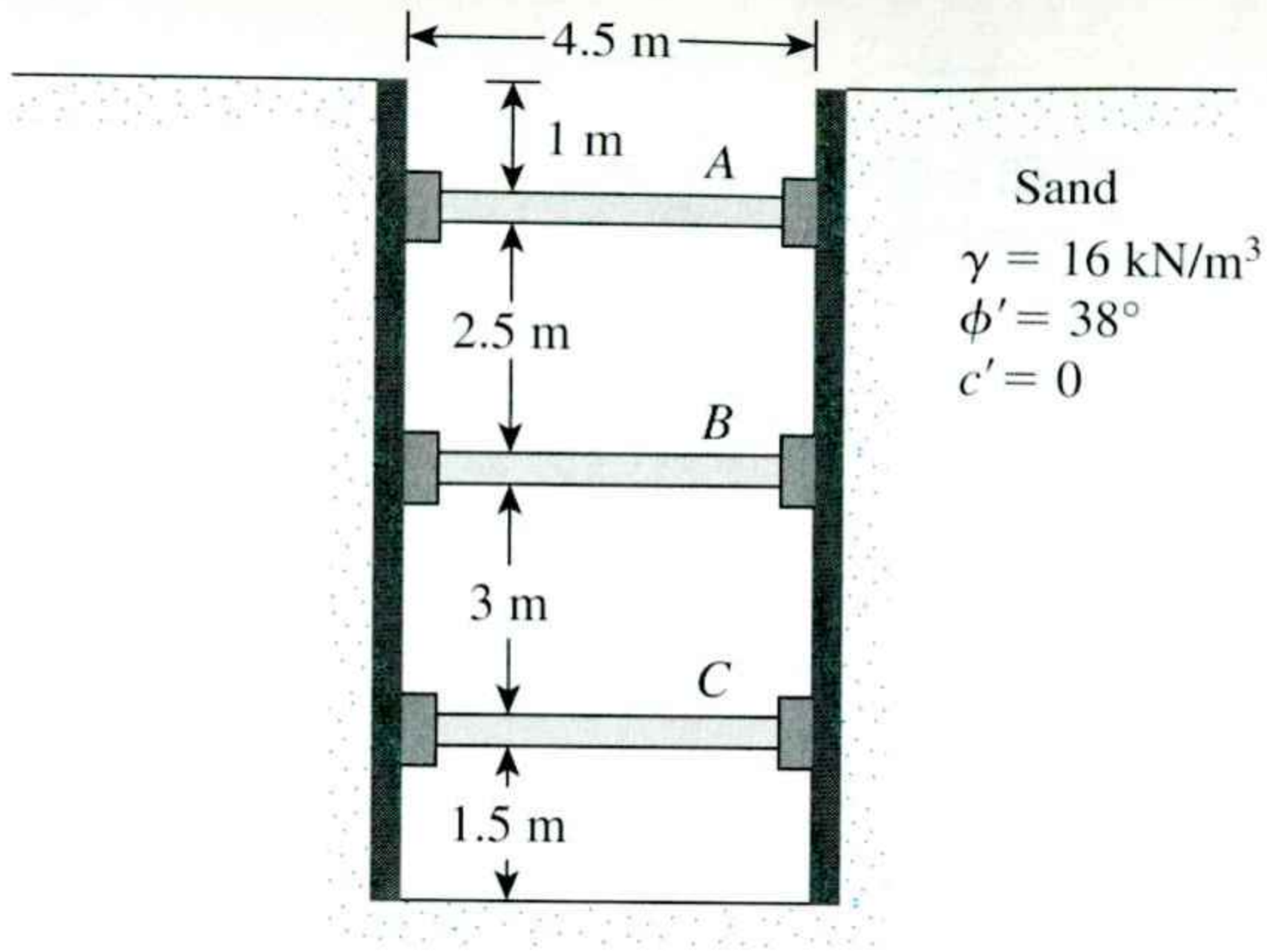


Figure P10.1

- 10.2** For the braced cut described in Problem 10.1, determine the following:
- The sheet-pile section modulus
 - The section modulus of the wales at level *B*
- Assume that $\sigma_{\text{all}} = 170 \text{ MN/m}^2$.
- 10.3** Refer to Fig. P10.3. Redo Problem 10.1 with $\gamma = 18 \text{ kN/m}^3$, $\phi' = 40^\circ$, $c' = 0$, and the center-to-center strut spacing in the plan = 4 m.
- 10.4** Determine the sheet-pile section modulus for the braced cut described in Problem 10.3. Given: $\sigma_{\text{all}} = 170 \text{ MN/m}^2$.
- 10.5** Refer to Figure 10.8a. For the braced cut, given $H = 6 \text{ m}$; $H_s = 2.5 \text{ m}$; $\gamma_s = 16.5 \text{ kN/m}^3$; angle of friction of sand, $\phi'_s = 35^\circ$; $H_c = 3.5 \text{ m}$; $\gamma_c = 17.5 \text{ kN/m}^3$; and unconfined compression strength of clay layer, $q_u = 62 \text{ kN/m}^2$.
- Estimate the average cohesion (c_{av}) and average unit weight (γ_{av}) for the construction of the earth-pressure envelope.
 - Plot the earth-pressure envelope.

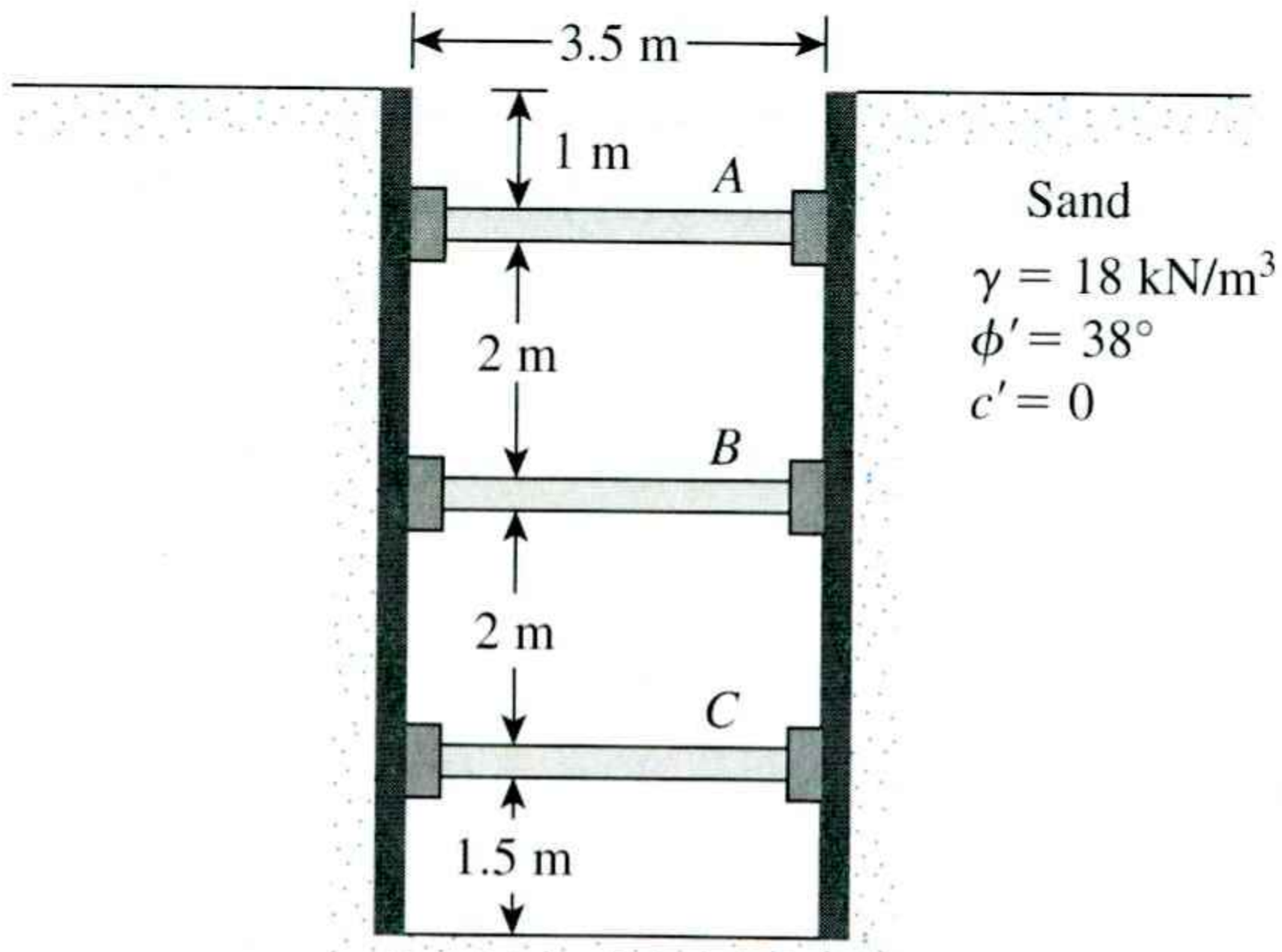


Figure P10.3

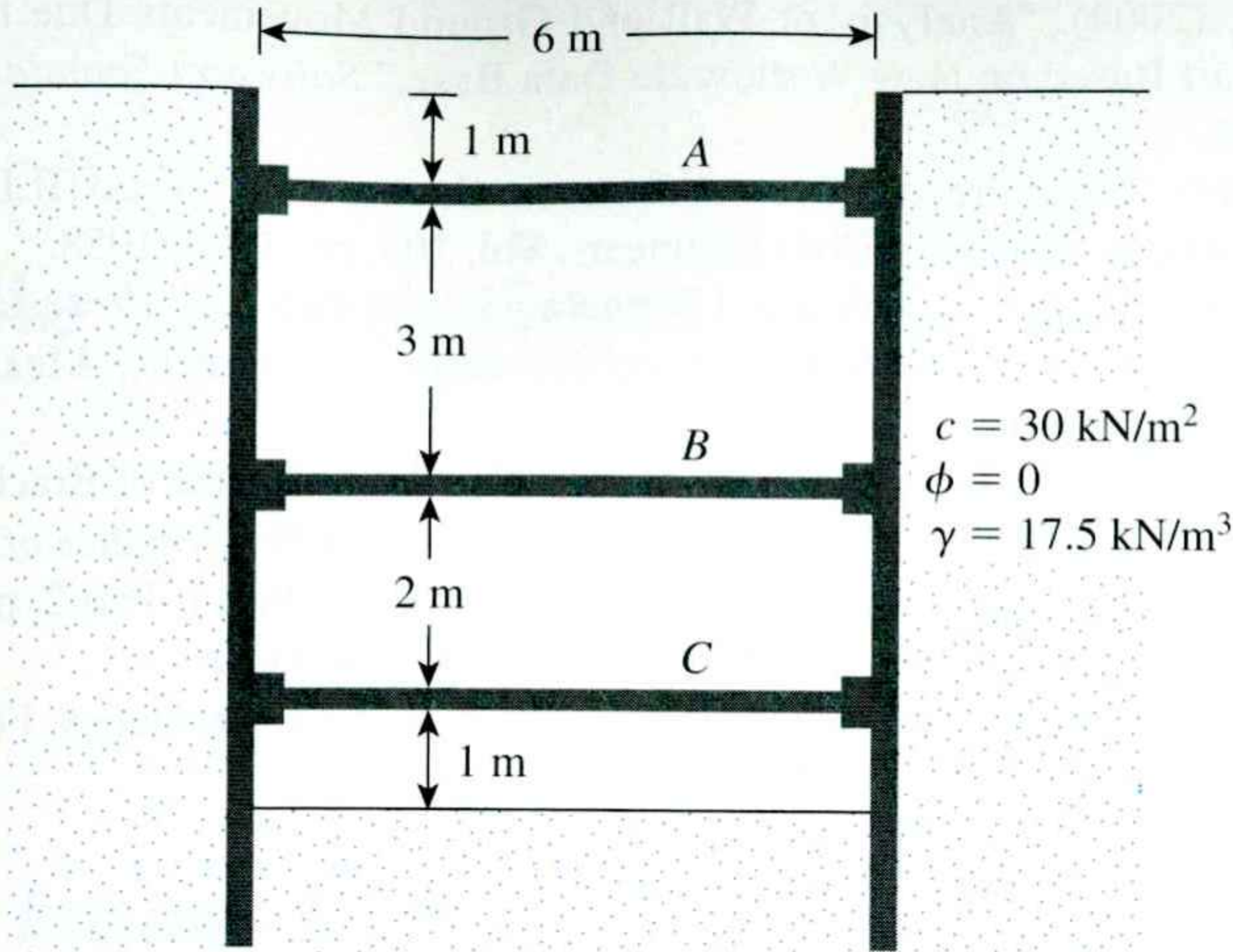


Figure P10.7

- 10.6** Refer to Figure 10.8b, which shows a braced cut in clay. Given: $H = 25 \text{ ft}$, $H_1 = 5 \text{ ft}$, $c_1 = 2125 \text{ lb/ft}^2$, $\gamma_1 = 111 \text{ lb/ft}^3$, $H_2 = 10 \text{ ft}$, $c_2 = 1565 \text{ lb/ft}^2$, $\gamma_2 = 107 \text{ lb/ft}^3$, $H_3 = 10 \text{ ft}$, $c_3 = 1670 \text{ lb/ft}^2$, and $\gamma_3 = 109 \text{ lb/ft}^3$.
- Determine the average cohesion (c_{av}) and average unit weight (γ_{av}) for the construction of the earth-pressure envelope.
 - Plot the earth-pressure envelope.
- 10.7** Refer to Figure P10.7. Given: $\gamma = 17.5 \text{ kN/m}^3$, $c = 30 \text{ kN/m}^2$, and center-to-center spacing of struts in the plan = 5 m. Draw the earth-pressure envelope and determine the strut loads at levels A, B, and C.
- 10.8** Determine the sheet-pile section modulus for the braced cut described in Problem 10.7. Use $\sigma_{all} = 170 \text{ MN/m}^2$.
- 10.9** Redo Problem 10.7 assuming that $c = 60 \text{ kN/m}^2$.
- 10.10** Determine the factor of safety against bottom heave for the braced cut described in Problem 10.7. Use Eq. (10.16) and assume the length of the cut, $L = 18 \text{ m}$.
- 10.11** Determine the factor of safety against bottom heave for the braced cut described in Problem 10.9. Use Eq. (10.15). The length of the cut is 12.5.

References

- BJERRUM, L., and EIDE, O. (1956). "Stability of Strutted Excavation in Clay," *Geotechnique*, Vol. 6, No. 1, pp. 32–47.
- CHANG, M. F. (2000). "Basal Stability Analysis of Braced Cuts in Clay," *Journal of Geotechnical and Geoenvironmental Engineering*, ASCE, Vol. 126, No. 3, pp. 276–279.
- HARR, M. E. (1962). *Groundwater and Seepage*, McGraw-Hill, New York.
- LAMBE, T. W. (1970). "Braced Excavations." *Proceedings of the Specialty Conference on Lateral Stresses in the Ground and Design of Earth-Retaining Structures*, American Society of Civil Engineers, pp. 149–218.

11 Pile Foundations

11.1 Introduction

Piles are structural members that are made of steel, concrete, or timber. They are used to build pile foundations, which are deep and which cost more than shallow foundations. (See Chapters 3, 4, and 5.) Despite the cost, the use of piles often is necessary to ensure structural safety. The following list identifies some of the conditions that require pile foundations (Vesic, 1977):

1. When one or more upper soil layers are highly compressible and too weak to support the load transmitted by the superstructure, piles are used to transmit the load to underlying bedrock or a stronger soil layer, as shown in Figure 11.1a. When bedrock is not encountered at a reasonable depth below the ground surface, piles are used to transmit the structural load to the soil gradually. The resistance to the applied structural load is derived mainly from the frictional resistance developed at the soil–pile interface. (See Figure 11.1b.)
2. When subjected to horizontal forces (see Figure 11.1c), pile foundations resist by bending, while still supporting the vertical load transmitted by the superstructure. This type of situation is generally encountered in the design and construction of earth-retaining structures and foundations of tall structures that are subjected to high wind or to earthquake forces.
3. In many cases, expansive and collapsible soils may be present at the site of a proposed structure. These soils may extend to a great depth below the ground surface. Expansive soils swell and shrink as their moisture content increases and decreases, and the pressure of the swelling can be considerable. If shallow foundations are used in such circumstances, the structure may suffer considerable damage. However, pile foundations may be considered as an alternative when piles are extended beyond the active zone, which is where swelling and shrinking occur. (See Figure 11.1d)

Soils such as loess are collapsible in nature. When the moisture content of these soils increases, their structures may break down. A sudden decrease in the void ratio of soil induces large settlements of structures supported by shallow foundations. In such

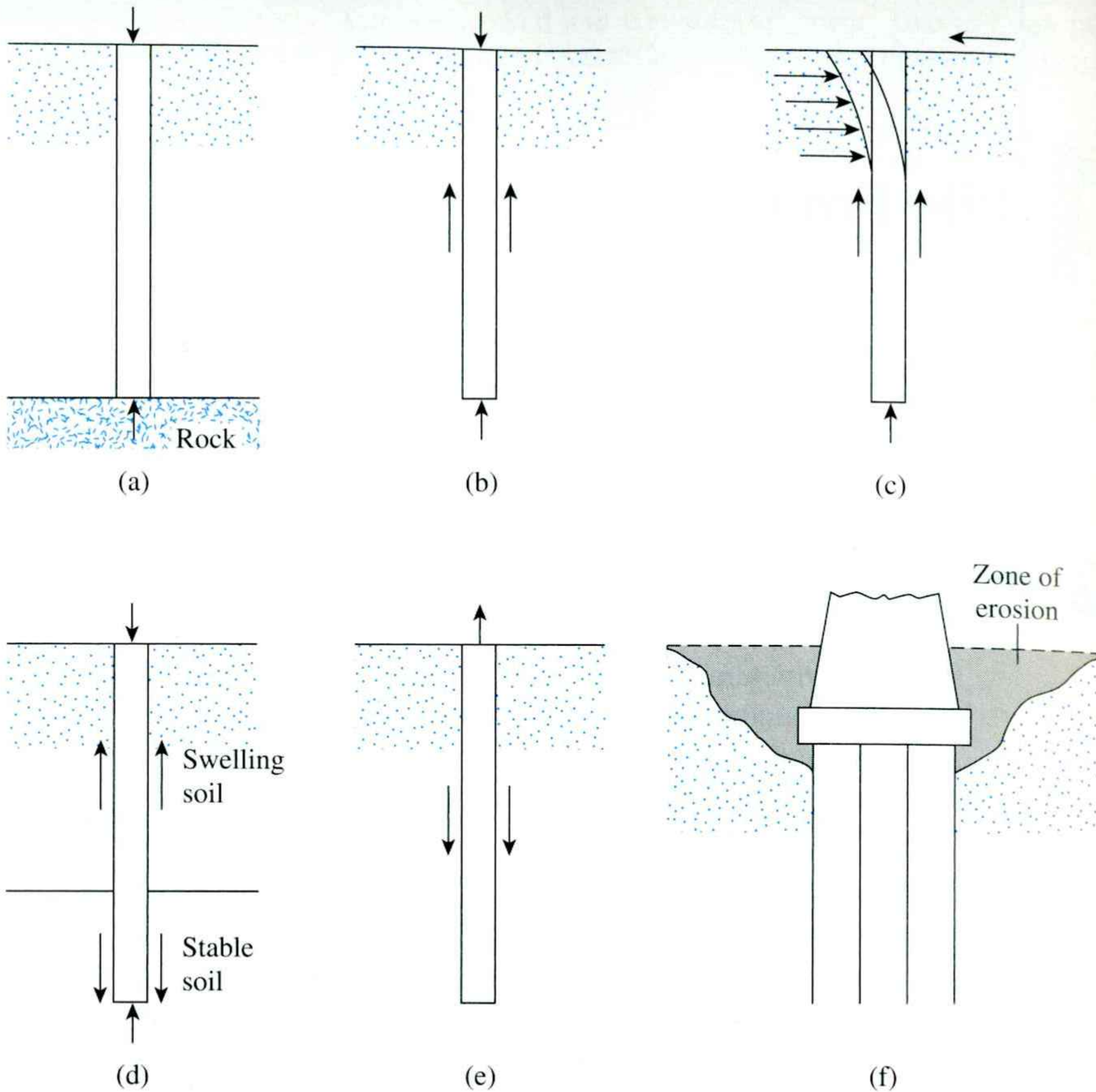


Figure 11.1 Conditions that require the use of pile foundations

cases, pile foundations may be used in which the piles are extended into stable soil layers beyond the zone where moisture will change.

4. The foundations of some structures, such as transmission towers, offshore platforms, and basement mats below the water table, are subjected to uplifting forces. Piles are sometimes used for these foundations to resist the uplifting force. (See Figure 11.1e.)
5. Bridge abutments and piers are usually constructed over pile foundations to avoid the loss of bearing capacity that a shallow foundation might suffer because of soil erosion at the ground surface. (See Figure 11.1f.)

Although numerous investigations, both theoretical and experimental, have been conducted in the past to predict the behavior and the load-bearing capacity of piles in granular and cohesive soils, the mechanisms are not yet entirely understood and may never be. The design and analysis of pile foundations may thus be considered somewhat of an art as a result of the uncertainties involved in working with some subsoil conditions. This chapter discusses the present state of the art.

Different types of piles are used in construction work, depending on the type of load to be carried, the subsoil conditions, and the location of the water table. Piles can be divided into the following categories: (a) steel piles, (b) concrete piles, (c) wooden (timber) piles, and (d) composite piles.

Steel Piles

Steel piles generally are either *pipe piles* or *rolled steel H-section piles*. Pipe piles can be driven into the ground with their ends open or closed. Wide-flange and I-section steel beams can also be used as piles. However, H-section piles are usually preferred because their web and flange thicknesses are equal. (In wide-flange and I-section beams, the web thicknesses are smaller than the thicknesses of the flange.) Table 11.1 gives the dimensions of some standard H-section steel piles used in the United States. Table 11.2 shows selected pipe sections frequency used for piling purposes. In many cases, the pipe piles are filled with concrete after they have been driven.

The allowable structural capacity for steel piles is

$$Q_{\text{all}} = A_s f_s \quad (11.1)$$

where

A_s = cross-sectional area of the steel

f_s = allowable stress of steel ($\approx 0.33 - 0.5 f_y$)

Once the design load for a pile is fixed, one should determine, on the basis of geotechnical considerations, whether $Q_{(\text{design})}$ is within the allowable range as defined by Eq. 11.1.

When necessary, steel piles are spliced by welding or by riveting. Figure 11.2a shows a typical splice by welding for an H-pile. A typical splice by welding for a pipe pile is shown in Figure 11.2b. Figure 11.2c is a diagram of a splice of an H-pile by rivets or bolts.

When hard driving conditions are expected, such as driving through dense gravel, shale, or soft rock, steel piles can be fitted with driving points or shoes. Figures 11.2d and 11.2e are diagrams of two types of shoe used for pipe piles.

Steel piles may be subject to corrosion. For example, swamps, peats, and other organic soils are corrosive. Soils that have a pH greater than 7 are not so corrosive. To offset the effect of corrosion, an additional thickness of steel (over the actual designed cross-sectional area) is generally recommended. In many circumstances factory-applied epoxy coatings on piles work satisfactorily against corrosion. These coatings are not easily damaged by pile driving. Concrete encasement of steel piles in most corrosive zones also protects against corrosion.

Following are some general facts about steel piles:

- Usual length: 15 m to 60 m (50 ft to 200 ft)
- Usual load: 300 kN to 1200 kN (67 kip to 265 kip)

- Advantages:
 - a. Easy to handle with respect to cutoff and extension to the desired length
 - b. Can stand high driving stresses
 - c. Can penetrate hard layers such as dense gravel and soft rock
 - d. High load-carrying capacity
- Disadvantages:
 - a. Relatively costly
 - b. High level of noise during pile driving
 - c. Subject to corrosion
 - d. H-piles may be damaged or deflected from the vertical during driving through hard layers or past major obstructions

Table 11.1a Common H-Pile Sections used in the United States (SI Units)

Designation, size (mm) × weight (kg/m)	Depth d_1 (mm)	Section area ($\text{m}^2 \times 10^{-3}$)	Flange and web thickness w (mm)	Flange width d_2 (mm)	Moment of inertia ($\text{m}^4 \times 10^{-6}$)	
					I_{xx}	I_{yy}
HP 200 × 53	204	6.84	11.3	207	49.4	16.8
HP 250 × 85	254	10.8	14.4	260	123	42
× 62	246	8.0	10.6	256	87.5	24
HP 310 × 125	312	15.9	17.5	312	271	89
× 110	308	14.1	15.49	310	237	77.5
× 93	303	11.9	13.1	308	197	63.7
× 79	299	10.0	11.05	306	164	62.9
HP 330 × 149	334	19.0	19.45	335	370	123
× 129	329	16.5	16.9	333	314	104
× 109	324	13.9	14.5	330	263	86
× 89	319	11.3	11.7	328	210	69
HP 360 × 174	361	22.2	20.45	378	508	184
× 152	356	19.4	17.91	376	437	158
× 132	351	16.8	15.62	373	374	136
× 108	346	13.8	12.82	371	303	109

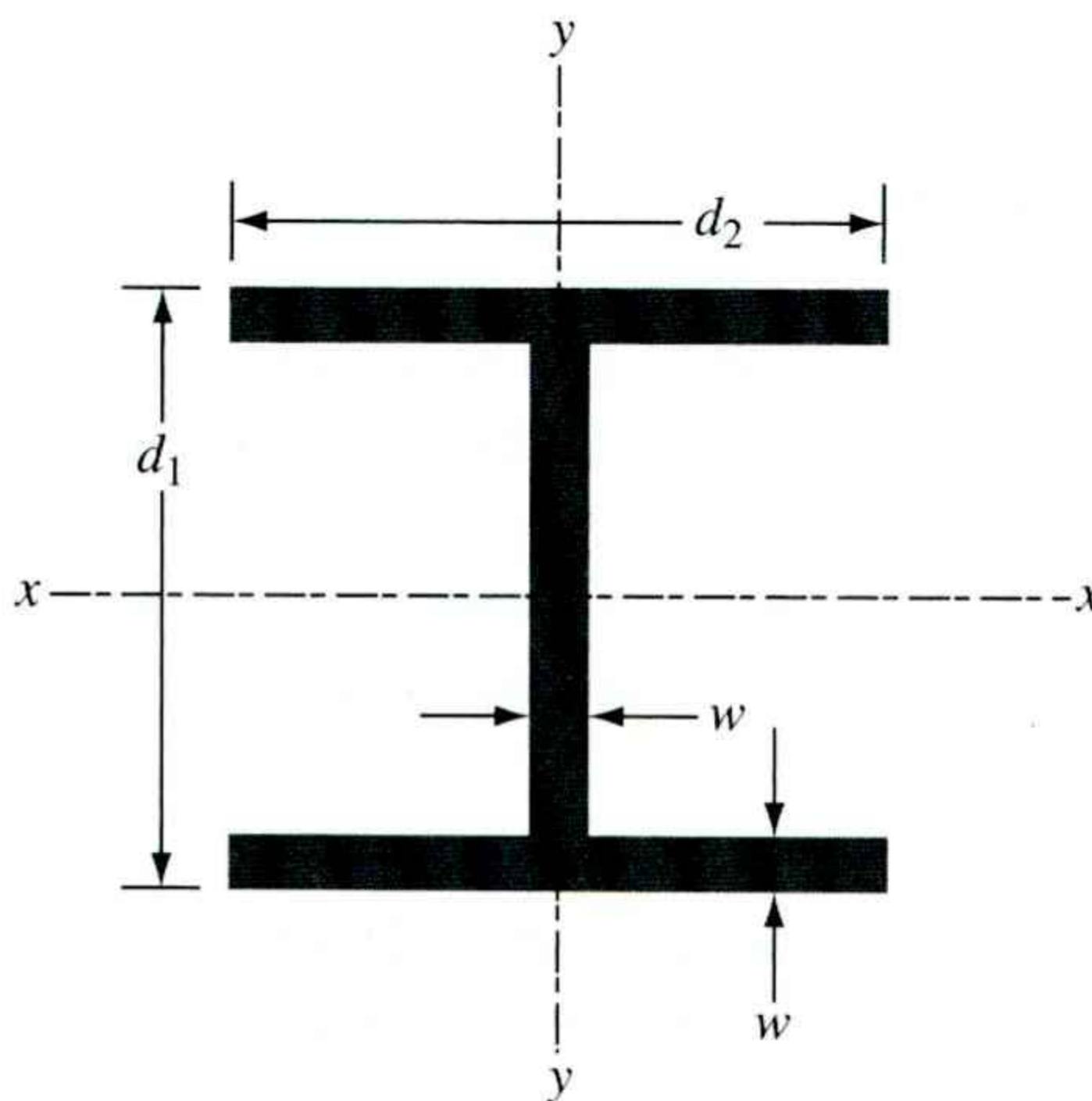


Table 11.1b Common H-Pile Sections used in the United States (English Units)

Designation size (in.) × weight (lb/ft)	Depth d_1 (in.)	Section area (in 2)	Flange and web thickness w (in.)	Flange width d_2 (in.)	Moment of inertia (in 4)	
					I_{xx}	I_{yy}
HP 8 × 36	8.02	10.6	0.445	8.155	119	40.3
HP 10 × 57	9.99	16.8	0.565	10.225	294	101
× 42	9.70	12.4	0.420	10.075	210	71.7
HP 12 × 84	12.28	24.6	0.685	12.295	650	213
× 74	12.13	21.8	0.610	12.215	570	186
× 63	11.94	18.4	0.515	12.125	472	153
× 53	11.78	15.5	0.435	12.045	394	127
HP 13 × 100	13.15	29.4	0.766	13.21	886	294
× 87	12.95	25.5	0.665	13.11	755	250
× 73	12.74	21.6	0.565	13.01	630	207
× 60	12.54	17.5	0.460	12.90	503	165
HP 14 × 117	14.21	34.4	0.805	14.89	1220	443
× 102	14.01	30.0	0.705	14.78	1050	380
× 89	13.84	26.1	0.615	14.70	904	326
× 73	13.61	21.4	0.505	14.59	729	262

Table 11.2a Selected Pipe Pile Sections (SI Units)

Outside diameter (mm)	Wall thickness (mm)	Area of steel (cm 2)
219	3.17	21.5
	4.78	32.1
	5.56	37.3
	7.92	52.7
254	4.78	37.5
	5.56	43.6
	6.35	49.4
305	4.78	44.9
	5.56	52.3
	6.35	59.7
406	4.78	60.3
	5.56	70.1
	6.35	79.8
457	5.56	80
	6.35	90
	7.92	112
508	5.56	88
	6.35	100
	7.92	125
610	6.35	121
	7.92	150
	9.53	179
	12.70	238

Table 11.2b Selected Pipe Pile Sections (English Units)

Outside diameter (in.)	Wall thickness (in.)	Area of steel (in 2)
8 $\frac{5}{8}$	0.125	3.34
	0.188	4.98
	0.219	5.78
	0.312	8.17
10	0.188	5.81
	0.219	6.75
	0.250	7.66
12	0.188	6.96
	0.219	8.11
	0.250	9.25
16	0.188	9.34
	0.219	10.86
	0.250	12.37
18	0.219	12.23
	0.250	13.94
	0.312	17.34
20	0.219	13.62
	0.250	15.51
	0.312	19.30
24	0.250	18.7
	0.312	23.2
	0.375	27.8
	0.500	36.9

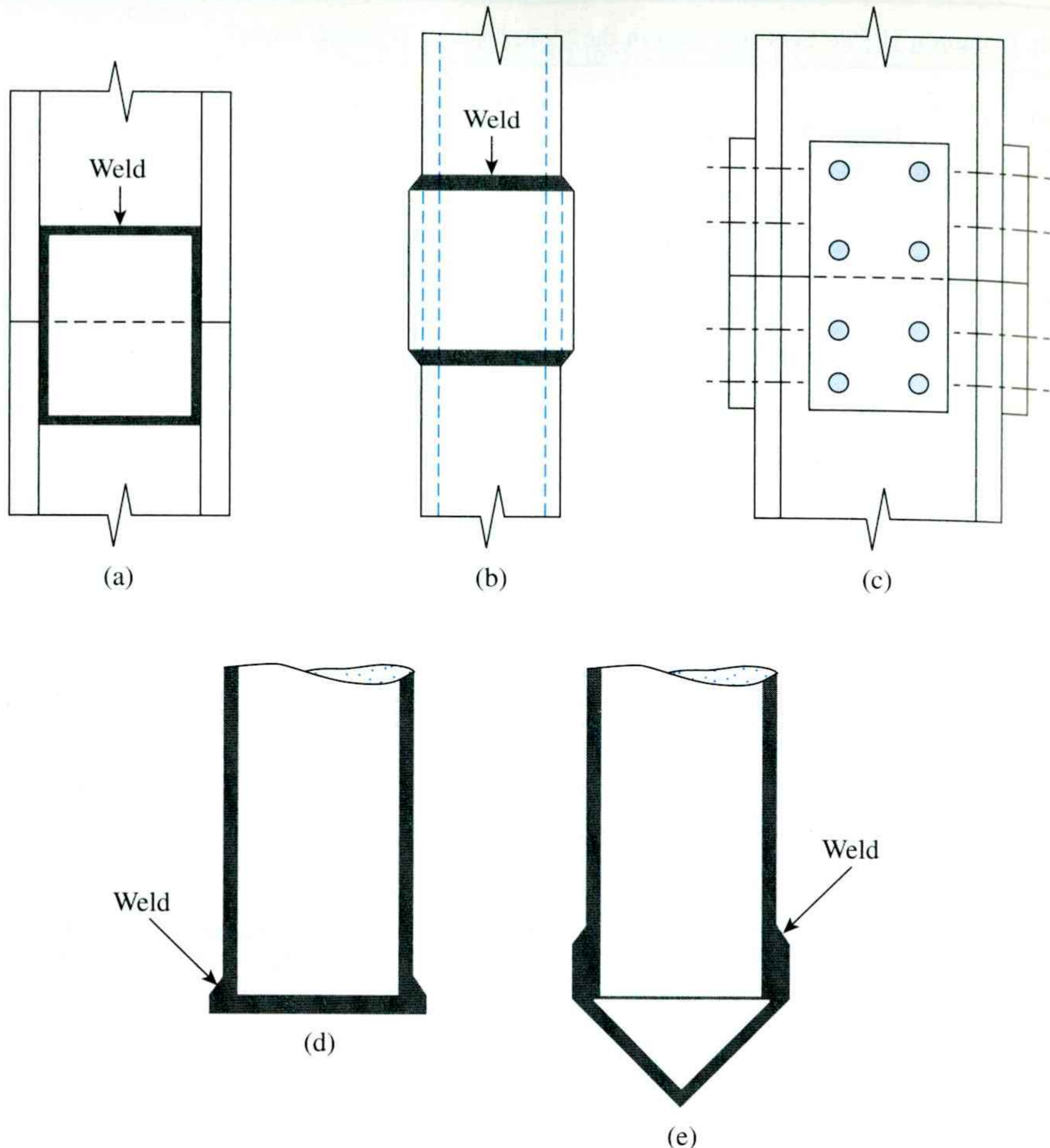


Figure 11.2 Steel piles: (a) splicing of H-pile by welding; (b) splicing of pipe pile by welding; (c) splicing of H-pile by rivets and bolts; (d) flat driving point of pipe pile; (e) conical driving point of pipe pile

Concrete Piles

Concrete piles may be divided into two basic categories: (a) precast piles and (b) cast-in-situ piles. *Precast piles* can be prepared by using ordinary reinforcement, and they can be square or octagonal in cross section. (See Figure 11.3.) Reinforcement is provided to enable the pile to resist the bending moment developed during pickup and transportation, the vertical load, and the bending moment caused by a lateral load. The piles are cast to desired lengths and cured before being transported to the work sites.

Some general facts about concrete piles are as follows:

- Usual length: 10 m to 15 m (30 ft to 50 ft)
- Usual load: 300 kN to 3000 kN (67 kip to 675 kip)
- Advantages:
 - a. Can be subjected to hard driving
 - b. Corrosion resistant
 - c. Can be easily combined with a concrete superstructure

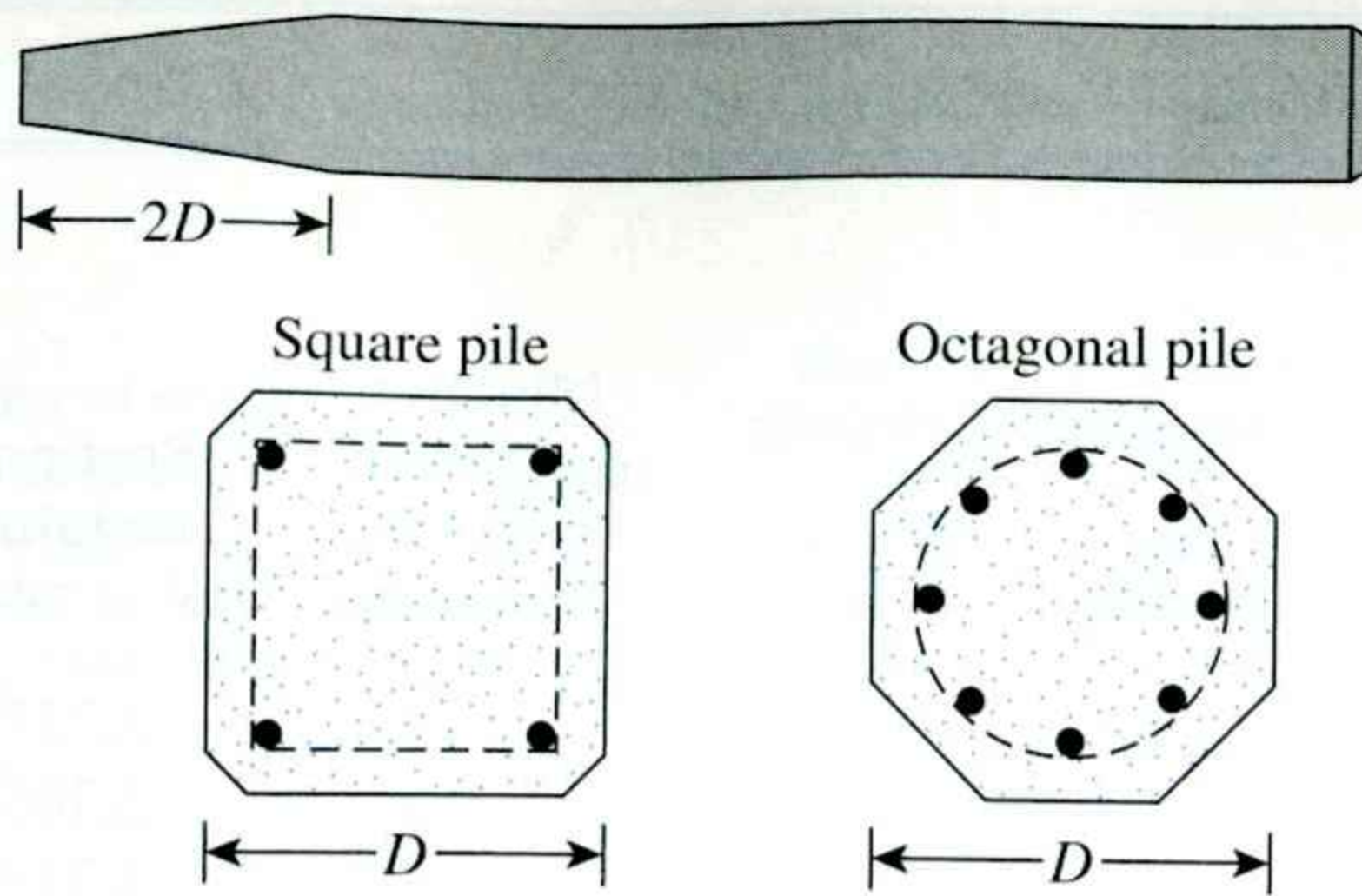


Figure 11.3 Precast piles with ordinary reinforcement

- Disadvantages:
 - Difficult to achieve proper cutoff
 - Difficult to transport

Precast piles can also be prestressed by the use of high-strength steel pre-stressing cables. The ultimate strength of these cables is about 1800 MN/m^2 ($\approx 260 \text{ ksi}$). During casting of the piles, the cables are pretensioned to about 900 to 1300 MN/m^2 (≈ 130 to 190 ksi), and concrete is poured around them. After curing, the cables are cut, producing a compressive force on the pile section. Table 11.3 gives additional information about prestressed concrete piles with square and octagonal cross sections.

Some general facts about precast prestressed piles are as follows:

- Usual length: 10 m to 45 m (30 ft to 150 ft)
- Maximum length: 60 m (200 ft)
- Maximum load: 7500 kN to 8500 kN (1700 kip to 1900 kip)

The advantages and disadvantages are the same as those of precast piles.

Cast-in-situ, or *cast-in-place*, piles are built by making a hole in the ground and then filling it with concrete. Various types of cast-in-place concrete piles are currently used in construction, and most of them have been patented by their manufacturers. These piles may be divided into two broad categories: (a) cased and (b) uncased. Both types may have a pedestal at the bottom.

Cased piles are made by driving a steel casing into the ground with the help of a mandrel placed inside the casing. When the pile reaches the proper depth the mandrel is withdrawn and the casing is filled with concrete. Figures 11.4a, 11.4b, 11.4c, and 11.4d show some examples of cased piles without a pedestal. Figure 11.4e shows a cased pile with a pedestal. The pedestal is an expanded concrete bulb that is formed by dropping a hammer on fresh concrete.

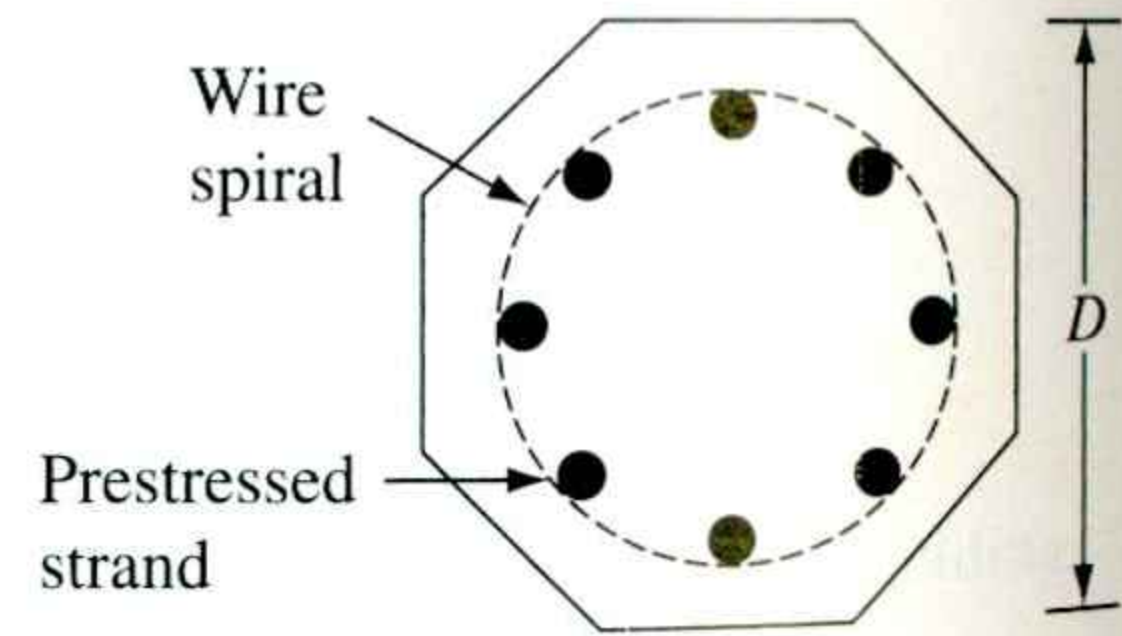
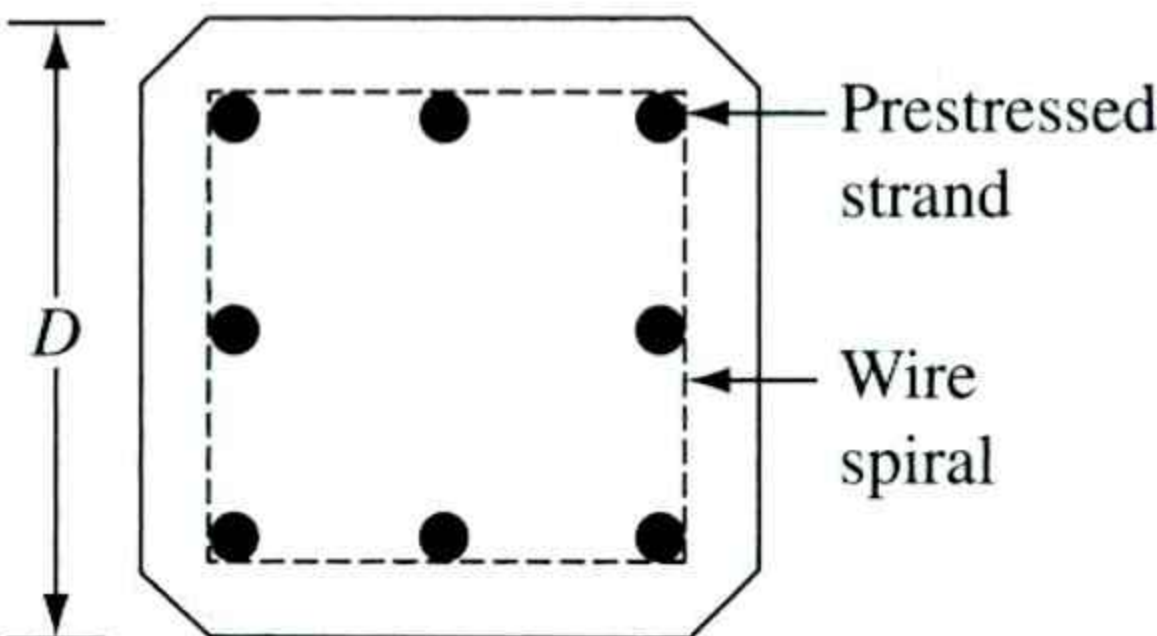
Some general facts about cased cast-in-place piles are as follows:

- Usual length: 5 m to 15 m (15 ft to 50 ft)
- Maximum length: 30 m to 40 m (100 ft to 130 ft)
- Usual load: 200 kN to 500 kN (45 kip to 115 kip)
- Approximate maximum load: 800 kN (180 kip)

Table 11.3a Typical Prestressed Concrete Pile in Use (SI Units)

Pile shape ^a	D (mm)	Area of cross section (cm ²)	Perimeter (mm)	Number of strands		Minimum effective prestress force (kN)	Section modulus (m ³ × 10 ⁻³)	Design bearing capacity (kN)	
				12.7-mm diameter	11.1-mm diameter			34.5	41.4
S	254	645	1016	4	4	312	2.737	556	778
O	254	536	838	4	4	258	1.786	462	555
S	305	929	1219	5	6	449	4.719	801	962
O	305	768	1016	4	5	369	3.097	662	795
S	356	1265	1422	6	8	610	7.489	1091	1310
O	356	1045	1168	5	7	503	4.916	901	1082
S	406	1652	1626	8	11	796	11.192	1425	1710
O	406	1368	1346	7	9	658	7.341	1180	1416
S	457	2090	1829	10	13	1010	15.928	1803	2163
O	457	1729	1524	8	11	836	10.455	1491	1790
S	508	2581	2032	12	16	1245	21.844	2226	2672
O	508	2136	1677	10	14	1032	14.355	1842	2239
S	559	3123	2235	15	20	1508	29.087	2694	3232
O	559	2587	1854	12	16	1250	19.107	2231	2678
S	610	3658	2438	18	23	1793	37.756	3155	3786
O	610	3078	2032	15	19	1486	34.794	2655	3186

^aS = square section; O = octagonal section



- Advantages:
 - a. Relatively cheap
 - b. Allow for inspection before pouring concrete
 - c. Easy to extend
- Disadvantages:
 - a. Difficult to splice after concreting
 - b. Thin casings may be damaged during driving
- Allowable load:

$$Q_{\text{all}} = A_s f_s + A_c f_c \quad (11.2)$$

where

A_s = area of cross section of steel

A_c = area of cross section of concrete

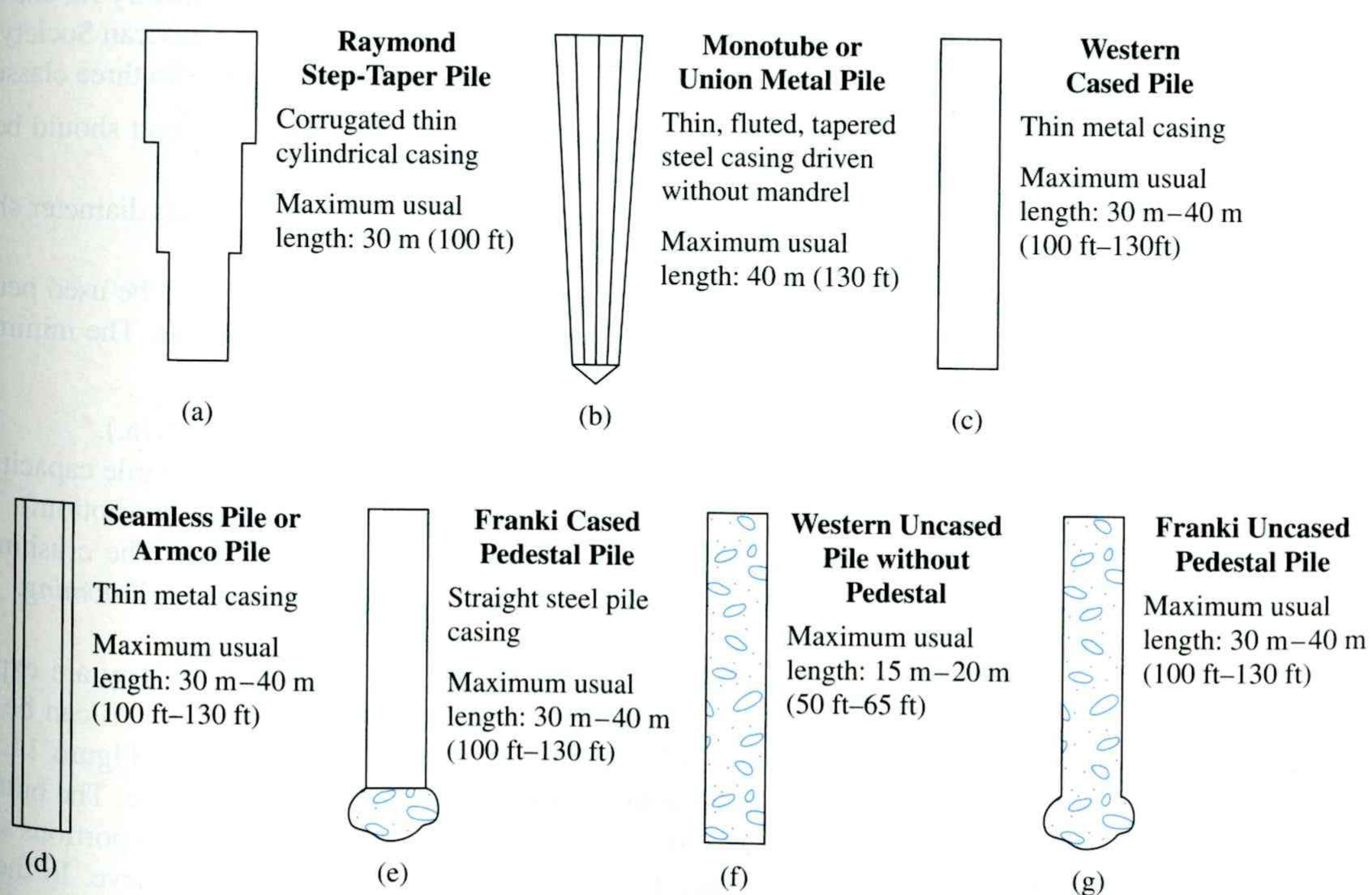
f_s = allowable stress of steel

f_c = allowable stress of concrete

Table 11.3b Typical Prestressed Concrete Pile in Use (English Units)

	Pile shape ^a	D (in.)	Area of cross section (in ²)	Perimeter (in.)	Number of strands		Minimum effective prestress force (kip)	Section modulus (in ³)	Design bearing capacity (kip)	
					½-in diameter	7/16-in diameter			Strength of concrete	5000 psi
41.4	S	10	100	40	4	4	70	167	125	175
778	O	10	83	33	4	4	58	109	104	125
555	S	12	144	48	5	6	101	288	180	216
962	O	12	119	40	4	5	83	189	149	178
795	S	14	196	56	6	8	137	457	245	295
1310	O	14	162	46	5	7	113	300	203	243
1082	S	16	256	64	8	11	179	683	320	385
1710	O	16	212	53	7	9	148	448	265	318
1416	S	18	324	72	10	13	227	972	405	486
2163	O	18	268	60	8	11	188	638	336	402
1790	S	20	400	80	12	16	280	1333	500	600
2672	O	20	331	66	10	14	234	876	414	503
2239	S	22	484	88	15	20	339	1775	605	727
3232	O	22	401	73	12	16	281	1166	502	602
2678	S	24	576	96	18	23	403	2304	710	851
3786	O	24	477	80	15	19	334	2123	596	716
3186										

^aS = square section; O = octagonal section

**Figure 11.4** Cast-in-place concrete piles

Figures 11.4f and 11.4g are two types of uncased pile, one with a pedestal and the other without. The uncased piles are made by first driving the casing to the desired depth and then filling it with fresh concrete. The casing is then gradually withdrawn.

Following are some general facts about uncased cast-in-place concrete piles:

- Usual length: 5 m to 15 m (15 ft to 50 ft)
- Maximum length: 30 m to 40 m (100 ft to 130 ft)
- Usual load: 300 kN to 500 kN (67 kip to 115 kip)
- Approximate maximum load: 700 kN (160 kip)
- Advantages:
 - a. Initially economical
 - b. Can be finished at any elevation
- Disadvantages:
 - a. Voids may be created if concrete is placed rapidly
 - b. Difficult to splice after concreting
 - c. In soft soils, the sides of the hole may cave in, squeezing the concrete
- Allowable load:

$$Q_{\text{all}} = A_c f_c \quad (11.3)$$

where

A_c = area of cross section of concrete

f_c = allowable stress of concrete

Timber Piles

Timber piles are tree trunks that have had their branches and bark carefully trimmed off. The maximum length of most timber piles is 10 to 20 m (30 to 65 ft). To qualify for use as a pile, the timber should be straight, sound, and without any defects. The American Society of Civil Engineers' *Manual of Practice*, No. 17 (1959), divided timber piles into three classes:

1. *Class A piles* carry heavy loads. The minimum diameter of the butt should be 356 mm (14 in.).
2. *Class B piles* are used to carry medium loads. The minimum butt diameter should be 305 to 330 mm (12 to 13 in.).
3. *Class C piles* are used in temporary construction work. They can be used permanently for structures when the entire pile is below the water table. The minimum butt diameter should be 305 mm (12 in.).

In any case, a pile tip should not have a diameter less than 150 mm (6 in.).

Timber piles cannot withstand hard driving stress; therefore, the pile capacity is generally limited. Steel shoes may be used to avoid damage at the pile tip (bottom). The tops of timber piles may also be damaged during the driving operation. The crushing of the wooden fibers caused by the impact of the hammer is referred to as *brooming*. To avoid damage to the top of the pile, a metal band or a cap may be used.

Splicing of timber piles should be avoided, particularly when they are expected to carry a tensile load or a lateral load. However, if splicing is necessary, it can be done by using *pipe sleeves* (see Figure 11.5a) or *metal straps and bolts* (see Figure 11.5b). The length of the sleeve should be at least five times the diameter of the pile. The butting ends should be cut square so that full contact can be maintained. The spliced portions should be carefully trimmed so that they fit tightly to the inside of the pipe sleeve. In the case of metal straps and bolts, the butting ends should also be cut square. The sides of the spliced portion should be trimmed plane for putting the straps on.

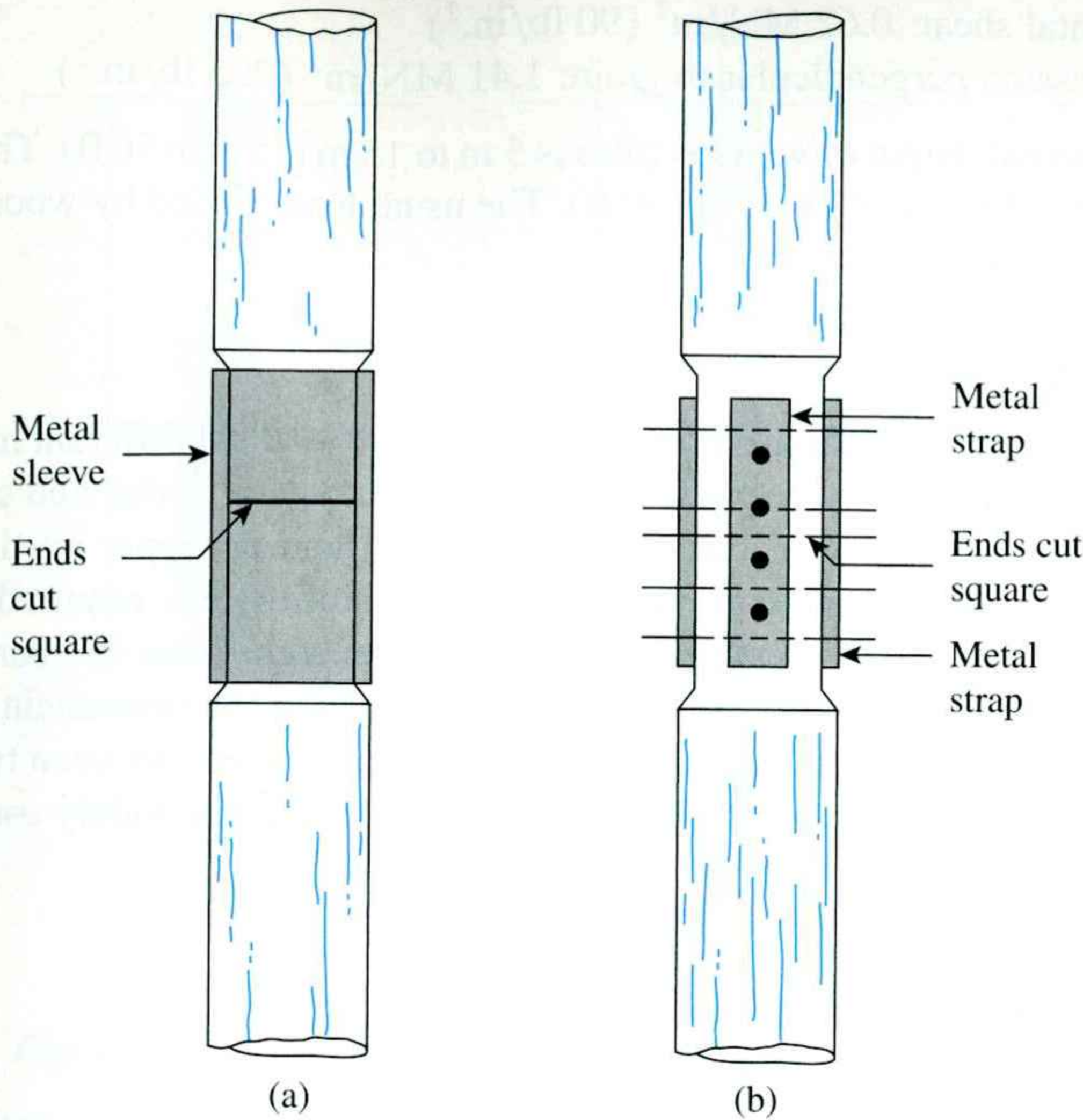


Figure 11.5 Splicing of timber piles: (a) use of pipe sleeves; (b) use of metal straps and bolts

Timber piles can stay undamaged indefinitely if they are surrounded by saturated soil. However, in a marine environment, timber piles are subject to attack by various organisms and can be damaged extensively in a few months. When located above the water table, the piles are subject to attack by insects. The life of the piles may be increased by treating them with preservatives such as creosote.

The allowable load-carrying capacity of wooden piles is

$$Q_{\text{all}} = A_p f_w \quad (11.4)$$

where

A_p = average area of cross section of the pile

f_w = allowable stress on the timber

The following allowable stresses are for pressure-treated round timber piles made from Pacific Coast Douglas fir and Southern pine used in hydraulic structures (ASCE, 1993):

Pacific Coast Douglas Fir

- Compression parallel to grain: 6.04 MN/m^2 (875 lb/in.^2)
- Bending: 11.7 MN/m^2 (1700 lb/in.^2)
- Horizontal shear: 0.66 MN/m^2 (95 lb/in.^2)
- Compression perpendicular to grain: 1.31 MN/m^2 (190 lb/in.^2)

Southern Pine

- Compression parallel to grain: 5.7 MN/m^2 (825 lb/in.^2)
- Bending: 11.4 MN/m^2 (1650 lb/in.^2)

- Horizontal shear: 0.62 MN/m^2 (90 lb/in.^2)
- Compression perpendicular to grain: 1.41 MN/m^2 (205 lb/in.^2)

The usual length of wooden piles is 5 m to 15 m (15 ft to 50 ft). The maximum length is about 30 m to 40 m (100 ft to 130 ft). The usual load carried by wooden piles is 300 kN to 500 kN (67 kip to 115 kip).

Composite Piles

The upper and lower portions of *composite piles* are made of different materials. For example, composite piles may be made of steel and concrete or timber and concrete. Steel-and-concrete piles consist of a lower portion of steel and an upper portion of cast-in-place concrete. This type of pile is used when the length of the pile required for adequate bearing exceeds the capacity of simple cast-in-place concrete piles. Timber-and-concrete piles usually consist of a lower portion of timber pile below the permanent water table and an upper portion of concrete. In any case, forming proper joints between two dissimilar materials is difficult, and for that reason, composite piles are not widely used.

11.3 Estimating Pile Length

Selecting the type of pile to be used and estimating its necessary length are fairly difficult tasks that require good judgment. In addition to being broken down into the classification given in Section 11.2, piles can be divided into three major categories, depending on their lengths and the mechanisms of load transfer to the soil: (a) point bearing piles, (b) friction piles, and (c) compaction piles.

Point Bearing Piles

If soil-boring records establish the presence of bedrock or rocklike material at a site within a reasonable depth, piles can be extended to the rock surface. (See Figure 11.6a.) In this case, the ultimate capacity of the piles depends entirely on the load-bearing capacity of the underlying material; thus, the piles are called *point bearing piles*. In most of these cases, the necessary length of the pile can be fairly well established.

If, instead of bedrock, a fairly compact and hard stratum of soil is encountered at a reasonable depth, piles can be extended a few meters into the hard stratum. (See Figure 11.6b.) Piles with pedestals can be constructed on the bed of the hard stratum, and the ultimate pile load may be expressed as

$$Q_u = Q_p + Q_s \quad (11.5)$$

where

Q_p = load carried at the pile point

Q_s = load carried by skin friction developed at the side of the pile (caused by shearing resistance between the soil and the pile)

If Q_s is very small,

$$Q_s \approx Q_p \quad (11.6)$$

In this case, the required pile length may be estimated accurately if proper subsoil exploration records are available.

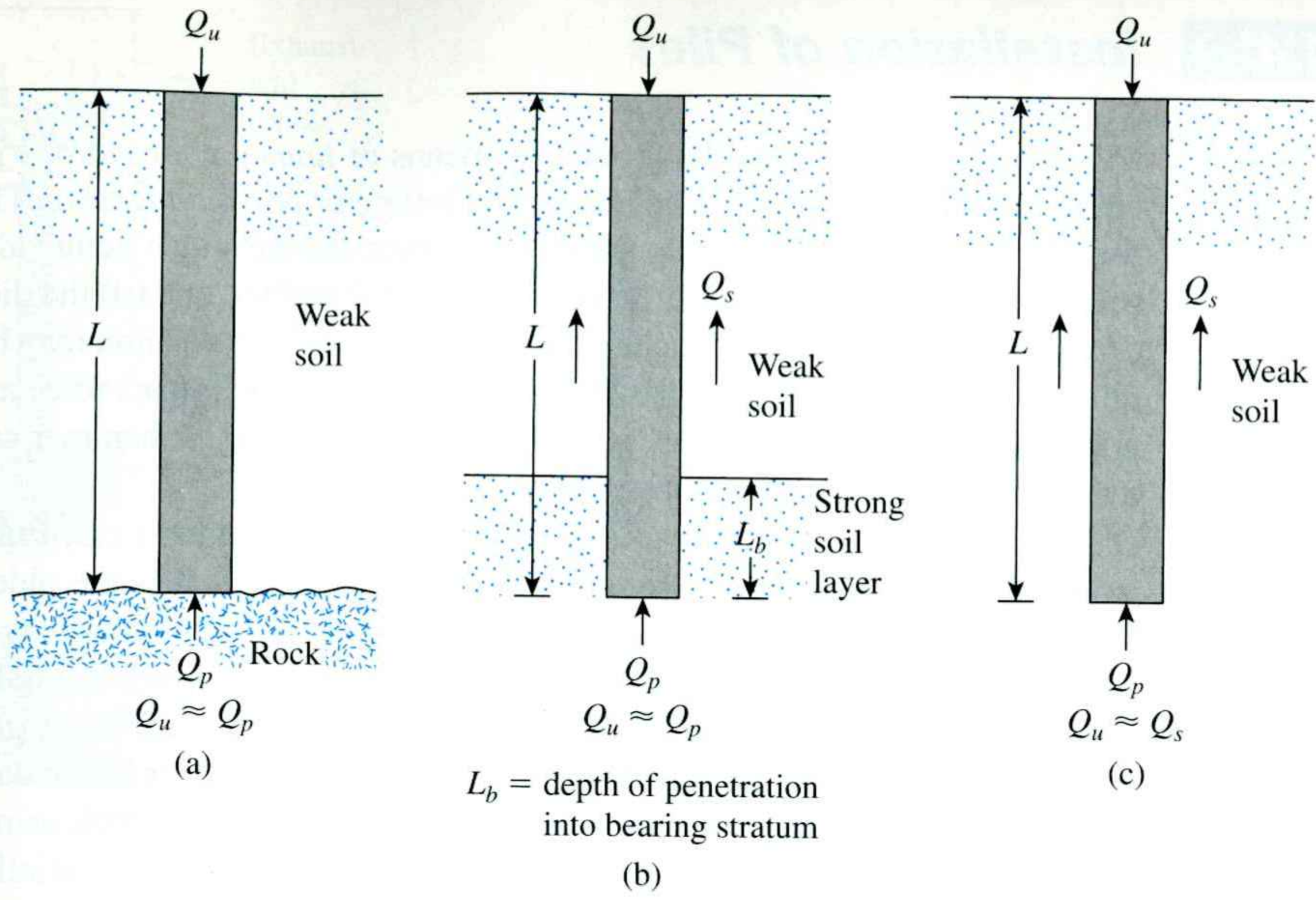


Figure 11.6 (a) and (b) Point bearing piles; (c) friction piles

Friction Piles

When no layer of rock or rocklike material is present at a reasonable depth at a site, point bearing piles become very long and uneconomical. In this type of subsoil, piles are driven through the softer material to specified depths. (See Figure 11.6c.) The ultimate load of the piles may be expressed by Eq. (11.5). However, if the value of Q_p is relatively small, then

$$Q_u \approx Q_s \quad (11.7)$$

These piles are called *friction piles*, because most of their resistance is derived from skin friction. However, the term *friction pile*, although used often in the literature, is a misnomer: In clayey soils, the resistance to applied load is also caused by *adhesion*.

The lengths of friction piles depend on the shear strength of the soil, the applied load, and the pile size. To determine the necessary lengths of these piles, an engineer needs a good understanding of soil–pile interaction, good judgment, and experience. Theoretical procedures for calculating the load-bearing capacity of piles are presented later in the chapter.

Compaction Piles

Under certain circumstances, piles are driven in granular soils to achieve proper compaction of soil close to the ground surface. These piles are called *compaction piles*. The lengths of compaction piles depend on factors such as (a) the relative density of the soil before compaction, (b) the desired relative density of the soil after compaction, and (c) the required depth of compaction. These piles are generally short; however, some field tests are necessary to determine a reasonable length.

11.4**Installation of Piles**

Most piles are driven into the ground by means of *hammers* or *vibratory drivers*. In special circumstances, piles can also be inserted by *jetting* or *partial augering*. The types of hammer used for pile driving include (a) the drop hammer, (b) the single-acting air or steam hammer, (c) the double-acting and differential air or steam hammer, and (d) the diesel hammer. In the driving operation, a cap is attached to the top of the pile. A cushion may be used between the pile and the cap. The cushion has the effect of reducing the impact force and spreading it over a longer time; however, the use of the cushion is optional. A hammer cushion is placed on the pile cap. The hammer drops on the cushion.

Figure 11.7 illustrates various hammers. A drop hammer (see Figure 11.7a) is raised by a winch and allowed to drop from a certain height H . It is the oldest type of hammer used for pile driving. The main disadvantage of the drop hammer is its slow rate of blows. The principle of the single-acting air or steam hammer is shown in Figure 11.7b. The striking part, or ram, is raised by air or steam pressure and then drops by gravity. Figure 11.7c shows the operation of the double-acting and differential air or steam hammer. Air or steam is used both to raise the ram and to push it downward, thereby increasing the impact velocity of the ram. The diesel hammer (see Figure 11.7d) consists essentially of a ram, an anvil block, and a fuel-injection system. First the ram is raised and fuel is injected near the anvil. Then the ram is released. When the ram drops, it compresses the air-fuel mixture, which ignites. This action, in effect, pushes the pile downward and raises the ram. Diesel hammers work well under hard driving conditions. In soft soils, the downward movement of the pile is rather large, and the upward movement of the ram is small. This differential may

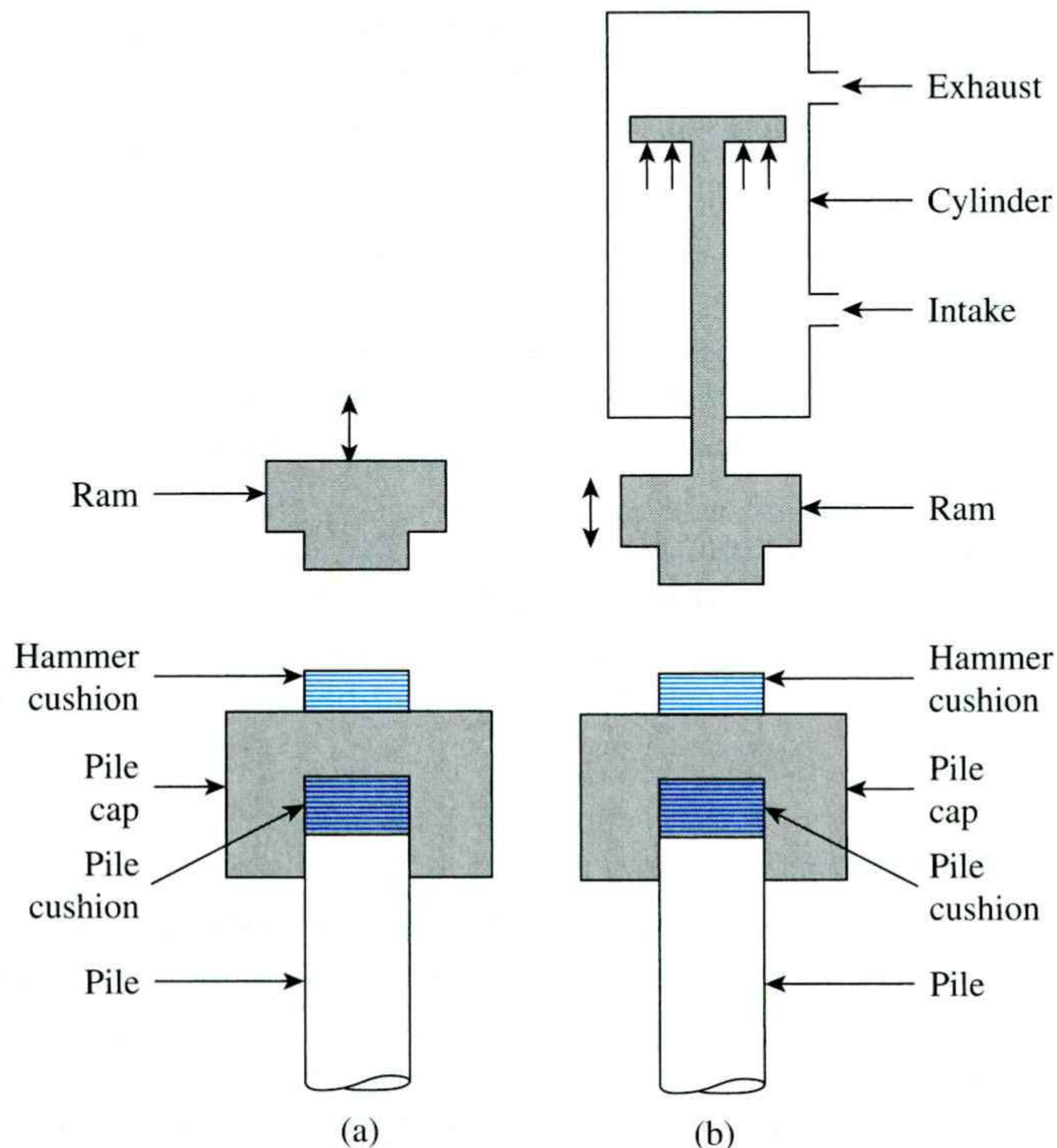


Figure 11.7 Pile-driving equipment: (a) drop hammer; (b) single-acting air or steam hammer

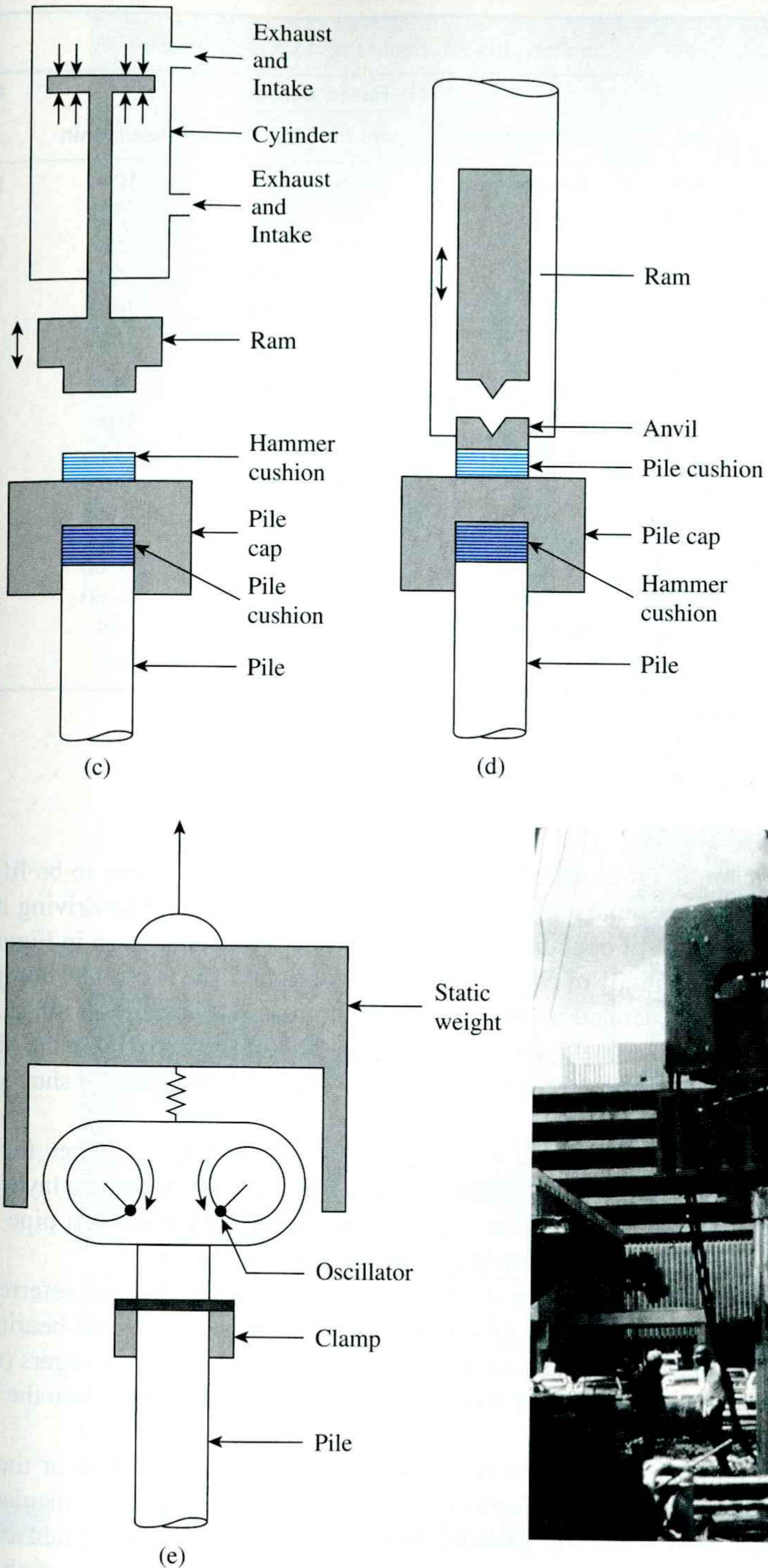


Figure 11.7 (continued) Pile-driving equipment: (c) double-acting and differential air or steam hammer; (d) diesel hammer; (e) vibratory pile driver; (f) photograph of a vibratory pile driver (Courtesy of Michael W. O'Neill, University of Houston)

Table 11.4 Examples of Commercially Available Pile-Driving Hammers

Maker of hammer [†]	Model No.	Hammer type	Rated energy			Ram weight	
			kN-m	kip-ft	Blows/min	kN	kip
V	400C	Single acting	153.9	113.5	100	177.9	40.0
M	S-20		81.3	60.0	60	89.0	20.0
M	S-8		35.3	26.0	53	35.6	8.0
M	S-5		22.0	16.3	60	22.2	5.0
R	5/O		77.1	56.9	44	77.8	17.5
R	2/O		44.1	32.5	50	44.5	10.0
V	200C	Double acting	68.1	50.2	98	89.0	20.0
V	140C	or	48.8	36.0	103	62.3	14.0
V	80C	differential	33.1	24.5	111	35.6	8.0
V	65C		26.0	19.2	117	28.9	6.5
R	150C		66.1	48.8	95–105	66.7	15.0
V	4N100	Diesel	58.8	43.4	50–60	23.5	5.3
V	IN100		33.4	24.6	50–60	13.3	3.0
M	DE40		43.4	32.0	48	17.8	4.0
M	DE30		30.4	22.4	48	12.5	2.8

[†]V—Vulcan Iron Works, Florida

M—McKiernan-Terry, New Jersey

R—Raymond International, Inc., Texas

not be sufficient to ignite the air-fuel system, so the ram may have to be lifted manually. Table 11.4 provides some examples of commercially available pile-driving hammers.

The principles of operation of a vibratory pile driver are shown in Figure 11.7e. This driver consists essentially of two counterrotating weights. The horizontal components of the centrifugal force generated as a result of rotating masses cancel each other. As a result, a sinusoidal dynamic vertical force is produced on the pile and helps drive the pile downward.

Figure 11.7f is a photograph of a vibratory pile driver. Figure 11.8 shows a pile-driving operation in the field.

Jetting is a technique that is sometimes used in pile driving when the pile needs to penetrate a thin layer of hard soil (such as sand and gravel) overlying a layer of softer soil. In this technique, water is discharged at the pile point by means of a pipe 50 to 75 mm (2 to 3 in.) in diameter to wash and loosen the sand and gravel.

Piles driven at an angle to the vertical, typically 14 to 20°, are referred to as *batter piles*. Batter piles are used in group piles when higher lateral load-bearing capacity is required. Piles also may be advanced by partial augering, with power augers (see Chapter 2) used to predrill holes part of the way. The piles can then be inserted into the holes and driven to the desired depth.

Piles may be divided into two categories based on the nature of their placement: *displacement piles* and *nondisplacement piles*. Driven piles are displacement piles, because they move some soil laterally; hence, there is a tendency for densification of soil surrounding them. Concrete piles and closed-ended pipe piles are high-displacement piles. However, steel H-piles displace less soil laterally during driving, so they are low-displacement piles. In contrast, bored piles are nondisplacement piles because their placement causes very little change in the state of stress in the soil.

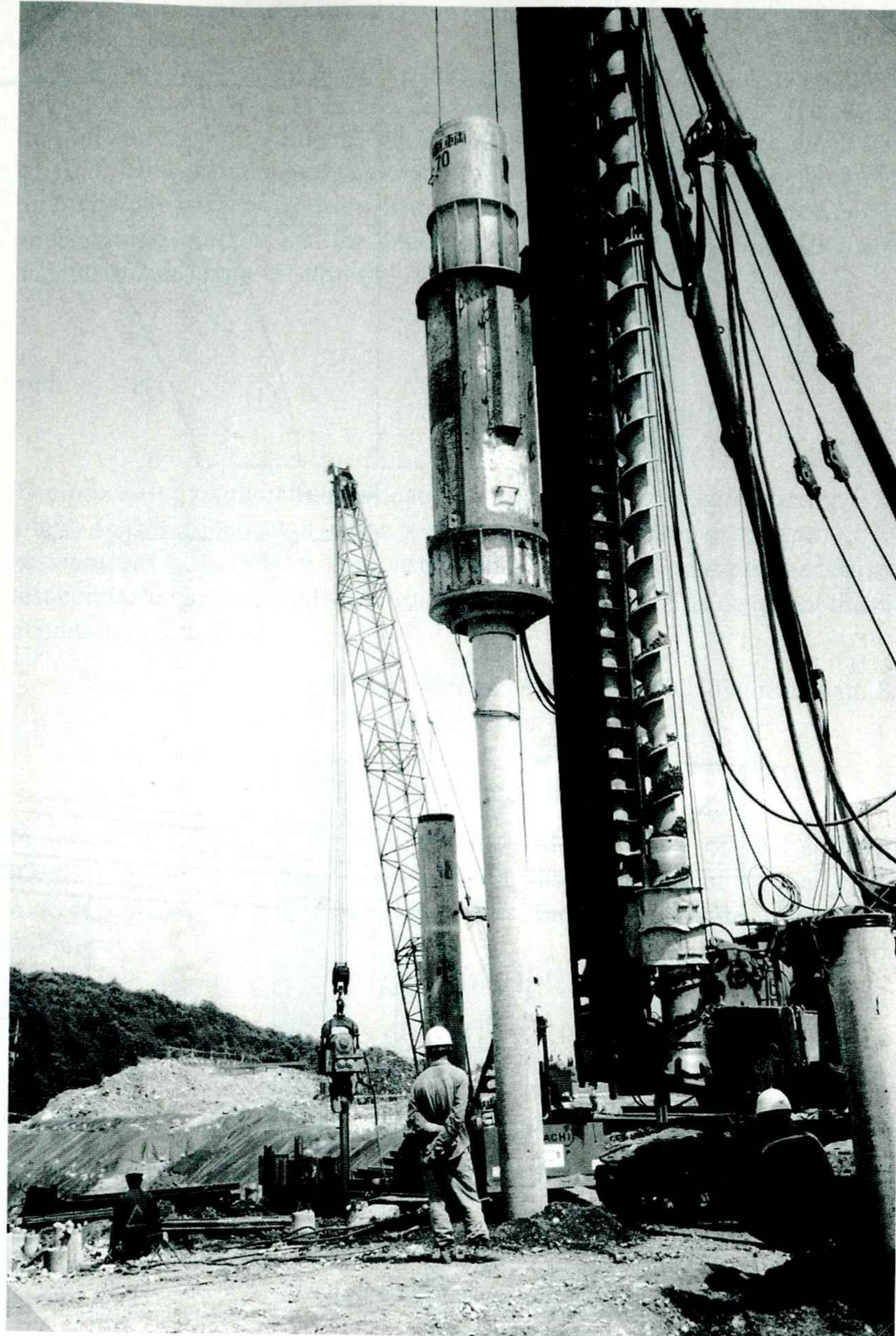


Figure 11.8 A pile-driving operation in the field (Courtesy of E. C. Shin, University of Incheon, Korea)

11.5

Load Transfer Mechanism

The load transfer mechanism from a pile to the soil is complicated. To understand it, consider a pile of length L , as shown in Figure 11.9a. The load on the pile is gradually increased from zero to $Q_{(z=0)}$ at the ground surface. Part of this load will be resisted by

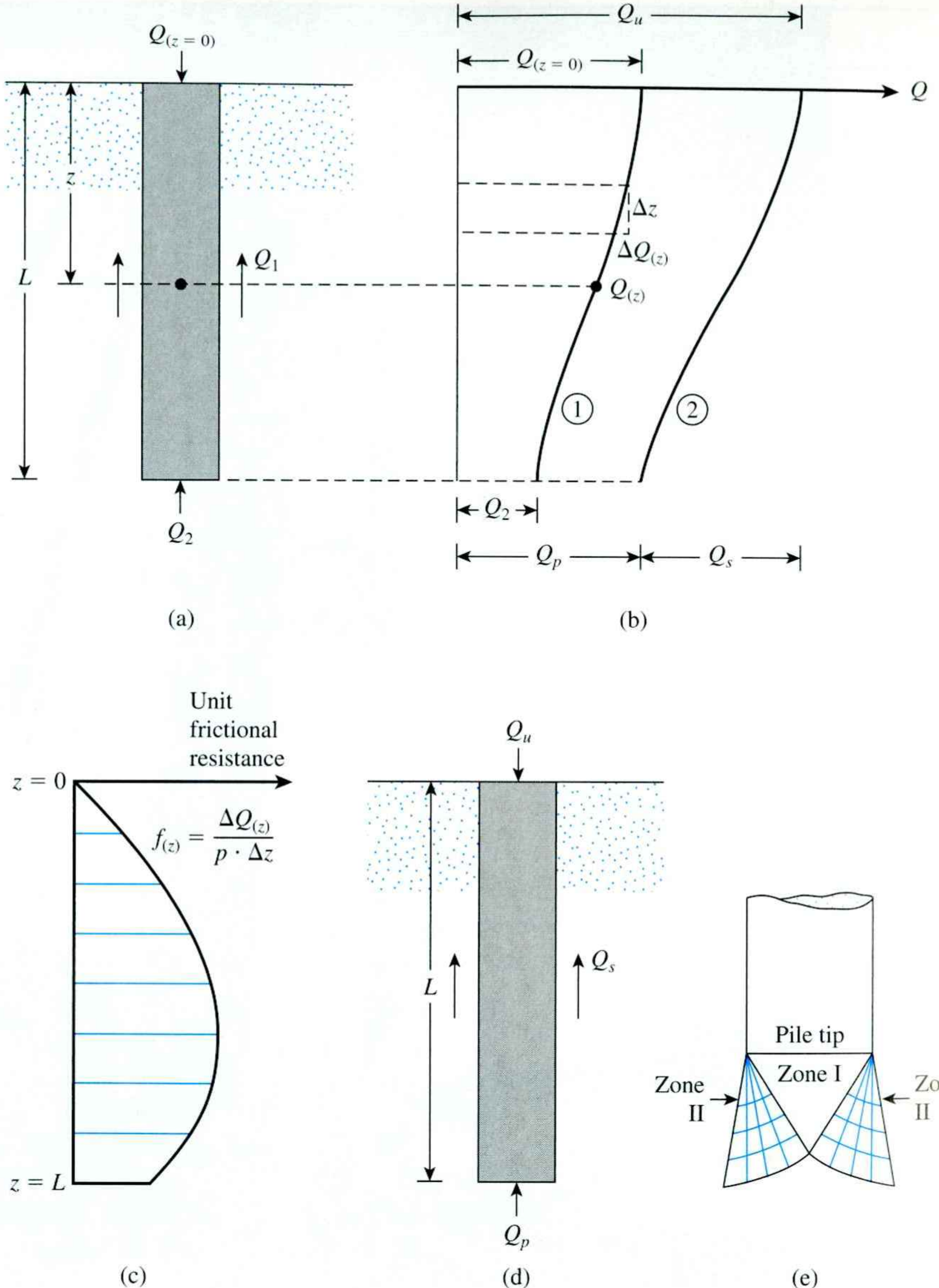


Figure 11.9 Load transfer mechanism for piles

the side friction developed along the shaft, Q_1 , and part by the soil below the tip of the pile, Q_2 . Now, how are Q_1 and Q_2 related to the total load? If measurements are made to obtain the load carried by the pile shaft, $Q_{(z)}$, at any depth z , the nature of the variation found will be like that shown in curve 1 of Figure 11.9b. The *frictional resistance per unit area* at any depth z may be determined as

$$f_{(z)} = \frac{\Delta Q_{(z)}}{(p)(\Delta z)} \quad (11.8)$$

where p = perimeter of the cross section of the pile. Figure 11.9c shows the variation of $f_{(z)}$ with depth.

If the load Q at the ground surface is gradually increased, maximum frictional resistance along the pile shaft will be fully mobilized when the relative displacement between the soil and the pile is about 5 to 10 mm (0.2 to 0.3 in.), irrespective of the pile size and length L . However, the maximum point resistance $Q_2 = Q_p$ will not be mobilized until the tip of the pile has moved about 10 to 25% of the pile width (or diameter). (The lower limit applies to driven piles and the upper limit to bored piles). At ultimate load (Figure 11.9d and curve 2 in Figure 11.9b), $Q_{(z=0)} = Q_u$. Thus,

$$Q_1 = Q_s$$

and

$$Q_2 = Q_p$$

The preceding explanation indicates that Q_s (or the unit skin friction, f , along the pile shaft) is developed at a *much smaller pile displacement compared with the point resistance, Q_p* . In order to demonstrate this point, let us consider the results of a pile load test conducted in the field by Mansur and Hunter (1970). The details of the pile and subsoil conditions are as follow:

Type of pile: Steel pile with 406 mm (16 in.) outside diameter with 8.15 mm (0.321 in.) wall thickness

Type of subsoil: Sand

Length of pile embedment: 16.8 m (55 ft)

Figure 11.10a shows the load test results, which is a plot of load at the top of the pile [$Q_{(z=0)}$] versus settlement(s). Figure 11.10b shows the plot of the load carried by the pile shaft [$Q_{(z)}$] at any depth. It was reported by Mansur and Hunter (1970) that, for this test, at failure

$$Q_u \approx 1601 \text{ kN} (360 \text{ kip})$$

$$Q_p \approx 416 \text{ kN} (93.6 \text{ kip})$$

and

$$Q_s \approx 1185 \text{ kN} (266.4 \text{ kip})$$

Now, let us consider the load distribution in Figure 11.10b when the pile settlement(s) is about 2.5 mm. For this condition,

$$Q_{(z=0)} \approx 667 \text{ kN}$$

$$Q_2 \approx 93 \text{ kN}$$

$$Q_1 \approx 574 \text{ kN}$$

Hence, at $s = 2.5 \text{ mm}$,

$$\frac{Q_2}{Q_p} = \frac{93}{416} (100) = 22.4\%$$

and

$$\frac{Q_1}{Q_s} = \frac{574}{1185} (100) = 48.4\%$$

Thus, it is obvious that the skin friction is mobilized faster at low settlement levels as compared to the point load.

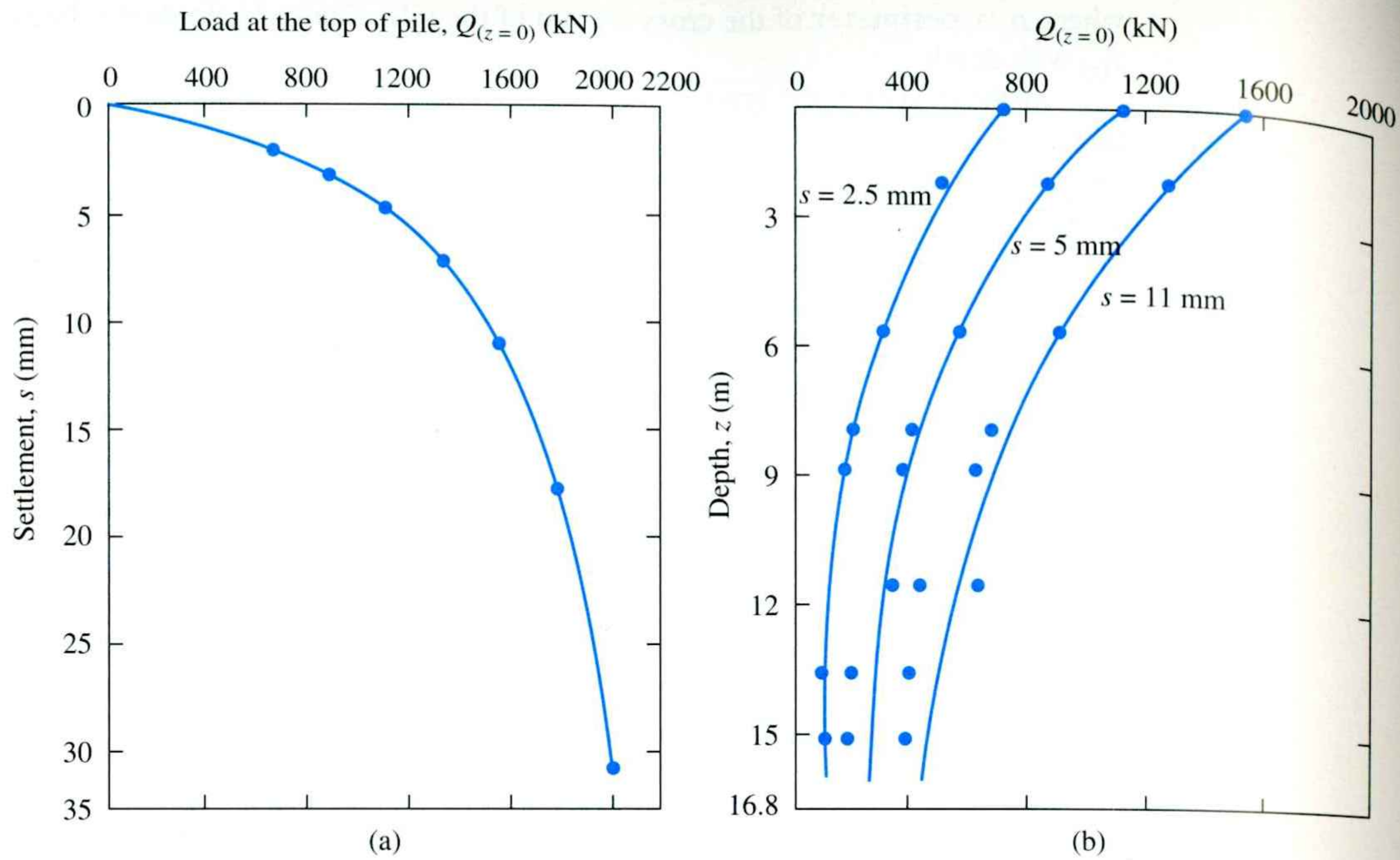


Figure 11.10 Load test results on a pipe pile in sand (Based on Mansur and Hunter, 1970)

At ultimate load, the failure surface in the soil at the pile tip (a bearing capacity failure caused by Q_p) is like that shown in Figure 11.9e. Note that pile foundations are deep foundations and that the soil fails mostly in a *punching mode*, as illustrated previously in Figures 3.1c and 3.3. That is, a *triangular zone*, I, is developed at the pile tip, which is pushed downward without producing any other visible slip surface. In dense sands and stiff clayey soils, a *radial shear zone*, II, may partially develop. Hence, the load displacement curves of piles will resemble those shown in Figure 3.1c.

11.6 Equations for Estimating Pile Capacity

The ultimate load-carrying capacity Q_u of a pile is given by the equation

$$Q_u = Q_p + Q_s \quad (11.9)$$

where

Q_p = load-carrying capacity of the pile point

Q_s = frictional resistance (skin friction) derived from the soil–pile interface (see Figure 11.11)

Numerous published studies cover the determination of the values of Q_p and Q_s . Excellent reviews of many of these investigations have been provided by Vesic (1977), Meyerhof (1976), and Coyle and Castello (1981). These studies afford an insight into the problem of determining the ultimate pile capacity.

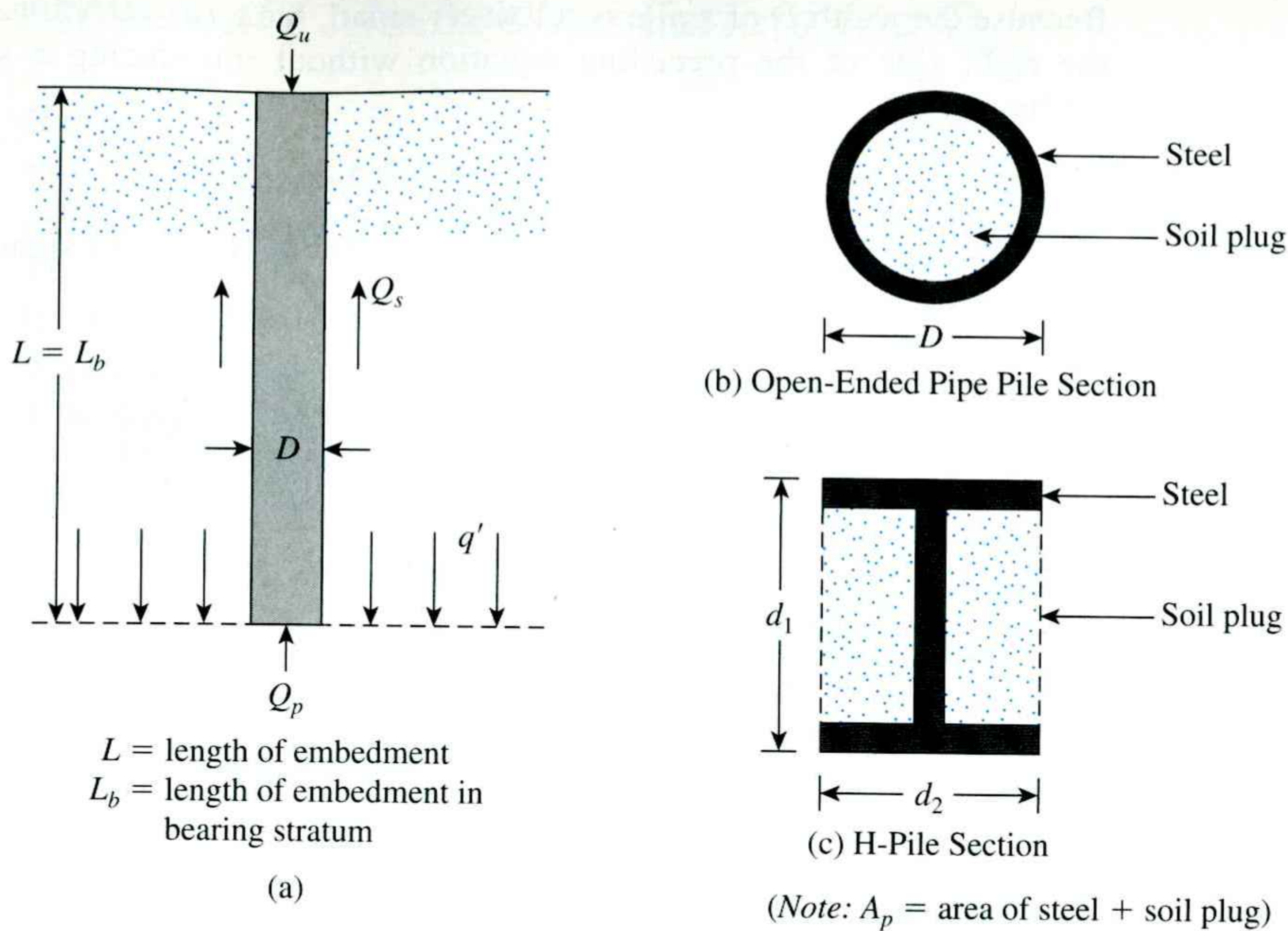


Figure 11.11 Ultimate load-carrying capacity of pile

Point Bearing Capacity, Q_p

The ultimate bearing capacity of shallow foundations was discussed in Chapter 3. According to Terzaghi's equations,

$$q_u = 1.3c'N_c + qN_q + 0.4\gamma BN_\gamma \quad (\text{for shallow square foundations})$$

and

$$q_u = 1.3c'N_c + qN_q + 0.3\gamma BN_\gamma \quad (\text{for shallow circular foundations})$$

Similarly, the general bearing capacity equation for shallow foundations was given in Chapter 3 (for vertical loading) as

$$q_u = c'N_c F_{cs}F_{cd} + qN_q F_{qs}F_{qd} + \frac{1}{2}\gamma BN_\gamma F_{ys}F_{yd}$$

Hence, in general, the ultimate load-bearing capacity may be expressed as

$$q_u = c'N_c^* + qN_q^* + \gamma BN_\gamma^* \quad (11.10)$$

where N_c^* , N_q^* , and N_γ^* are the bearing capacity factors that include the necessary shape and depth factors.

Pile foundations are deep. However, the ultimate resistance per unit area developed at the pile tip, q_p , may be expressed by an equation similar in form to Eq. (11.10), although the values of N_c^* , N_q^* , and N_γ^* will change. The notation used in this chapter for the width of a pile is D . Hence, substituting D for B in Eq. (11.10) gives

$$q_u = q_p = c'N_c^* + qN_q^* + \gamma DN_\gamma^* \quad (11.11)$$

Because the width D of a pile is relatively small, the term $\gamma D N_g^*$ may be dropped from the right side of the preceding equation without introducing a serious error; thus, we have

$$q_p = c'N_c^* + q'N_q^* \quad (11.12)$$

Note that the term q has been replaced by q' in Eq. (11.12), to signify effective vertical stress. Thus, the point bearing of piles is

$$Q_p = A_p q_p = A_p (c'N_c^* + q'N_q^*) \quad (11.13)$$

where

- A_p = area of pile tip
- c' = cohesion of the soil supporting the pile tip
- q_p = unit point resistance
- q' = effective vertical stress at the level of the pile tip
- N_c^*, N_q^* = the bearing capacity factors

Frictional Resistance, Q_s

The frictional, or skin, resistance of a pile may be written as

$$Q_s = \Sigma p \Delta L f \quad (11.14)$$

where

- p = perimeter of the pile section
- ΔL = incremental pile length over which p and f are taken to be constant
- f = unit friction resistance at any depth z

The various methods for estimating Q_p and Q_s are discussed in the next several sections. It needs to be reemphasized that, in the field, for full mobilization of the point resistance (Q_p), the pile tip must go through a displacement of 10 to 25% of the pile width (or diameter).

Allowable Load, Q_{all}

After the total ultimate load-carrying capacity of a pile has been determined by summing the point bearing capacity and the frictional (or skin) resistance, a reasonable factor of safety should be used to obtain the total allowable load for each pile, or

$$Q_{\text{all}} = \frac{Q_u}{\text{FS}}$$

where

- Q_{all} = allowable load-carrying capacity for each pile
- FS = factor of safety

The factor of safety generally used ranges from 2.5 to 4, depending on the uncertainties surrounding the calculation of ultimate load.

Sand

The point bearing capacity, q_p , of a pile in sand generally increases with the depth of embedment in the bearing stratum and reaches a maximum value at an embedment ratio of $L_b/D = (L_b/D)_{cr}$. Note that in a homogeneous soil L_b is equal to the actual embedment length of the pile, L . However, where a pile has penetrated into a bearing stratum, $L_b < L$. Beyond the critical embedment ratio, $(L_b/D)_{cr}$, the value of q_p remains constant ($q_p = q_l$). That is, as shown in Figure 11.12 for the case of a homogeneous soil, $L = L_b$.

For piles in sand, $c' = 0$, and Eq. (11.13) simplifies to

$$Q_p = A_p q_p = A_p q' N_q^* \quad (11.15)$$

The variation of N_q^* with soil friction angle ϕ' is shown in Figure 11.13. The interpolated values of N_q^* for various friction angles are also given in Table 11.5. However, Q_p should not exceed the limiting value $A_p q_l$; that is,

$$Q_p = A_p q' N_q^* \leq A_p q_l \quad (11.16)$$

Figure 11.13 Variation of the maximum values of N_q^* with soil friction angle ϕ' (From Meyerhof, G. G. (1976). "Bearing Capacity and Settlement of Pile Foundations," Journal of the Geotechnical Engineering Division, American Society of Civil Engineers, Vol. 102, No. GT3, pp. 197–228. With permission from ASCE.)

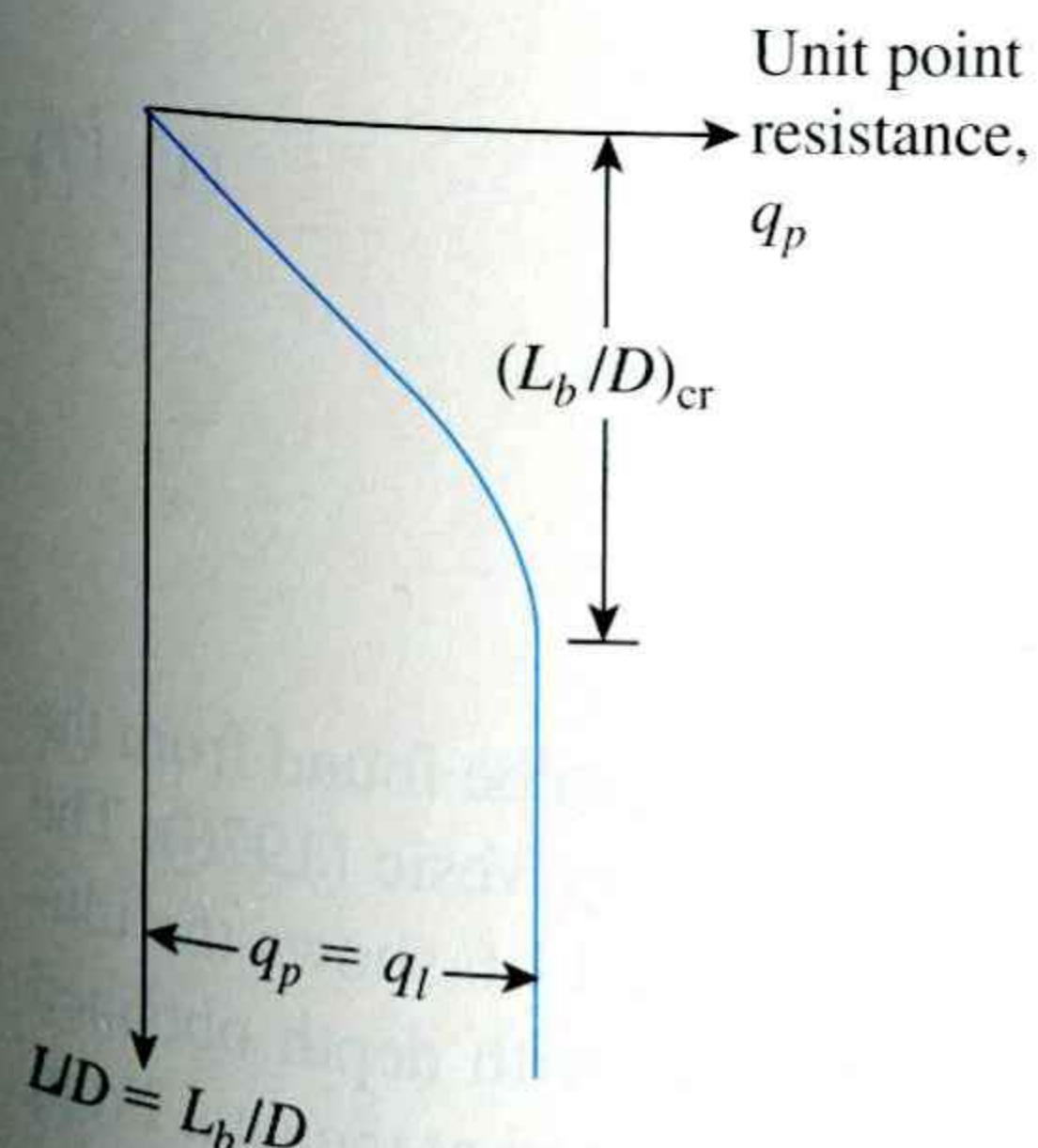


Figure 11.12 Nature of variation of unit point resistance in a homogeneous sand

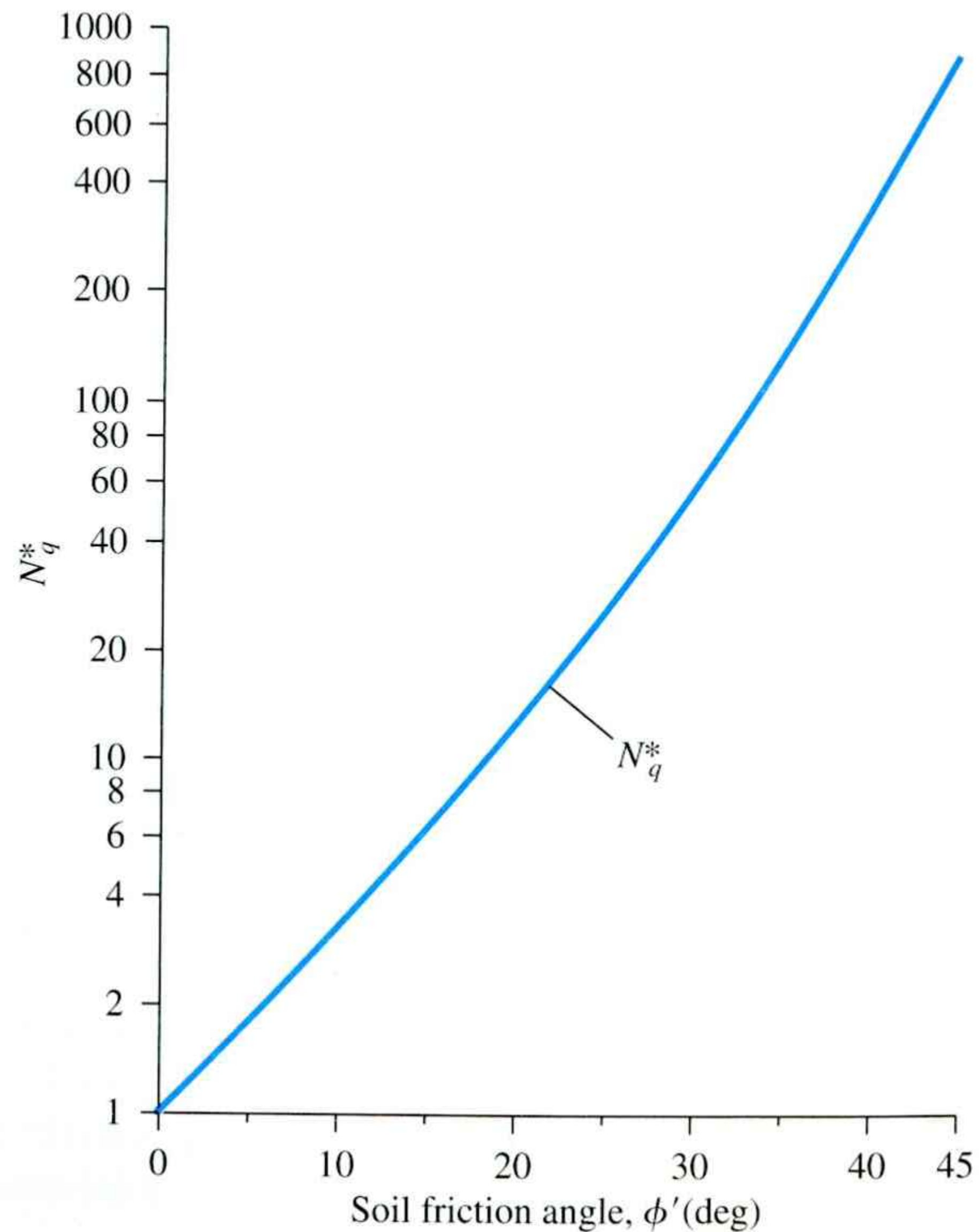


Table 11.5 Interpolated Values of N_q^* Based on Meyerhof's Theory

Soil friction angle, ϕ (deg)	N_q^*
20	12.4
21	13.8
22	15.5
23	17.9
24	21.4
25	26.0
26	29.5
27	34.0
28	39.7
29	46.5
30	56.7
31	68.2
32	81.0
33	96.0
34	115.0
35	143.0
36	168.0
37	194.0
38	231.0
39	276.0
40	346.0
41	420.0
42	525.0
43	650.0
44	780.0
45	930.0

The limiting point resistance is

$$q_l = 0.5 p_a N_q^* \tan \phi' \quad (11.17)$$

where

p_a = atmospheric pressure ($= 100 \text{ kN/m}^2$ or 2000 lb/ft^2)

ϕ' = effective soil friction angle of the bearing stratum

A good example of the concept of the critical embedment ratio can be found from the field load tests on a pile in sand at the Ogeechee River site reported by Vesic (1970). The pile tested was a steel pile with a diameter of 457 mm (18 in.). Table 11.6 shows the ultimate resistance at various depths. Figure 11.14 shows the plot of q_p with depth obtained from the field tests along with the range of standard penetration resistance at the site. From the figure, the following observations can be made.

1. There is a limiting value of q_p . For the tests under consideration, it is about $12,000 \text{ kN/m}^2$.
2. The $(L/D)_{cr}$ value is about 16 to 18.

Table 11.6 Ultimate Point Resistance, q_p , of Test Pile at the Ogeechee River Site As reported by Vesic (1970)

Pile diameter, D (m)	Depth of embedment, L (m)	L/D	q_p (kN/m ²)
0.457	3.02	6.61	3,304
0.457	6.12	13.39	9,365
0.457	8.87	19.4	11,472
0.457	12.0	26.26	11,587
0.457	15.00	32.82	13,971

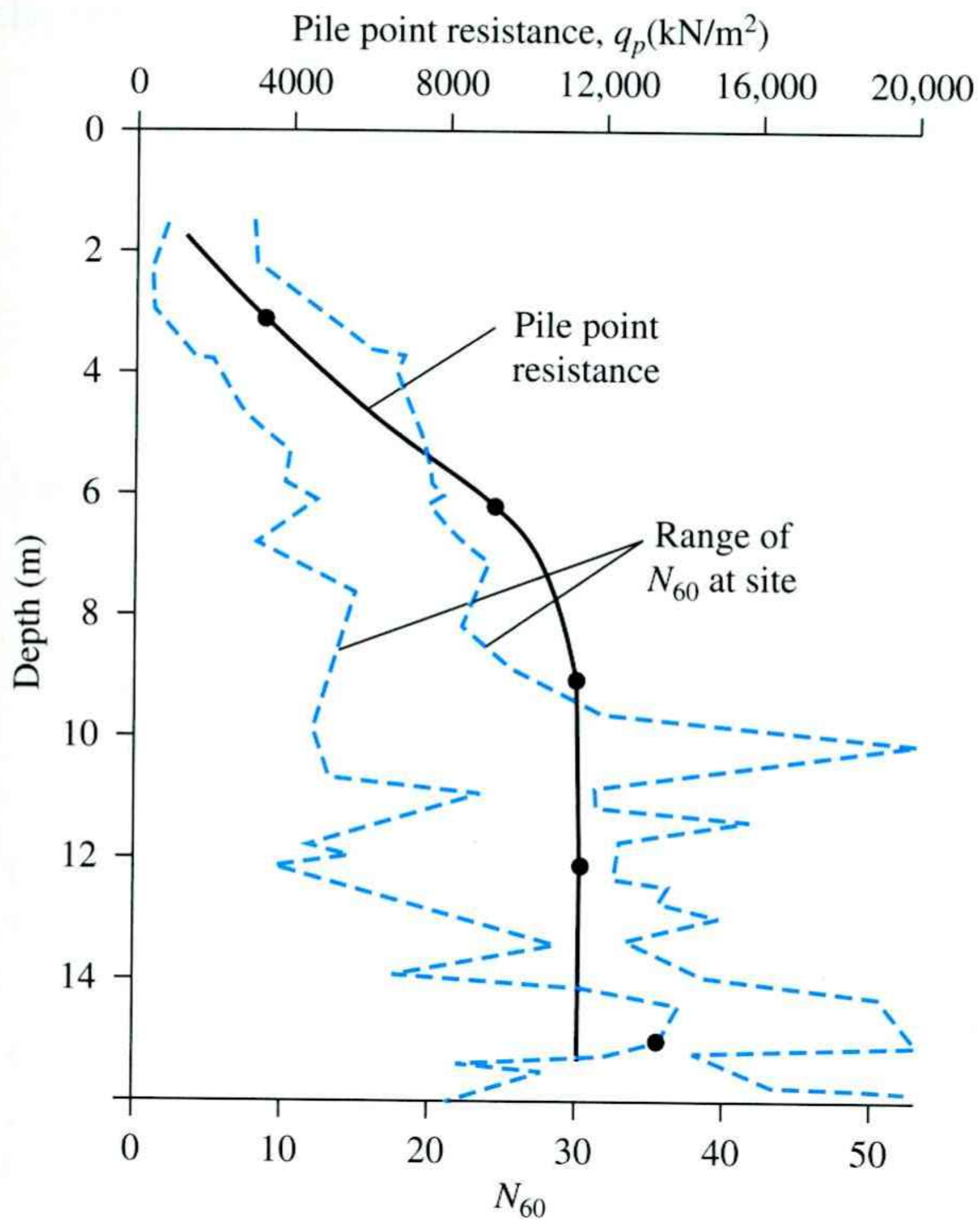


Figure 11.14 Vesic's pile test (1970) result—variation of q_p and N_{60} with depth

3. The average N_{60} value is about 30 for $L/D \geq (L/D)_{cr}$. Using Eq. (11.37), the limiting point resistance is $4p_a N_{60} = (4)(100)(30) = 12,000$ kN/m². This value is generally consistent with the field observation.

Clay ($\phi = 0$)

For piles in *saturated clays* under undrained conditions ($\phi = 0$), the net ultimate load can be given as

$$Q_p \approx N_c^* c_u A_p = 9c_u A_p \quad (11.18)$$

where c_u = undrained cohesion of the soil below the tip of the pile.

Sand

Vesic (1977) proposed a method for estimating the pile point bearing capacity based on the theory of *expansion of cavities*. According to this theory, on the basis of effective stress parameters, we may write

$$Q_p = A_p q_p = A_p \bar{\sigma}'_o N_\sigma^* \quad (11.19)$$

where

$\bar{\sigma}'_o$ = mean effective normal ground stress at the level of the pile point

$$= \left(\frac{1 + 2K_o}{3} \right) q' \quad (11.20)$$

$$K_o = \text{earth pressure coefficient at rest} = 1 - \sin \phi' \quad (11.21)$$

and

N_σ^* = bearing capacity factor

Note that Eq. (11.19) is a modification of Eq. (11.15) with

$$N_\sigma^* = \frac{3N_q^*}{(1 + 2K_o)} \quad (11.22)$$

According to Vesic's theory,

$$N_\sigma^* = f(I_{rr}) \quad (11.23)$$

where I_{rr} = reduced rigidity index for the soil. However,

$$I_{rr} = \frac{I_r}{1 + I_r \Delta} \quad (11.24)$$

where

$$I_r = \text{rigidity index} = \frac{E_s}{2(1 + \mu_s) q' \tan \phi'} = \frac{G_s}{q' \tan \phi'} \quad (11.25)$$

E_s = modulus of elasticity of soil

μ_s = Poisson's ratio of soil

G_s = shear modulus of soil

Δ = average volumatic strain in the plastic zone below the pile point

The general ranges of I_r for various soils are

Sand (relative density = 50% to 80%): 75 to 150

Silt : 50 to 75

In order to estimate I_r [Eq. (11.25)] and hence I_{rr} [Eq. (11.24)], the following approximations may be used (Chen and Kulhawy, 1994)

$$\frac{E_s}{p_a} = m \quad (11.26)$$

where

p_a = atmospheric pressure ($\approx 100 \text{ kN/m}^2$ or 2000 lb/ft^2)

$$m = \begin{cases} 100 \text{ to } 200 & (\text{loose soil}) \\ 200 \text{ to } 500 & (\text{medium dense soil}) \\ 500 \text{ to } 1000 & (\text{dense soil}) \end{cases}$$

$$\mu_s = 0.1 + 0.3 \left(\frac{\phi' - 25}{20} \right) \quad (\text{for } 25^\circ \leq \phi' \leq 45^\circ) \quad (11.27)$$

$$\Delta = 0.005 \left(1 - \frac{\phi' - 25}{20} \right) \frac{q'}{p_a} \quad (11.28)$$

On the basis of cone penetration tests in the field, Baldi et al. (1981) gave the following correlations for I_r :

$$I_r = \frac{300}{F_r(\%)} \quad (\text{for mechanical cone penetration}) \quad (11.29)$$

and

$$I_r = \frac{170}{F_r(\%)} \quad (\text{for electric cone penetration}) \quad (11.30)$$

For the definition of F_r , see Eq. (2.41). Table 11.7 gives the values of N_c^* for various values of I_{rr} and ϕ' .

Clay ($\phi = 0$)

In saturated clay ($\phi = 0$ condition), the net ultimate point bearing capacity of a pile can be approximated as

$$Q_p = A_p q_p = A_p c_u N_c^* \quad (11.31)$$

where c_u = undrained cohesion

According to the *expansion of cavity* theory of Vesic (1977),

$$N_c^* = \frac{4}{3} (\ln I_{rr} + 1) + \frac{\pi}{2} + 1 \quad (11.32)$$

The variations of N_c^* with I_{rr} for $\phi = 0$ condition are given in Table 11.8.

Now, referring to Eq. (11.24) for saturated clay with no volume change, $\Delta = 0$. Hence,

$$I_{rr} = I_r \quad (11.33)$$

Table 11.7 Bearing Capacity Factors N_{σ}^* Based on the Theory of Expansion of Cavities

ϕ'	I_{rr}									
	10	20	40	60	80	100	200	300	400	500
25	12.12	15.95	20.98	24.64	27.61	30.16	39.70	46.61	52.24	57.06
26	13.18	17.47	23.15	27.30	30.69	33.60	44.53	52.51	59.02	64.62
27	14.33	19.12	25.52	30.21	34.06	37.37	49.88	59.05	66.56	73.04
28	15.57	20.91	28.10	33.40	37.75	41.51	55.77	66.29	74.93	82.40
29	16.90	22.85	30.90	36.87	41.79	46.05	62.27	74.30	84.21	92.80
30	18.24	24.95	33.95	40.66	46.21	51.02	69.43	83.14	94.48	104.33
31	19.88	27.22	37.27	44.79	51.03	56.46	77.31	92.90	105.84	117.11
32	21.55	29.68	40.88	49.30	56.30	62.41	85.96	103.66	118.39	131.24
33	23.34	32.34	44.80	54.20	62.05	68.92	95.46	115.51	132.24	146.87
34	25.28	35.21	49.05	59.54	68.33	76.02	105.90	128.55	147.51	164.12
35	27.36	38.32	53.67	65.36	75.17	83.78	117.33	142.89	164.33	183.16
36	29.60	41.68	58.68	71.69	82.62	92.24	129.87	158.65	182.85	204.14
37	32.02	45.31	64.13	78.57	90.75	101.48	143.61	175.95	203.23	227.26
38	34.63	49.24	70.03	86.05	99.60	111.56	158.65	194.94	225.62	252.71
39	37.44	53.50	76.45	94.20	109.24	122.54	175.11	215.78	250.23	280.71
40	40.47	58.10	83.40	103.05	119.74	134.52	193.13	238.62	277.26	311.50
41	43.74	63.07	90.96	112.68	131.18	147.59	212.84	263.67	306.94	345.34
42	47.27	68.46	99.16	123.16	143.64	161.83	234.40	291.13	339.52	382.53
43	51.08	74.30	108.08	134.56	157.21	177.36	257.99	321.22	375.28	423.39
44	55.20	80.62	117.76	146.97	172.00	194.31	283.80	354.20	414.51	468.28
45	59.66	87.48	128.28	160.48	188.12	212.79	312.03	390.35	457.57	517.58

From "Design of Pile Foundations," by A. S. Vesic. SYNTHESIS OF HIGHWAY PRACTICE by AMERICAN ASSOCIATION OF STATE HIGHWAY AND TRANSPORT. Copyright 1969 by TRANSPORTATION RESEARCH BOARD. Reproduced with permission of TRANSPORTATION RESEARCH BOARD in the format Textbook via Copyright Clearance Center.

Table 11.8 Variation of N_c^* with I_{rr} for $\phi = 0$ Condition based on Vesic's Theory

I_{rr}	N_c^*
10	6.97
20	7.90
40	8.82
60	9.36
80	9.75
100	10.04
200	10.97
300	11.51
400	11.89
500	12.19

For $\phi = 0$,

$$I_r = \frac{E_s}{3c_u} \quad (11.34)$$

O' Neill and Reese (1999) suggested the following approximate relationships for I_r and the undrained cohesion, c_u .

$\frac{c_u}{p_a}$	I_r
0.24	50
0.48	150
≥ 0.96	250–300

Note: p_a = atmospheric pressure
 $\approx 100 \text{ kN/m}^2$ or 2000 lb/ft^2 .

The preceding values can be approximated as

$$I_r = 347\left(\frac{c_u}{p_a}\right) - 33 \leq 300 \quad (11.35)$$

11.9

Coyle and Castello's Method for Estimating Q_p in Sand

Coyle and Castello (1981) analyzed 24 large-scale field load tests of driven piles in sand. On the basis of the test results, they suggested that, in sand,

$$Q_p = q' N_q^* A_p \quad (11.36)$$

where

- q' = effective vertical stress at the pile tip
- N_q^* = bearing capacity factor

Figure 11.15 shows the variation of N_q^* with L/D and the soil friction angle ϕ' .

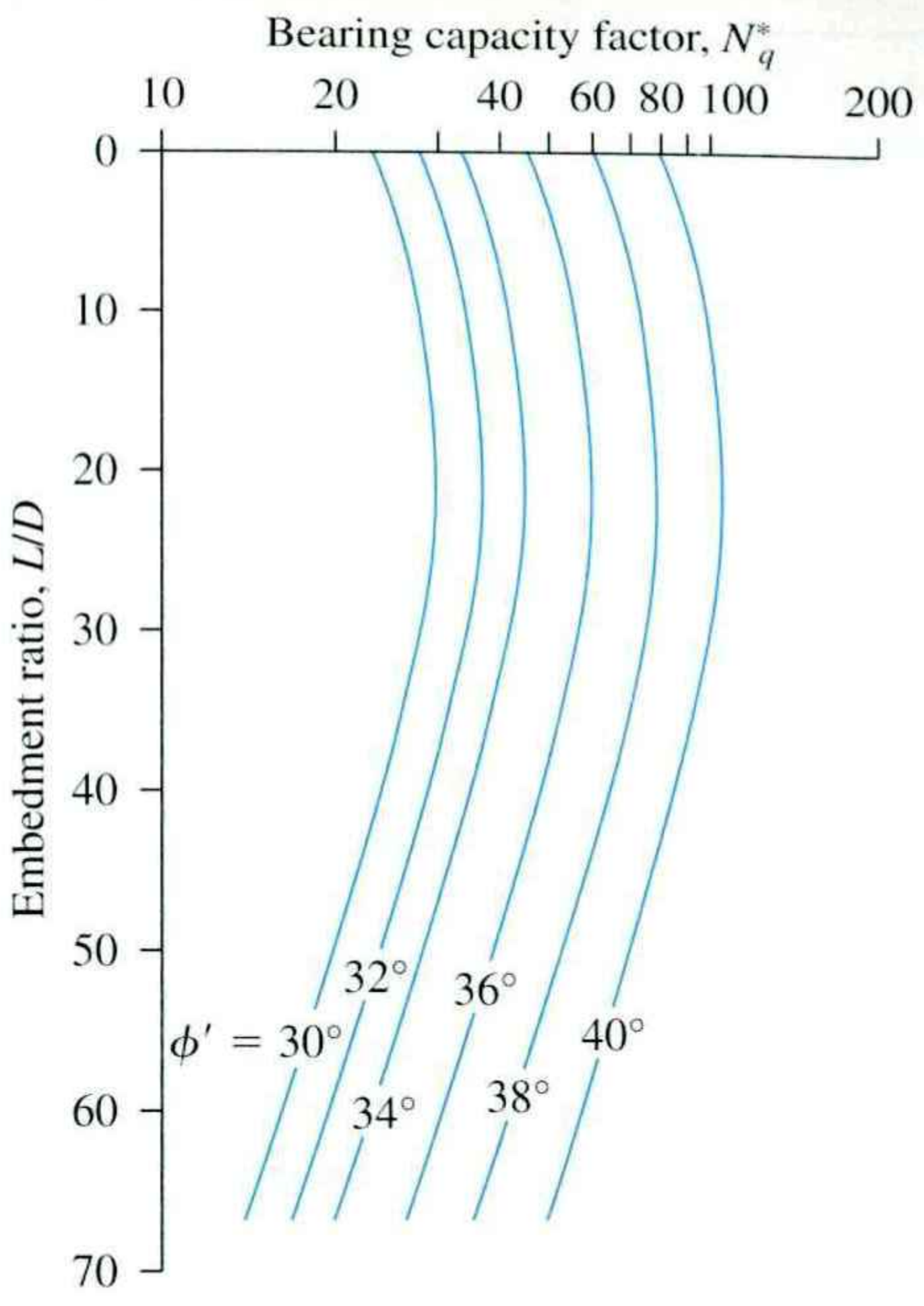


Figure 11.15 Variation of N_q^* with L/D
(Redrawn after Coyle and Costello, 1981)

Example 11.1

Consider a 15-m long concrete pile with a cross section of $0.45\text{ m} \times 0.45\text{ m}$ fully embedded in sand. For the sand, given: unit weight, $\gamma = 17\text{kN/m}^3$; and soil friction angle, $\phi' = 35^\circ$. Estimate the ultimate point Q_p with each of the following:

- Meyerhof's method
- Vesic's method
- The method of Coyle and Castello
- based on the results of parts a, b, and c, adopt a value for Q_p

Solution

Part a

From Eqs. (11.16) and (11.17),

$$Q_p = A_p q' N_q^* \leq A_p (0.5 p_a N_q^* \tan \phi')$$

For $\phi' = 35^\circ$, the value of $N_q^* \approx 143$ (Table 11.5). Also, $q' = \gamma L = (17)(15) = 255\text{kN/m}^2$.

Thus,

$$A_p q' N_q^* = (0.45 \times 0.45)(255)(143) \approx 7384\text{kN}$$

Again,

$$A_p (0.5 p_a N_q^* \tan \phi') = (0.45 \times 0.45)[(0.5)(100)(143)(\tan 35)] \approx 1014\text{kN}$$

Hence, $Q_p = 1014\text{ kN}$.

Part b

From Eq. (11.19),

$$Q_p = A_p \bar{\sigma}'_o N_\sigma^*$$

$$\bar{\sigma}'_o = \left[\frac{1 + 2(1 - \sin \phi')}{3} \right] q' = \left(\frac{1 + 2(1 - \sin 35)}{3} \right) (17 \times 15)$$

$$= 139.96 \text{ kN/m}^2$$

From Eq. (11.26),

$$\frac{E_s}{p_a} = m$$

Assume $m \approx 250$ (medium sand). So,

$$E_s = (250)(100) = 25,000 \text{ kN/m}^2$$

From Eq. (11.27),

$$\mu_s = 0.1 + 0.3 \left(\frac{\phi' - 25}{20} \right) = 0.1 + 0.3 \left(\frac{35 - 25}{20} \right) = 0.25$$

From Eq. (11.28),

$$\Delta = 0.005 \left(1 - \frac{\phi' - 25}{20} \right) \left(\frac{q'}{p_a} \right) = 0.005 \left(1 - \frac{35 - 25}{20} \right) \left(\frac{17 \times 15}{100} \right) = 0.0064$$

From Eq. (11.25),

$$I_r = \frac{E_s}{2(1 + \mu_s)q' \tan \phi'} = \frac{25,000}{(2)(1 + 0.25)(17 \times 15)(\tan 35)} = 56$$

From Eq. (11.24),

$$I_{rr} = \frac{I_r}{1 + I_r \Delta} = \frac{56}{1 + (56)(0.0064)} = 41.2$$

From Table 11.7, for $\phi' = 35^\circ$ and $I_{rr} = 41.2$, the value of $N_\sigma^* \approx 55$. Hence,

$$Q_p = A_p \bar{\sigma}'_o N_\sigma^* = (0.45 \times 0.45)(139.96)(55) \approx 1559 \text{ kN}$$

Part c

From Eq. (11.36),

$$Q_p = q' N_q^* A_p$$

$$\frac{L}{D} = \frac{15}{0.45} = 33.3$$

For $\phi' = 35^\circ$ and $L/D = 33.3$, the value of N_q^* is about 48 (Figure 11.15). Thus,

$$Q_p = q' N_q^* A_p = (15 \times 17)(48)(0.45 \times 0.45) \approx 2479 \text{ kN}$$

Part d

It appears that Q_p obtained from the method of Coyle and Castello is too large. Thus, the average of the results from parts a and b is

$$\frac{1014 + 1559}{2} = 1286.5 \text{ kN}$$

Use $Q_p = 1250 \text{ kN}$.

Example 11.2

Consider a pipe pile (flat driving point—see Figure 11.2d) having an outside diameter of 406 mm. The embedded length of the pile in layered saturated clay is 30 m. The following are the details of the subsoil:

Depth from ground surface (m)	Saturated unit weight, $\gamma (\text{kN/m}^3)$	$c_u (\text{kN/m}^2)$
0–5	18	30
5–10	18	30
10–30	19.6	100

The groundwater table is located at a depth of 5 m from the ground surface. Estimate Q_p by using

- a. Meyerhof's method
- b. Vesic's method

Solution

Part a

From Eq. (11.18),

$$Q_p = 9c_u A_p$$

The tip of the pile is resting on a clay with $c_u = 100 \text{ kN/m}^2$. So,

$$Q_p = (9)(100) \left[\left(\frac{\pi}{4} \right) \left(\frac{406}{1000} \right)^2 \right] = 116.5 \text{ kN}$$

Part b

From Eq. (11.31),

$$Q_p = A_p c_u N_c^*$$

From Eq. (11.35),

$$I_r = I_{rr} = 347 \left(\frac{c_u}{p_a} \right) - 33 = 347 \left(\frac{100}{100} \right) - 33 = 314$$

So we use $I_{rr} = 300$.

From Table 11.8 for $I_{rr} = 300$, the value of $N_c^* = 11.51$. Thus,

$$Q_p = A_p c_u N_c^* = \left[\left(\frac{\pi}{4} \right) \left(\frac{406}{1000} \right)^2 \right] (100) (11.51) = 149.0 \text{ kN}$$

Note: The average value of Q_p is

$$\frac{116.5 + 149.0}{2} \approx 133 \text{ kN}$$

11.10

Correlations for Calculating Q_p with SPT and CPT Results

On the basis of field observations, Meyerhof (1976) also suggested that the ultimate point resistance q_p in a homogeneous granular soil ($L = L_b$) may be obtained from standard penetration numbers as

$$q_p = 0.4 p_a N_{60} \frac{L}{D} \leq 4 p_a N_{60} \quad (11.37)$$

where

N_{60} = the average value of the standard penetration number near the pile point (about $10D$ above and $4D$ below the pile point)

p_a = atmospheric pressure ($\approx 100 \text{ kN/m}^2$ or 2000 lb/ft^2)

Briaud et al. (1985) suggested the following correlation for q_p in granular soil with the standard penetration resistance N_{60} .

$$q_p = 19.7 p_a (N_{60})^{0.36} \quad (11.38)$$

Meyerhof (1956) also suggested that

$$q_p \approx q_c \text{ (in granular soil)} \quad (11.39)$$

where q_c = cone penetration resistance.

Example 11.3

Consider a concrete pile that is 12 in. \times 12 in. in cross section in sand. The pile is 50 ft long. The following are the variations of N_{60} with depth.

Depth below ground surface (ft)	N_{60}
5	8
10	10
15	9
20	12
25	14
30	18
35	11
40	17
45	20
50	28
55	29
60	32
65	30
70	27

- Estimate Q_p using Eq. (11.37).
- Estimate Q_p using Eq. (11.38).

Solution

Part a

The tip of the pile is 50 ft below the ground surface. For the pile, $D = 1$ ft. The average of N_{60} 10D above and about 5D below the pile tip is

$$N_{60} = \frac{17 + 20 + 28 + 29}{4} = 23.5 \approx 24$$

From Eq. (11.37)

$$\begin{aligned} Q_p &= A_p(q_p) = A_p \left[0.4 p_a N_{60} \left(\frac{L}{D} \right) \right] \leq A_p (4 p_a N_{60}) \\ A_p \left[0.4 p_a N_{60} \left(\frac{L}{D} \right) \right] &= (1 \times 1) \left[(0.4)(2000)(24) \left(\frac{50}{1} \right) \right] = 960,000 \text{ lb} \\ A_p (4 p_a N_{60}) &= (1 \times 1)[(4)(2000)(24)] = 192,000 \text{ lb} \end{aligned}$$

Thus, $Q_p = 192,000 \text{ lb} = \mathbf{192 \text{ kip}}$

Part b

From Eq. (11.38),

$$\begin{aligned} Q_p &= A_p q_p = A_p [19.7 p_a (N_{60})^{0.36}] = (1 \times 1) [(19.7)(2000)(24)^{0.36}] \\ &= 123,700 \text{ lb} = \mathbf{123.7 \text{ kip}} \end{aligned}$$

11.11

Frictional Resistance (Q_s) in Sand

According to Eq. (11.14), the frictional resistance

$$Q_s = \Sigma p \Delta L f$$

The unit frictional resistance, f , is hard to estimate. In making an estimation of f , several important factors must be kept in mind:

- The nature of the pile installation. For driven piles in sand, the vibration caused during pile driving helps densify the soil around the pile. The zone of sand densification may be as much as 2.5 times the pile diameter, in the sand surrounding the pile.
- It has been observed that the nature of variation of f in the field is approximately as shown in Figure 11.16. The unit skin friction increases with depth more or

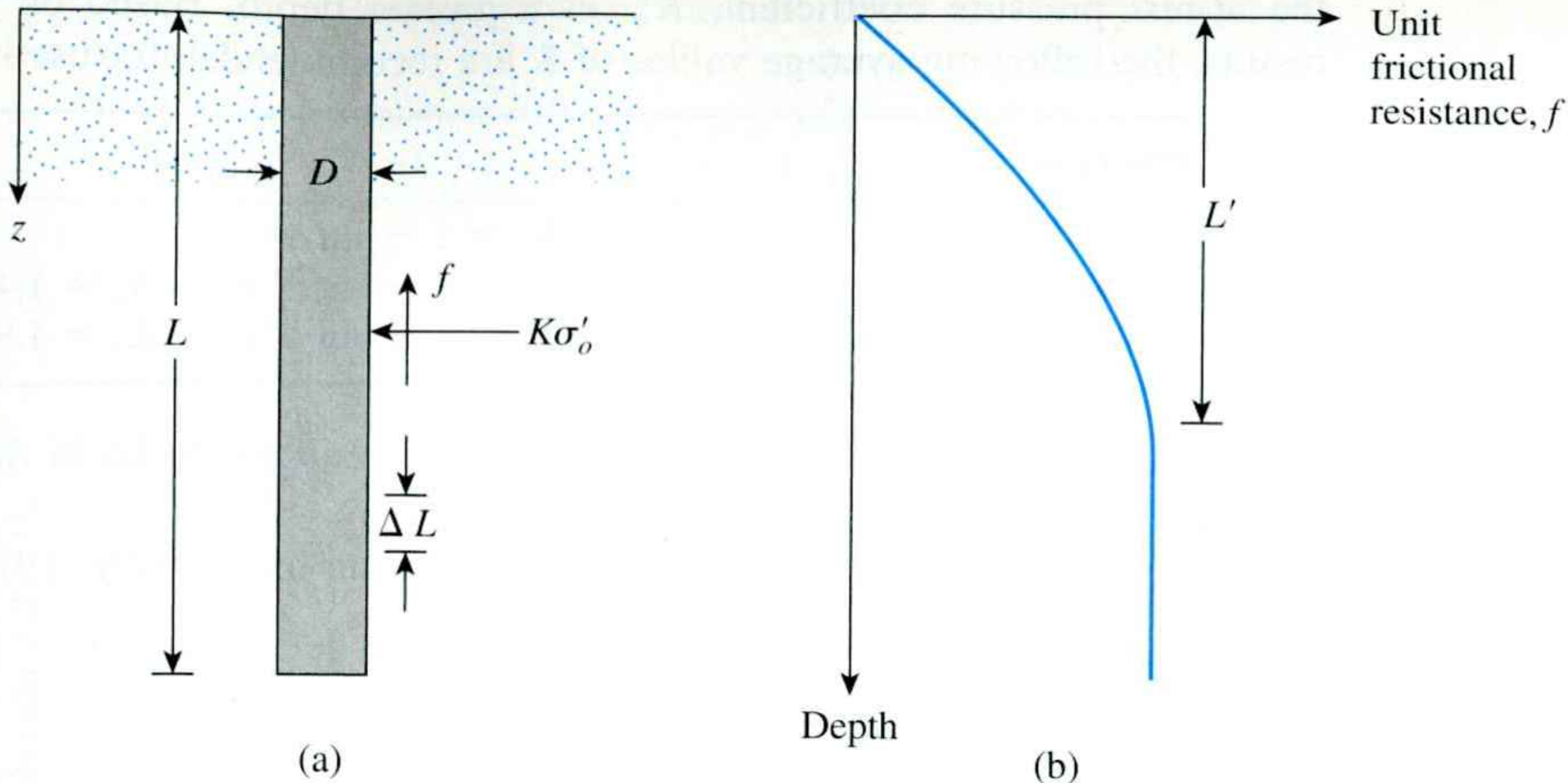


Figure 11.16 Unit frictional resistance for piles in sand

less linearly to a depth of L' and remains constant thereafter. The magnitude of the critical depth L' may be 15 to 20 pile diameters. A conservative estimate would be

$$L' \approx 15D \quad (11.40)$$

3. At similar depths, the unit skin friction in loose sand is higher for a high-displacement pile, compared with a low-displacement pile.
 4. At similar depths, bored, or jetted, piles will have a lower unit skin friction compared with driven piles.

Taking into account the preceding factors, we can give the following approximate relationship for f (see Figure 11.16):

For $z = 0$ to L' ,

$$f = K\sigma'_o \tan \delta' \quad (11.41)$$

and for $z = L'$ to L ,

$$f = f_{z=L} \quad (11.42)$$

In these equations,

K = effective earth pressure coefficient

σ'_o = effective vertical stress at the depth under consideration

δ' = soil-pile friction angle

In reality, the magnitude of K varies with depth; it is approximately equal to the Rankine passive earth pressure coefficient, K_p , at the top of the pile and may be less than

the at-rest pressure coefficient, K_o , at a greater depth. Based on presently available results, the following average values of K are recommended for use in Eq. (11.41):

Pile type	K
Bored or jetted	$\approx K_o = 1 - \sin \phi'$
Low-displacement driven	$\approx K_o = 1 - \sin \phi'$ to $1.4K_o = 1.4(1 - \sin \phi')$
High-displacement driven	$\approx K_o = 1 - \sin \phi'$ to $1.8K_o = 1.8(1 - \sin \phi')$

The values of δ' from various investigations appear to be in the range from $0.5\phi'$ to $0.8\phi'$.

Based on load test results in the field, Mansur and Hunter (1970) reported the following average values of K .

$$\text{H-piles} \dots K = 1.65$$

$$\text{Steel pipe piles} \dots K = 1.26$$

$$\text{Precast concrete piles} \dots K = 1.5$$

Coyle and Castello (1981), in conjunction with the material presented in Section 11.9, proposed that

$$Q_s = f_{av} pL = (K \bar{\sigma}'_o \tan \delta') pL \quad (11.43)$$

where

$\bar{\sigma}'_o$ = average effective overburden pressure

δ' = soil–pile friction angle = $0.8\phi'$

The lateral earth pressure coefficient K , which was determined from field observations, is shown in Figure 11.17. Thus, if that figure is used,

$$Q_s = K \bar{\sigma}'_o \tan(0.8\phi') pL \quad (11.44)$$

Correlation with Standard Penetration Test Results

Meyerhof (1976) indicated that the average unit frictional resistance, f_{av} , for high-displacement driven piles may be obtained from average standard penetration resistance values as

$$f_{av} = 0.02 p_a (\bar{N}_{60}) \quad (11.45)$$

where

(\bar{N}_{60}) = average value of standard penetration resistance

p_a = atmospheric pressure ($\approx 100 \text{ kN/m}^2$ or 2000 lb/ft^2)

For low-displacement driven piles

$$f_{av} = 0.01 p_a (\bar{N}_{60}) \quad (11.46)$$

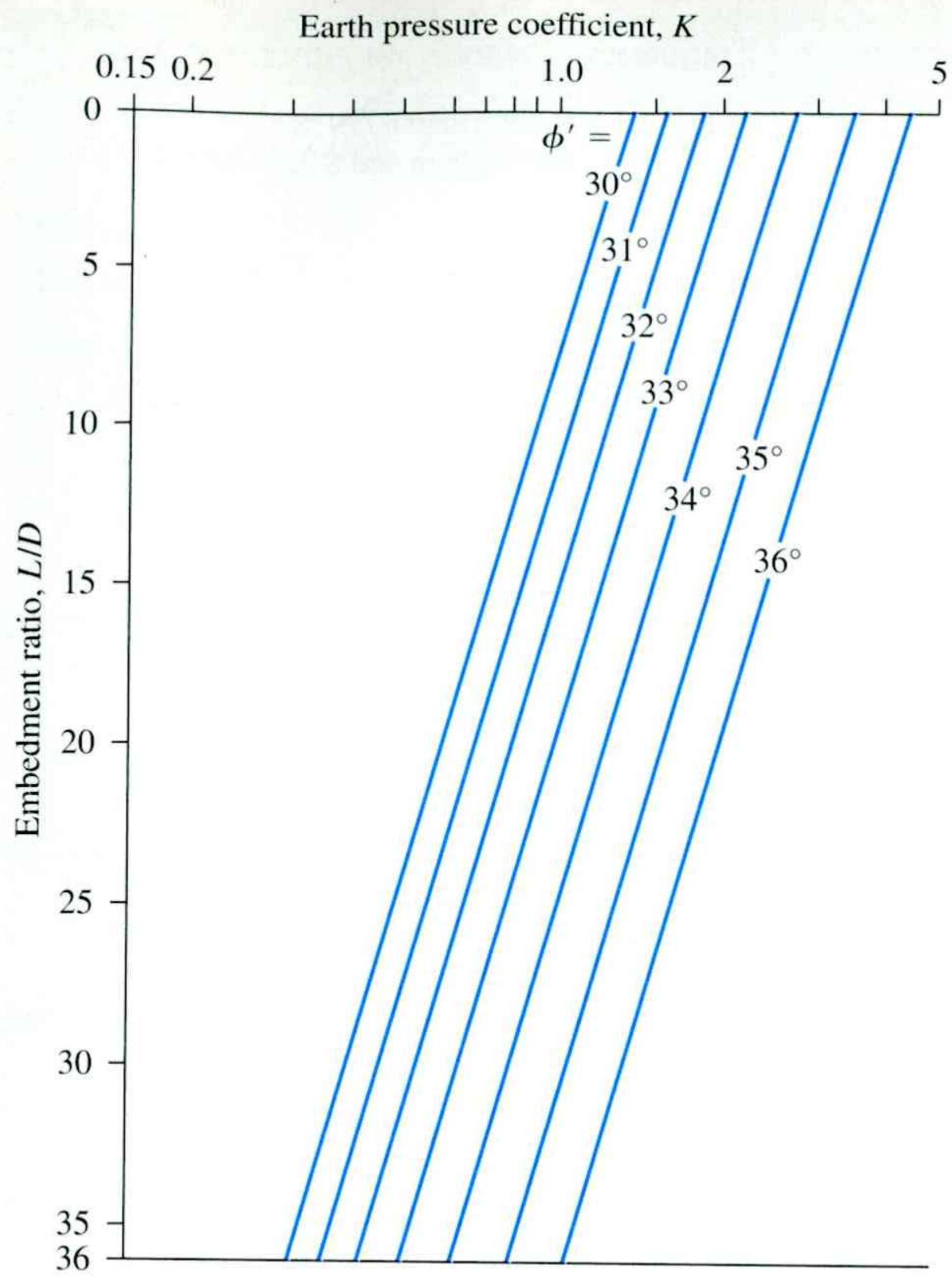


Figure 11.17 Variation of K with L/D (Redrawn after Coyle and Castello, 1981)

Briaud et al. (1985) suggested that

$$f_{av} \approx 0.224 p_a (\bar{N}_{60})^{0.29} \quad (11.47)$$

Thus,

$$Q_s = p L f_{av} \quad (11.48)$$

Correlation with Cone Penetration Test Results

Nottingham and Schmertmann (1975) and Schmertmann (1978) provided correlations for estimating Q_s using the frictional resistance (f_c) obtained during cone penetration tests. According to this method

$$f = \alpha' f_c \quad (11.49)$$

The variations of α' with z/D for electric cone and mechanical cone penetrometers are shown in Figures 11.18 and 11.19, respectively. We have

$$Q_s = \sum p(\Delta L) f = \sum p(\Delta L) \alpha' f_c \quad (11.50)$$

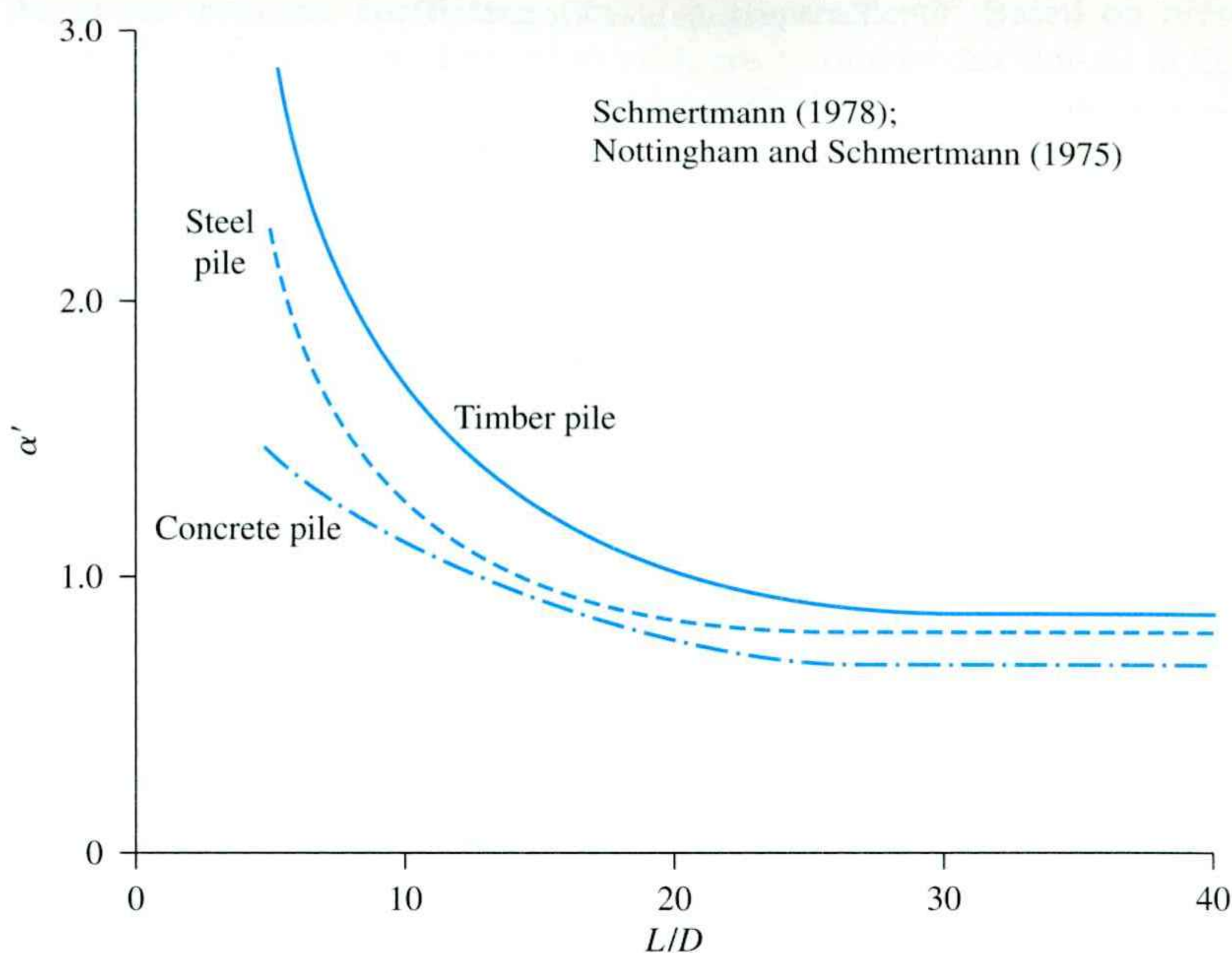


Figure 11.18 Variation of α' with embedment ratio for pile in sand: electric cone penetrometer

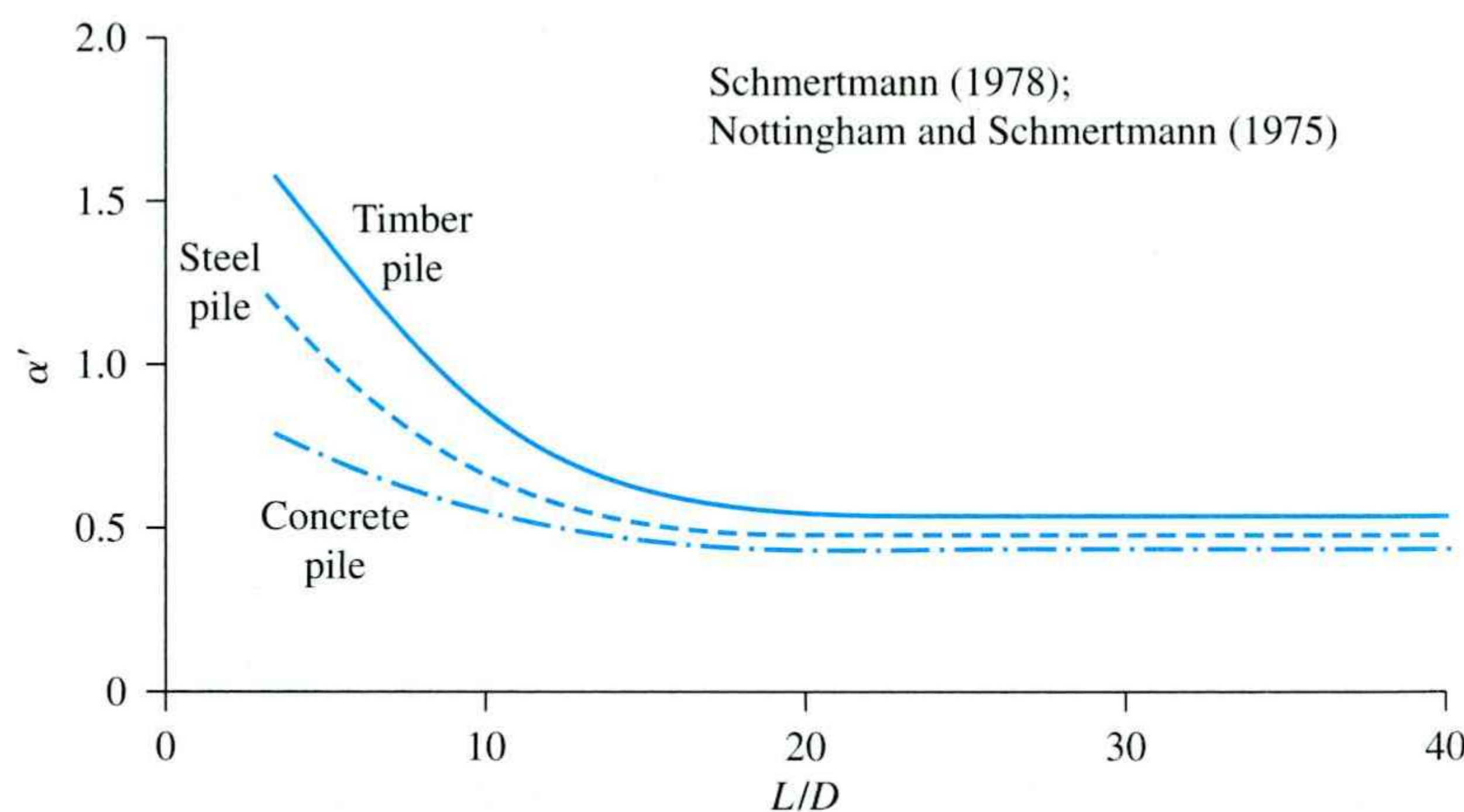


Figure 11.19 Variation of α' with embedment ratio for piles in sand: mechanical cone penetrometer

Example 11.4

Refer to the pile described in Example 11.3. Estimate the magnitude of Q_s for the pile.

- Use Eq. (11.45).
- Use Eq. (11.47).

- c. Considering the results in Example 11.3, determine the allowable load-carrying capacity of the pile based on Meyerhof's method and Briaud's method. Use a factor of safety, FS = 3.

Solution

The average \bar{N}_{60} value for the sand for the top 50 ft is

$$\bar{N}_{60} = \frac{8 + 10 + 9 + 12 + 14 + 18 + 11 + 17 + 20 + 28}{10} = 14.7 \approx 15$$

Part a

From Eq. (11.45),

$$f_{av} = 0.02p_a(\bar{N}_{60}) = (0.02)(2000)(15) = 600 \text{ lb/ft}^2$$

$$Q_s = pL f_{av} = (4 \times 1)(50)(600) = 120,000 \text{ lb} = \mathbf{120 \text{ kip}}$$

Part b

From Eq. (11.47),

$$f_{av} = 0.224p_a(\bar{N}_{60})^{0.29} = (0.224)(2000)(15)^{0.29} = 982.5 \text{ lb/ft}^2$$

$$Q_s = pL f_{av} = (4 \times 1)(50)(982.5) = 196,500 \text{ lb} = \mathbf{196.5 \text{ kip}}$$

Part c

$$\text{Meyerhof's method: } Q_{all} = \frac{Q_p + Q_s}{FS} = \frac{192 + 120}{3} = \mathbf{104 \text{ kip}}$$

$$\text{Briaud's method: } Q_{all} = \frac{Q_p + Q_s}{FS} = \frac{123.7 + 196.5}{3} = \mathbf{106.7 \text{ kip}}$$

So the allowable pile capacity may be taken to be about **105 kip**. ■

Example 11.5

Refer to Example 11.1. For the pile, estimate the frictional resistance Q_s

- Based on Eqs. (11.41) and (11.42). Use $K = 1.3$ and $\delta' = 0.8\phi'$.
- Based on Eq. (11.44).
- Using the results of Part d of Example 11.1, estimate the allowable bearing capacity of the pile. Use FS = 3.

Solution

Part a

From Eq. (11.40), $L' = 15D = (15)(0.45) = 6.75 \text{ m}$. Refer to Eq. (11.41):

$$\begin{aligned} \text{At } z = 0: \quad \sigma'_o &= 0 \\ &f = 0 \end{aligned}$$

$$\text{At } z = 6.75 \text{ m: } \sigma'_o = (6.75)(17) = 114.75 \text{ kN/m}^2$$

So

$$f = K\sigma'_o \tan \delta = (1.3)(114.75)[\tan(0.8 \times 35)] = 79.3 \text{ kN/m}^3$$

Thus,

$$\begin{aligned} Q_s &= \frac{(f_{z=0} + f_{z=6.75\text{m}})}{2} pL' + f_{z=6.75\text{m}} p(L - L') \\ &= \left(\frac{0 + 79.3}{2}\right)(4 \times 0.45)(6.75) + (79.3)(4 \times 0.45)(15 - 6.75) \\ &= 481.75 + 1177.61 = 1659.36 \text{ kN} \approx \mathbf{1659 \text{ kN}} \end{aligned}$$

Part b

From Eq. (11.44),

$$\begin{aligned} Q_s &= K\bar{\sigma}'_o \tan(0.8\phi') pL \\ \bar{\sigma}'_o &= \frac{(15)(17)}{2} = 127.5 \text{ kN/m}^2 \\ \frac{L}{D} &= \frac{15}{0.45} = 33.3; \phi' = 35^\circ \end{aligned}$$

From Figure 11.17, $K = 0.93$

$$Q_s = (1.3)(127.5) \tan[(0.8 \times 35)](4 \times 0.45)(15) = \mathbf{2380 \text{ kN}}$$

Part c

The average value of Q_s from parts a and b is

$$Q_{s(\text{average})} = \frac{1659 + 2380}{2} = 2019.5 \approx 2020 \text{ kN} - \text{USE}$$

From part d of Example 11.1, $Q_p = 1250 \text{ kN}$. Thus,

$$Q_{\text{all}} = \frac{Q_p + Q_s}{\text{FS}} = \frac{1250 + 2020}{3} = \mathbf{1090 \text{ kN}}$$

Example 11.6

Consider an 18-m long concrete pile (cross section: $0.305 \text{ m} \times 0.305 \text{ m}$) fully embedded in a sand layer. For the sand layer, the following is an approximation of the cone penetration resistance q_c (mechanical cone) and the frictional resistance f_c with depth. Estimate the allowable load that the pile can carry. Use FS = 3.

Depth from ground surface (m)	q_c (kN/m ²)	f_c (kN/m ²)
0–5	3040	73
5–15	4560	102
15–25	9500	226

Solution

$$Q_u = Q_p + Q_s$$

From Eq. (11.39),

$$q_p \approx q_c$$

At the pile tip (i.e., at a depth of 18 m), $q_c \approx 9500 \text{ kN/m}^2$. Thus,

$$Q_p = A_p q_c = (0.305 \times 0.305)(9500) = 883.7 \text{ kN}$$

To determine Q_s , the following table can be prepared. (Note: $L/D = 18/0.305 = 59$.)

Depth from ground surface (m)	ΔL (m)	f_c (kN/m^2)	α' (Figure 11.19)	$p\Delta L\alpha'f_c$ (kN)
0–5	5	73	0.44	195.9
5–15	10	102	0.44	547.5
15–18	3	226	0.44	363.95
				$Q_s = 1107.35 \text{ kN}$

Hence,

$$Q_u = Q_p + Q_s = 883.7 + 1107.35 = 1991.05 \text{ kN}$$

$$Q_{\text{all}} = \frac{Q_u}{\text{FS}} = \frac{1991.05}{3} = 663.68 \approx 664 \text{ kN}$$

11.12

Frictional (Skin) Resistance in Clay

Estimating the frictional (or skin) resistance of piles in clay is almost as difficult a task as estimating that in sand (see Section 11.11), due to the presence of several variables that cannot easily be quantified. Several methods for obtaining the unit frictional resistance of piles are described in the literature. We examine some of them next.

λ Method

This method, proposed by Vijayvergiya and Focht (1972), is based on the assumption that the displacement of soil caused by pile driving results in a passive lateral pressure at any depth and that the average unit skin resistance is

$$f_{av} = \lambda(\bar{\sigma}'_o + 2c_u) \quad (11.51)$$

where

$\bar{\sigma}'_o$ = mean effective vertical stress for the entire embedment length

c_u = mean undrained shear strength ($\phi = 0$)

Table 11.9 Variation of λ with pile embedment length, L

Embedment length, L (m)	λ
0	0.5
5	0.336
10	0.245
15	0.200
20	0.173
25	0.150
30	0.136
35	0.132
40	0.127
50	0.118
60	0.113
70	0.110
80	0.110
90	0.110

The value of λ changes with the depth of penetration of the pile. (See Table 11.9.) Thus, the total frictional resistance may be calculated as

$$Q_s = pL f_{av}$$

Care should be taken in obtaining the values of $\bar{\sigma}'_o$ and c_u in layered soil. Figure 11.20 helps explain the reason. Figure 11.20a shows a pile penetrating three layers of clay. According to Figure 11.20b, the mean value of c_u is $(c_{u(1)}L_1 + c_{u(2)}L_2 + \dots)/L$. Similarly, Figure 11.20c shows the plot of the variation of effective stress with depth. The mean effective stress is

$$\bar{\sigma}'_o = \frac{A_1 + A_2 + A_3 + \dots}{L} \quad (11.52)$$

where A_1, A_2, A_3, \dots = areas of the vertical effective stress diagrams.

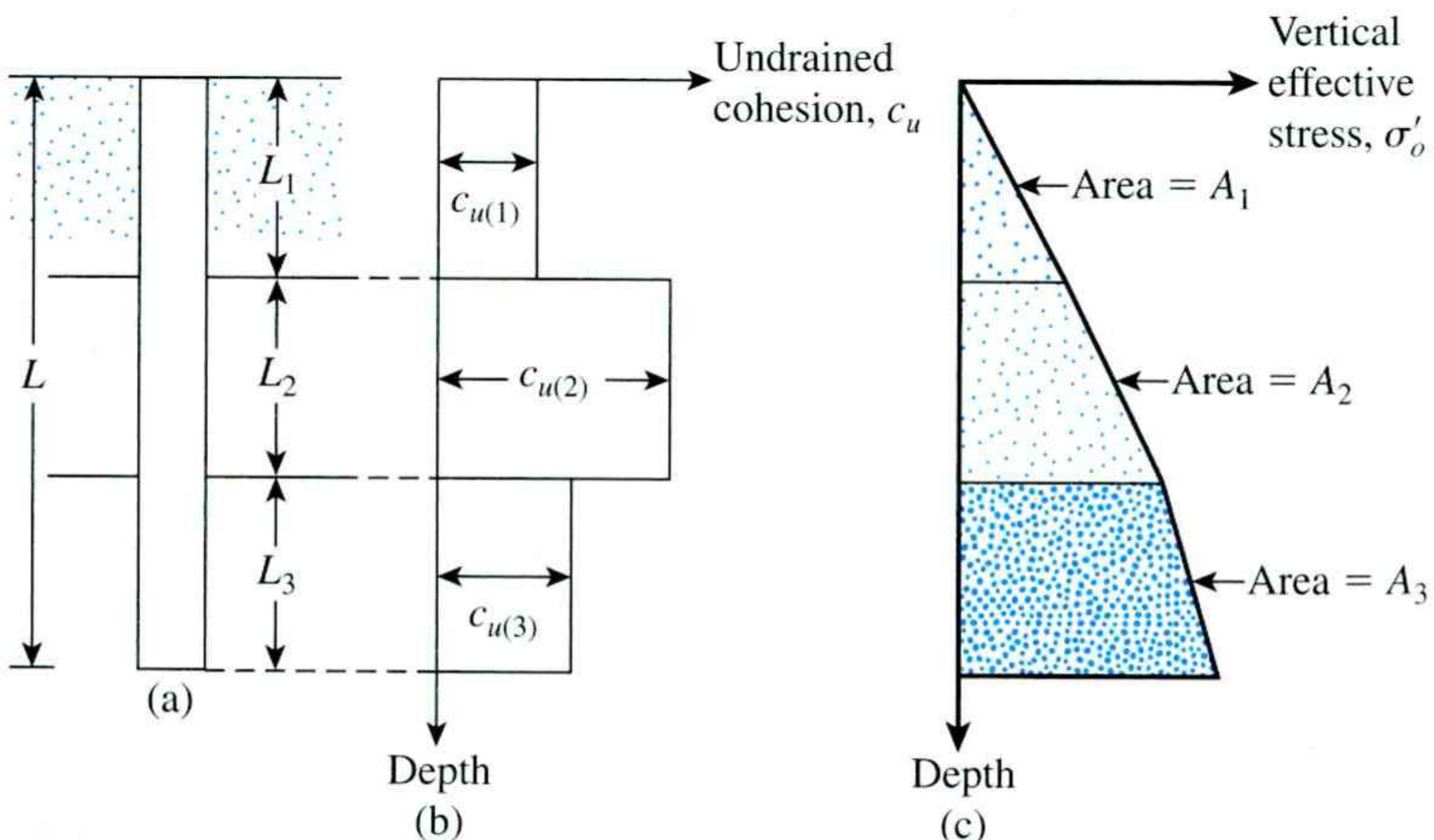


Figure 11.20 Application of λ method in layered soil

α Method

According to the α method, the unit skin resistance in clayey soils can be represented by the equation

$$f = \alpha c_u \quad (11.53)$$

where α = empirical adhesion factor. The approximate variation of the value of α is shown in Table 11.10. It is important to realize that the values of α given in Table 11.10 may vary somewhat, since α is actually a function of vertical effective stress and the undrained cohesion. Sladen (1992) has shown that

$$\alpha = C \left(\frac{\bar{\sigma}'_o}{c_u} \right)^{0.45} \quad (11.54)$$

where

$\bar{\sigma}'_o$ = average vertical effective stress

$C \approx 0.4$ to 0.5 for bored piles and ≥ 0.5 for driven piles

The ultimate side resistance can thus be given as

$$Q_s = \sum f p \Delta L = \sum \alpha c_u p \Delta L \quad (11.55)$$

Table 11.10 Variation of α (interpolated values based on Terzaghi, Peck and Mesri, 1996)

$\frac{c_u}{p_a}$	α
≤ 0.1	1.00
0.2	0.92
0.3	0.82
0.4	0.74
0.6	0.62
0.8	0.54
1.0	0.48
1.2	0.42
1.4	0.40
1.6	0.38
1.8	0.36
2.0	0.35
2.4	0.34
2.8	0.34

Note: p_a = atmospheric pressure
 $\approx 100 \text{ kN/m}^2$ or 2000 lb/ft^2

β Method

When piles are driven into saturated clays, the pore water pressure in the soil around the piles increases. The excess pore water pressure in normally consolidated clays may be four to six times c_u . However, within a month or so, this pressure gradually dissipates. Hence, the unit frictional resistance for the pile can be determined on the basis of the effective stress parameters of the clay in a remolded state ($c' = 0$). Thus, at any depth,

$$f = \beta \sigma'_o \quad (11.56)$$

where

$$\begin{aligned} \sigma'_o &= \text{vertical effective stress} \\ \beta &= K \tan \phi'_R \\ \phi'_R &= \text{drained friction angle of remolded clay} \\ K &= \text{earth pressure coefficient} \end{aligned} \quad (11.57)$$

Conservatively, the magnitude of K is the earth pressure coefficient at rest, or

$$K = 1 - \sin \phi'_R \quad (\text{for normally consolidated clays}) \quad (11.58)$$

and

$$K = (1 - \sin \phi'_R) \sqrt{\text{OCR}} \quad (\text{for overconsolidated clays}) \quad (11.59)$$

where OCR = overconsolidation ratio.

Combining Eqs. (11.56), (11.57), (11.58), and (11.59), for normally consolidated clays yields

$$f = (1 - \sin \phi'_R) \tan \phi'_R \sigma'_o \quad (11.60)$$

and for overconsolidated clays,

$$f = (1 - \sin \phi'_R) \tan \phi'_R \sqrt{\text{OCR}} \sigma'_o \quad (11.61)$$

With the value of f determined, the total frictional resistance may be evaluated as

$$Q_s = \sum f p \Delta L$$

Correlation with Cone Penetration Test Results

Nottingham and Schmertmann (1975) and Schmertmann (1978) found the correlation for unit skin friction in clay (with $\phi = 0$) to be

$$f = \alpha' f_c \quad (11.62)$$

The variation of α' with the frictional resistance f_c is shown in Figure 11.21. Thus,

$$Q_s = \sum f p(\Delta L) = \sum \alpha' f_c p(\Delta L) \quad (11.63)$$

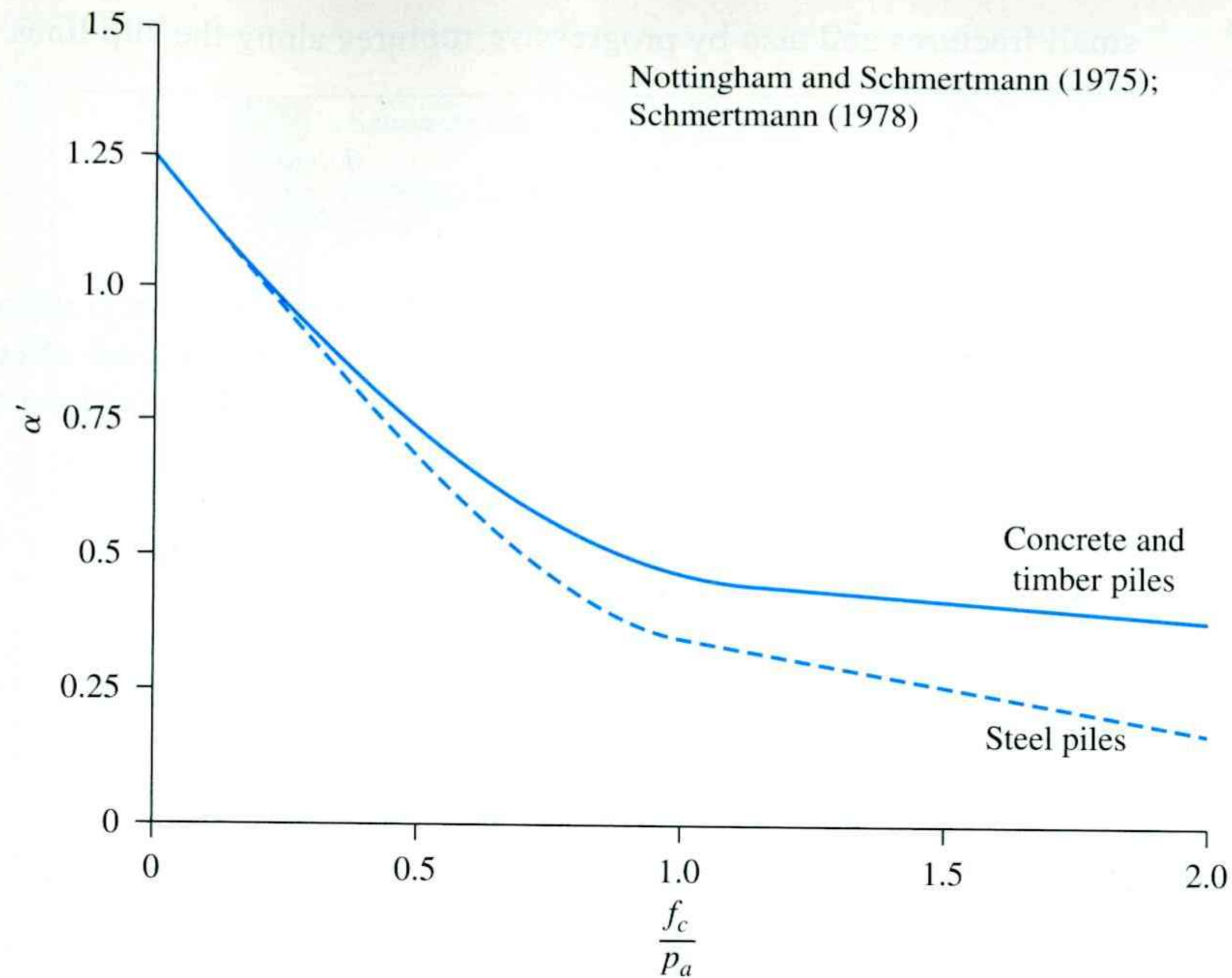


Figure 11.21 Variation of α' with f_c/p_a for piles in clay (p_a = atmospheric pressure $\approx 100 \text{ kN/m}^2$ or 2000 lb/ft^2)

11.13 Point Bearing Capacity of Piles Resting on Rock

Sometimes piles are driven to an underlying layer of rock. In such cases, the engineer must evaluate the bearing capacity of the rock. The ultimate unit point resistance in rock (Goodman, 1980) is approximately

$$q_p = q_u(N_\phi + 1) \quad (11.64)$$

where

$$N_\phi = \tan^2(45 + \phi'/2)$$

q_u = unconfined compression strength of rock

ϕ' = drained angle of friction

The unconfined compression strength of rock can be determined by laboratory tests on rock specimens collected during field investigation. However, extreme caution should be used in obtaining the proper value of q_u , because laboratory specimens usually are small in diameter. As the diameter of the specimen increases, the unconfined compression strength decreases—a phenomenon referred to as the *scale effect*. For specimens larger than about 1 m (3 ft) in diameter, the value of q_u remains approximately constant. There appears to be a fourfold to fivefold reduction of the magnitude of q_u in this process. The scale effect in rock is caused primarily by randomly distributed large and

small fractures and also by progressive ruptures along the slip lines. Hence, we always recommend that

$$q_{u(\text{design})} = \frac{q_{u(\text{lab})}}{5} \quad (11.65)$$

Table 11.11 lists some representative values of (laboratory) unconfined compression strengths of rock. Representative values of the rock friction angle ϕ' are given in Table 11.12.

A factor of safety of at least 3 should be used to determine the allowable point bearing capacity of piles. Thus,

$$Q_{p(\text{all})} = \frac{[q_{u(\text{design})}(N_\phi + 1)]A_p}{\text{FS}} \quad (11.66)$$

Table 11.11 Typical Unconfined Compressive Strength of Rocks

Type of rock	MN/m ²	lb/in ²
Sandstone	70–140	10,000–20,000
Limestone	105–210	15,000–30,000
Shale	35–70	5000–10,000
Granite	140–210	20,000–30,000
Marble	60–70	8500–10,000

Table 11.12 Typical Values of Angle of Friction ϕ' of Rocks

Type of rock	Angle of friction, ϕ' (deg)
Sandstone	27–45
Limestone	30–40
Shale	10–20
Granite	40–50
Marble	25–30

Example 11.7

Refer to the pile in saturated clay shown in Figure 11.22. For the pile,

- Calculate the skin resistance (Q_s) by (1) the α method, (2) the λ method, and (3) the β method. For the β method, use $\phi'_R = 30^\circ$ for all clay layers. The top 10 m of clay is normally consolidated. The bottom clay layer has an OCR = 2. (Note: diameter of pile = 406 mm)
- Using the results of Example 11.2, estimate the allowable pile capacity (Q_{all}). Use FS = 4.

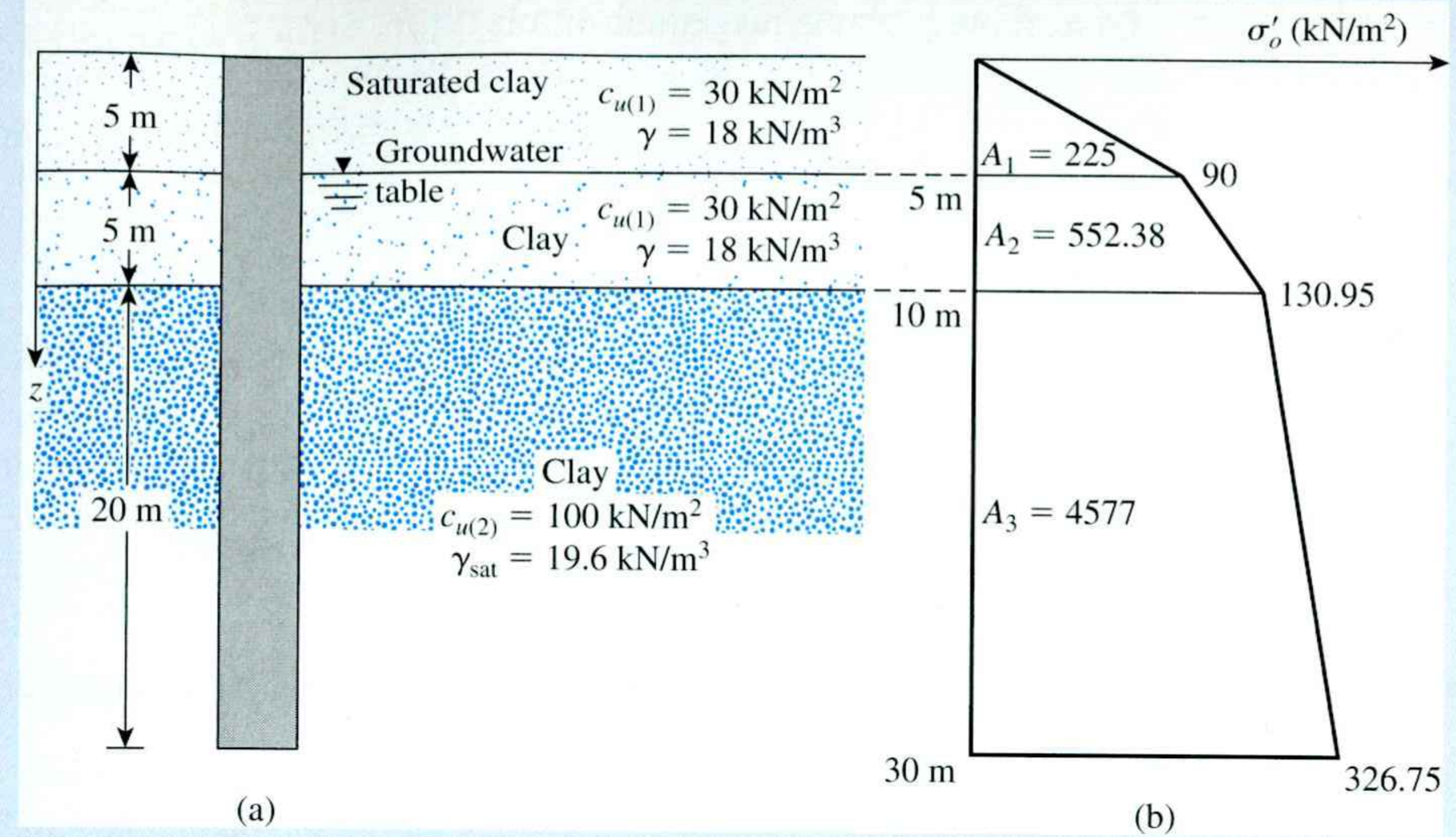


Figure 11.22 Estimation of the load bearing capacity of a driven-pipe pile

Solution

Part a

(1) From Eq. (11.55),

$$Q_s = \sum \alpha c_u p \Delta L$$

[Note: $p = \pi(0.406) = 1.275\text{m}$] Now the following table can be prepared.

Depth (m)	ΔL (m)	c_u (kN/m ²)	α (Table 11.10)	$\alpha c_u p \Delta L$ (kN)
0–5	5	30	0.82	156.83
5–10	5	30	0.82	156.83
10–30	20	100	0.48	1224.0

$$Q_s \approx 1538 \text{ kN}$$

(2) From Eq. 11.51, $f_{av} = \lambda(\bar{\sigma}'_o + 2c_u)$. Now, the average value of c_u is

$$\frac{c_{u(1)}(10) + c_{u(2)}(20)}{30} = \frac{(30)(10) + (100)(20)}{30} = 76.7 \text{ kN/m}^2$$

To obtain the average value of $\bar{\sigma}'_o$, the diagram for vertical effective stress variation with depth is plotted in Figure 11.22b. From Eq. (11.52),

$$\bar{\sigma}'_o = \frac{A_1 + A_2 + A_3}{L} = \frac{225 + 552.38 + 4577}{30} = 178.48 \text{ kN/m}^2$$

From Table 11.9, the magnitude of λ is 0.136. So

$$f_{av} = 0.136[178.48 + (2)(76.7)] = 45.14 \text{ kN/m}^2$$

Hence,

$$Q_s = pLf_{av} = \pi(0.406)(30)(45.14) = 1727 \text{ kN}$$

(3) The top layer of clay (10 m) is normally consolidated, and $\phi'_R = 30^\circ$. For $z = 0\text{--}5 \text{ m}$, from Eq. (11.60), we have

$$\begin{aligned} f_{av(1)} &= (1 - \sin \phi'_R) \tan \phi'_R \bar{\sigma}'_o \\ &= (1 - \sin 30^\circ)(\tan 30^\circ) \left(\frac{0 + 90}{2} \right) = 13.0 \text{ kN/m}^2 \end{aligned}$$

Similarly, for $z = 5\text{--}10 \text{ m}$.

$$f_{av(2)} = (1 - \sin 30^\circ)(\tan 30^\circ) \left(\frac{90 + 130.95}{2} \right) = 31.9 \text{ kN/m}^2$$

For $z = 10\text{--}30 \text{ m}$ from Eq. (11.61),

$$f_{av} = (1 - \sin \phi'_R) \tan \phi'_R \sqrt{\text{OCR}} \bar{\sigma}'_o$$

For OCR = 2,

$$f_{av(3)} = (1 - \sin 30^\circ)(\tan 30^\circ) \sqrt{2} \left(\frac{130.95 + 326.75}{2} \right) = 93.43 \text{ kN/m}^2$$

So,

$$\begin{aligned} Q_s &= p[f_{av(1)}(5) + f_{av(2)}(5) + f_{av(3)}(20)] \\ &= (\pi)(0.406)[(13)(5) + (31.9)(5) + (93.43)(20)] = 2670 \text{ kN} \end{aligned}$$

Part b

$$Q_u = Q_p + Q_s$$

From Example 11.2,

$$Q_p \approx \frac{116.5 + 149}{2} \approx 133 \text{ kN}$$

Again, the values of Q_s from the α method and λ method are close. So,

$$Q_s \approx \frac{1538 + 1727}{2} = 1632.5 \text{ kN}$$

$$Q_{\text{all}} = \frac{Q_u}{\text{FS}} = \frac{133 + 1632.5}{4} = 441.4 \text{ kN} \approx 441 \text{ kN}$$